The Thesis Committee for Sarah Lynn Williams
certifies that this is the approved version of the following thesis:

Toward the Development of Robust Self-Healing Concrete Using Vegetative Microorganisms

APPROVED BY
SUPERVISING COMMITTEE:

Supervisor: _____
Raissa Douglas Ferron

Co-supervisor: _____
Mary Jo Kirisits

Toward the Development of Robust Self-Healing Concrete Using Vegetative Microorganisms

by

Sarah Lynn Williams, B.S.C.E.

Thesis

Presented to the Faculty of the Graduate School of

The University of Texas at Austin

in Partial Fulfillment

of the Requirements

for the Degree of

Master of Science in Engineering

The University of Texas at Austin

May 2015

Dedication

To my parents for their unconditional love, support, and encouragement.

Acknowledgements

I would like to express my sincerest gratitude to my advisors, Dr. Raissa Ferron and Dr. Mary Jo Kirisits, for introducing me to this project and providing valuable insight over the years. Having access to each of your expertise was critical for the success of this research, and I've genuinely enjoyed all of the time spent learning together and challenging each other. I am a better researcher for having working with each of you. I am also grateful to Dr. Kirisits for being kind and patient with me while I learned microbiology. You were always helpful and encouraging when I had questions, no matter how simple they were.

To call Dr. Zeynep Bundur an influential person in my life is an understatement. I was incredibly fortunate to be assigned as your undergraduate research assistant nearly four years ago, and I absolutely could not have completed this thesis without your guidance and encouragement. To my CMRG and Kirisits group friends, I am thankful for all of your support and assistance over the years. I am particularly grateful to Racheal Lute and Sarah Keithley for their help around the lab and for always making me feel welcome. Stephen Stacey, Fred Aguayo, Trevor Williamson, Beth Anne Feero, Aasiyah Baig, Nicolás Tiburzi, Thano Drimalas, Qian Wu, Alex Olivas, Bryant Chambers, Emily Palmer, Sungwoo Bae, Gustavo Ochoa, Taegyu Kim, and Bruk Berhanu also deserve my thanks for providing both technical and moral support over the years. I would like to thank my undergraduate research assistants Stephanie Chu, Emily Bolyard, and Jamie Hufnagel for their hard work and also for keeping me company around the lab. Acknowledgments are also due to Dr. Maria Juenger and my future co-workers at ERDC for their support throughout my time in graduate school.

To my Texas Gymnastics family, I am so blessed to have such an amazing group of people in my life that I might have never met if we hadn't fallen in love with the same

crazy sport growing up. Being a part of this team for the past six years has been an amazing experience, and I am grateful to all of you for helping me find balance in my life. I see so many great things in each and every one of your futures, and I am looking forward to the lifelong friendships we will share.

Most importantly, I must thank my amazing family for their steadfast support, love, and encouragement. Mom and Dad, I cannot thank you enough for raising me to be an independent thinker and instilling the traits of ambition and perseverance in me from a young age. You always said I could do anything I set my mind to, even when I couldn't see it. Luke, Matt, and Heather, thank you for your constant support, for always making me laugh, and for reminding me not to take life too seriously. I love all of you with all my heart, and I am so lucky to call you my family.

Toward the Development of Robust Self-Healing Concrete Using Vegetative Microorganisms

Sarah Lynn Williams, M.S.E.

The University of Texas at Austin, 2015

Supervisors: Raissa Ferron; Mary Jo Kirisits

Robust self-healing concrete, which requires less maintenance and repair throughout its service life than ordinary concrete, can be used for the development of sustainable infrastructure. Li and Herbert [1] stated that a true robust self-healing concrete should meet six critical robustness criteria; the self-healing mechanism should

1. possess a *long shelf life* comparable to the service life of the structure;
2. be *pervasive* throughout the material;
3. exhibit good *quality* as indicated by the percentage of recovery provided;
4. be *reliable*;
5. be *versatile* in various environmental conditions;
6. be *repeatable* over the service life of the structure;

Although many approaches can be used to promote self-healing in cement-based materials, use of biomineralization (the process by which organisms stimulate the formation of minerals) for this purpose has generated considerable interest. Previous research on biomineralization, specifically microbial-induced calcium carbonate precipitation, suggested that this process can improve durability and remediate cracks in concrete.

This thesis presents the results of a multifaceted research program undertaken to evaluate the robustness of microbial concrete containing vegetative *Sporosarcina pasteurii*. Specifically, the criteria of *versatility* and *quality* were assessed. *Versatility* was evaluated by examining the influence of environmental factors on the polymorph selection process of calcium carbonate precipitated due to the activity of *S. pasteurii*, and it was determined that calcium concentration and overall ionic strength impacted morphology as did pH and substrate mineralogy. Another aspect of *versatility* that was addressed was the ability of vegetative *S. pasteurii* to remain viable and metabolically active when subjected to harsh conditions that might occur inside concrete including heat, high pH, and nutrient depletion.

Quality was assessed by comparing properties of biogenic calcium carbonate and synthetic calcium carbonate, and it was determined that the former exhibited greater kinetic and thermodynamic stability than the latter. *Quality* was further examined by determining the ability of biomineralization to heal flexural cracks in mortar and provide strength recovery. Finally, the chemical constituents of the growth medium for *S. pasteurii* were optimized to mitigate severe retardation in cement hydration kinetics that has been observed when vegetative bacteria suspended in growth medium are added to cement, which improved the feasibility of microbial concrete.

Table of Contents

List of Tables

List of Figures

Chapter 1: Introduction

Over the past half-century, society has become more aware of dwindling natural resources and the harmful effects of environmental pollution [2]. Increased awareness of these issues has sparked newfound interest in developing ecofriendly technologies, and implementation of stricter environmental regulations has prompted product and process redesign to include greener materials, systems for life cycle management, and recycling or reuse [3]. "Biomimetics," a relatively new scientific field concerned with understanding and unlocking the secrets of nature, has been identified as an important part of this effort [4]. Although humans have made incredible scientific advancements over the past century, our understanding of nature is still considerably lacking. In particular, the mechanisms of many biological processes continue to elude us, which could be attributed to the fact that these processes often display high levels of complexity. Thus, biomimetics researchers seek to emulate natural models, systems, and processes to solve human problems, and they aim to develop systems that more closely mimic nature.

The concrete industry, and by extension the portland cement industry, is no exception to this newfound desire to go green. Concrete is the world's most widely used construction material with over six billion tons produced on an annual basis [5], and production of portland cement accounts for 5-7% of global anthropogenic CO_2 emissions due to the decarbonation of limestone during clinker production and burning of fossil fuels to heat the kiln reactors [6-11]. Thus, significant research efforts are aimed at developing more ecofriendly cement and concrete technologies, and recent research in this area has produced many innovative processes that have the potential to effect real change. As stated above, a major goal of biomimetics research is to develop systems and products that more closely mimic nature. Interestingly, the concrete industry has already began the journey to

embracing the laws of nature. These basic laws, as defined by Benyus [12], are listed below along with examples of how green trends in concrete are working to embody each law:

1. *Nature runs on sunlight*: Solar thermal reactors have been examined to replace fossil fuel heat sources for clinker production [13], and researchers at The George Washington University have developed a new type of cement that uses solar power and molten salt chemistry to decarbonate $CaCO_3$ without any CO_2 production [14].
2. *Nature uses only the energy it needs*: The widespread implementation of preheater and precalciners in cement plants has substantially reduced energy consumption during cement production [15].
3. *Nature fits form to function*: Concrete originates in a flowable, deformable state and ultimately stiffens to become rigid and durable; thus, its shape can be customized to meet the function for which it is intended. For example, the shape of buried concrete arches can be optimized using numerical modeling to reduce bending and flexural stresses [16, 17].
4. *Nature recycles everything*: Recycled concrete aggregates have recently generated a lot of interest [18-23], and the development of a carbon-negative, sustainable concrete that recovers CO_2 over its lifetime has shown promise in initial studies [24]. Use of waste fuel sources, such as rubber tires, medical waste, municipal sewage, agricultural waste, for clinker production also has received attention for the dual benefit of eliminating waste substances that would otherwise go to landfill and reducing use of fossil fuel sources [25-27].
5. *Nature rewards cooperation*: Supplementary cementing materials (SCMs) are increasingly being used in industry for technical, environmental, and economic benefits [28, 29]. These materials work in cooperation with ordinary cement to form hydrated phases through either hydraulic or pozzolanic activity.

6. *Nature banks on diversity:* The mineralogy and chemical composition of cementitious materials, filler materials, and aggregates used in concrete are very diverse, and this variation contributes to the great degree customizability and diversity in concrete. Critical characteristics of concrete such as density and compressive strength are heavily influenced by the mechanical, physical, and chemical properties of the aggregates [30-32] and the chemical composition of cement [33].
7. *Nature demands local expertise*: Responsible, local sourcing of materials has long been a priority of the concrete industry for economic and environmental benefits. The concrete industry was the first to link its sustainable construction strategy to the responsible sourcing standard developed by the Building Research Establishment (BRE), BES 6001 – "Framework Standard for the Responsible Sourcing of Construction Products" in the U.K. [34, 35].
8. *Nature curbs excesses from within:* The reuse of waste wash water, which is produced in ready-mixed concrete plants, in mixing water for new concrete and mortars has been investigated as a means to conserve water and eliminate disposal of this high pH liquid that is considered hazardous by the EPA [36, 37].
9. *Nature taps the power of limits*: The concrete industry has proven its creativity through the development of new technologies such as self-consolidating concrete (SCC), ultra-high performance concrete (UHPC), and geopolymer concrete. SCC can be placed purely by means of its self-weight, eliminating the need for mechanical vibration [38]. UHPC possesses excellent mechanical properties that have enabled optimization of structural elements, and its enhanced durability can extend design life [39]. Geopolymer concrete is produced through the chemical

action of inorganic materials, such as fly ash, without the use of portland cement [40].

Considering this list of examples, which is by no means exhaustive, the concrete industry has made great progress in recent years towards reducing its environmental footprint. Another approach that could accomplish this goal while simultaneously providing performance-related benefits in concrete is the creation of a biomimetic material that contains living microorganisms inside the bulk matrix [41]. Certain microorganisms can induce biomineralization (the process by which organisms stimulate the formation of minerals) of calcium carbonate [42, 43], and this can lead to a reduction of permeability [44, 45] and/or sealing of cracks [46] in concrete. Further, the microorganisms might be able to survive and remain metabolically active inside the concrete over time such that when a crack occurs, the microorganisms could autogenously seal the crack with biogenic calcium carbonate [1, 47-51]. This bacterial, self-healing concrete is biomimetic since it takes inspiration from the process by which a bone heals itself when cracked [52].

1.1 RESEARCH SCOPE

Previous studies have indicated that biomineralization could be used to improve durability [53, 44] and compressive strength [54-56] of portland cement-based materials as well as to remediate cracks [44, 46]. Although these studies show great promise, some key questions remain unanswered. The majority of these concerns are related to the feasibility and scalability of microbial concrete (concrete containing microorganisms) systems, which also is related to the robustness. Microbial concrete studies in the literature have hitherto consisted almost exclusively of small batch mortar mixes conducted in a controlled laboratory setting. Although this controlled environment is useful in initial research, it is

not realistic for field use of microbial concrete where the temperature, humidity, and available curing conditions might vary considerably.

Another factor that currently prohibits the scalability of microbial concrete is cost. Silva et al. [57] estimated that the cost of concrete at an industrial scale could be increased from 60-75 €/m^3 (approximately \$50-62/yd^3) for ordinary concrete to 5760 €/m^3 (approximately \$4787/yd^3) for concrete with a bio-based additive consisting of encapsulated endospores (metabolically dormant microorganisms) that are added before casting. This sharp increase was primarily attributed to the necessity of aseptic laboratory conditions needed to produce endospores, labor, and the cost of encapsulating endospores [57]. As such, it is clear that a more cost-effective bio-based additive is needed for MICCP to be implemented at the field-scale.

The following items were addressed in this research, and together they constitute the scope of this thesis:

- Thermodynamic stability and mechanical strength have been reported to vary considerably among the polymorphs of calcium carbonate [58, 59], and factors influencing the morphology of calcium carbonate precipitated by microorganisms are not well understood [60]. To improve this understanding, the influence of pH, dissolved calcium concentration and ionic strength, and substrate mineralogy on the polymorph selection process was examined (Chapter 4).
- Biominerals often have considerably different structures and properties as compared to their synthetic counterparts [61-64]. The stability of biogenic calcium carbonate was investigated by comparing dissolution kinetics, thermodynamic solubility, and morphology of biogenic calcium carbonate and abiogenic calcium carbonate (Chapter 5).

- Metabolic activity and surface charge of bacterial cells are believed to have considerable influence on the biomineralization process. However, it is currently unclear how these parameters are affected by environmental conditions that might occur in concrete (e.g., high pH, lack of nutrients, heat generated from cement hydration). Thus, the effects of these conditions on metabolic activity and surface charge of bacteria were investigated (Chapter 6).
- The incorporation of microorganisms for biomineralization has been shown to benefit concrete in numerous ways, but some undesirable effects have been observed such as the retardation of cement hydration kinetics [47, 54]. This delay in hydration is undesirable because it could correspond to longer construction times and increased costs [65]. Thus, the chemical constituents of the microbial growth medium were optimized to mitigate retardation (Chapter 7).
- It has been recognized that biomineralization in cement-based materials can seal surface cracks [46, 47, 51, 66], but strength recovery has not been fully addressed in the literature. The ability of biomineralization by bacteria in cracked concrete to recover strength, and therefore restore structural integrity, was assessed (Chapter 8).

This thesis addresses the aforementioned concerns and thus provides useful information about the robustness, feasibility, and scalability of microbial concrete.

Chapter 2: Literature Review

2.1 BIOMIMETICS AND BIOMINERALIZATION

Natural, biological processes have been harnessed to produce materials for human consumption since the early days of civilization [4]. These processes have undergone continuous evolution over hundreds of millions of years to meet the demands of life, and this fine-tuning has enabled them to reach extraordinary degrees of intricacy that have been largely unattainable in man-made systems [67]. Furthermore, biological processes are often cost-effective, environmentally-friendly, and simple to induce [4].

Biomimetics, an interdisciplinary field uniting concepts from biology, nanotechnology, chemistry, and materials science, has received interest in recent years as the desire to understand and exploit biological processes has grown [68]. Between 1985 and 2005, the number of U.S. patents with titles containing the word "biomimetic" or "bioinspired" increased by a factor of 93 as compared to a 2.7 times rise in the total number of patents [69]. This sharp increase could be attributed to a number of benefits associated with bioinspired design, such as the possibility of developing safer, more environmentally-friendly chemicals. Many industrial chemicals possess characteristics that are harmful to humans and the environment. Biomimicry has been identified as a promising approach to alleviate these concerns, and considerable research efforts are aimed at designing biologically safe, ecologically sustainable substances by mimicking processes that organisms use to make materials [70].

Although biomimetics has only recently gained recognition as an area for scientific research, biomimicry has been used in design processes throughout history [63, 71-74]. In fact, many prevalent items and technologies in modern society were inspired from biology. Leonardo da Vinci studied the structure and anatomy of birds to create sketches of

proposed “human flying machines,” and the Wright brothers used observations of pigeons in flight to create the first airplane in 1903 [75]. Similarly, the shape of a kingfisher’s beak was used to derive the ideal shape for the Shinkansen bullet train to minimize air resistance [76]. Humpback whale fins have inspired the creation of more efficient wind turbines, and Velcro was created by imitation of hook-ended burr needles [77]. Even the texture of lotus leaves, which enables rainwater to roll across the surface and remove dirt, was used as inspiration to create self-cleaning paint [78].

Another potential application of biomimicry resides in the realm of electrical engineering. It has been postulated that the “hardware and software” of biological systems could observed to develop more sophisticated optimization algorithms and feedback control systems. This bioinspiration, obtained from observations of the functional operation of biological systems, could lead to the injection of new ideas, techniques, and perspectives that have the potential to extend current levels of sophistication in automation [79]. Interestingly, biomimicry has even received interest from the graphic design community as a method to develop sustainable, timeless design solutions [80].

Human beings can learn a lot from the elegance and resiliency of nature, and researchers have recently turned to nature for inspiration to improve architecture and structural design. The closed loop systems for water, oxygen, and food found in oak trees have been used to derive sustainable architecture [81], and the geometric configurations of a beehive were used as inspiration for design of a hexagonal steel moment frame [82]. Additionally, the emulation of spatial relationships exhibited between coral reefs and their surroundings was proposed as a possible method to improve buffering effectiveness of shoreline stabilization structures [83].

Motivation to replicate biological processes also has been generated by the fact that many biogenic minerals possess excellent mechanical properties [61, 62, 64, 68], which is

partly attributable to their hierarchical organization at the nano-, micro-, and meso- scale [74]. Accordingly, a great deal of interest is focused on understanding and inducing biomineralization processes, where organisms stimulate the formation of minerals. Chen et al. [83] reported that coral skeletal material, which is composed of calcium carbonate, exhibited greater porosity but similar strength as compared to common man-made infrastructure materials. According to the authors, this suggested that biomineralization could lead to the development of structural materials with higher strength-to-weight ratios. Over 60 different biological minerals have been observed in nature, and they typically contain essential elements such as H, C, O, Mg, Si, P, Ca, Mn, and Fe. Calcium phosphate and calcium carbonate minerals are some of the most widespread biominerals because they are stable in many biological environments due to their high lattice energies and low solubilities [62].

2.2 MICROBIAL-INDUCED CALCIUM CARBONATE PRECIPITATION (MICCP)

Just as there are over 60 unique biominerals, there are countless different biomineralization processes that organisms use to create them. One of these processes, microbial-induced calcium carbonate precipitation (MICCP), has been identified as a natural method to enhance properties of porous materials, particularly construction materials. MICCP can be achieved through numerous mechanisms, and MICCP by urea hydrolysis is one of the most common approaches used by researchers because ureolytic bacteria are widespread in the environment [84].

2.2.1 Chemical reactions in MICCP by urea hydrolysis

MICCP by urea hydrolysis is triggered by microorganisms that possess the urease enzyme. Urease catalyzes the hydrolysis of urea, which results in the production of

ammonia and carbon dioxide (Reaction 2.1). These products participate in acid-base reactions (Reactions 2.2-2.4), which result in an increase in pH that induces calcium carbonate precipitation if dissolved calcium is present (Reaction 2.5) [42, 85, 86].

$$CO(NH_2)_2 + H_2O \rightarrow 2NH_3 + CO_2 \quad (2.1)$$

$$NH_4^+ \leftrightarrow NH_3 + H^+ \quad pK_a = 9.3 \quad (2.2)$$

$$H_2CO_3^* \leftrightarrow HCO_3^- + H^+ \quad pK_a = 6.3 \quad (2.3)$$

$$HCO_3^- \leftrightarrow CO_3^{2-} + H^+ \quad pK_a = 10.3 \quad (2.4)$$

$$CaCO_3 \leftrightarrow CO_3^{2-} + Ca^{2+} \quad K_{sp} = 3.8 \times 10^{-9} \quad (2.5)$$

2.2.2 MICCP as a soil improvement technique

Early studies on MICCP in construction applications focused on improving soil properties. Soil often needs to be stabilized to enhance its cohesion and durability, which is typically achieved by injecting synthetic materials into the soil to act as a binding agent between particles. However, these synthetic materials can be costly, difficult to uniformly distribute throughout the soil, and might introduce hazardous elements to the system [87]. MICCP is a natural, alternative method to stabilize soil, and has been shown to substantially increase strength and stiffness [88].

MICCP can be employed to enhance the suitability of soil for construction practices using the mechanisms of bioclogging and biocementation [89, 90]. Bioclogging refers to the production of inorganic, pore-filling materials by bacteria. These materials can plug the voids between grains of soil, which leads to a reduction in the porosity and hydraulic conductivity of soil systems. Biocementation is similar to bioclogging in methodology, but it differs in the fact that it leads to the production of a particle-binding material that can improve the cohesion and shear strength of the soil as opposed to a material that simply fills the pores of the soil system. Initial investigations in this area focused almost

exclusively on bioclogging, but recent studies have suggested that biocementation can be achieved using MICCP [89-95] in soil. Hui et al. [91, 95] reported that permeability, stiffness, compressive strength, shear strength, and volumetric behavior were improved in loose soil particles due to the precipitation of microorganism-based cementitious material, and similar findings were reported by Soon et al. [96] and Chu et al. [90]. Thus, it is apparent that MICCP is a good option to improve strength and durability of soil systems.

2.2.3 Preservation of historical architecture using MICCP

In addition to acting as a stabilization agent for soil, MICCP has shown great promise as a natural preservation agent for historical architecture. Biodeposition of carbonate layers on the surface of monuments and buildings could be an effective repair and/or restoration technique, particularly for structures comprised of porous marble or limestone [97]. Further, use of microorganisms for remediation provides conservators with an option that does not require the use of synthetic materials [98]. A surface skin is often produced by these synthetic repair materials that can deteriorate over time and peel off, requiring frequent maintenance and damaging the aesthetic quality of the structure [99]. Synthetic resins, often silane or polysiloxane, used for this application also require large quantities of organic solvents, which contribute to environmental pollution [98]. Other possible disadvantages of conventional repair techniques include a change in color due to the application of foreign substances on the surface, an adverse impact on the movement of salts within the stone structure, and removal of excessive amounts of the original surface [100].

Initial studies on restoration using bacteria have produced promising results. Dick et al. [101] reported a decrease in water absorption for corroded limestone treated with *Lysinibacillus sphaericus* (previously *Bacillus sphaericus*) or *Bacillus lentus*, which was

attributed deposition of a dense layer of calcium carbonate on the damaged limestone surface. Similarly, Li and Qu [97] observed a 22.2% decrease in porosity of marble due to biodeposition of calcium carbonate by *Sporosarcina pasteurii*, and it was stated that the calcium carbonate crystals were strongly attached to the marble substrate. Rodriguez-Navarro et al. [102] determined that *Myxococcus xanthus* was able to produce a carbonate cement layer on the surface of ornamental stone, and sonication tests demonstrated that the newly formed calcium carbonate crystals were strongly attached to the substrate due to epitaxial growth on pre-existing crystals.

Despite these encouraging studies, some researchers have expressed concerns about using MICCP as a repair method. Tiano et al. [103] suggested that any decrease in porosity observed due to the bacteria in these systems is mostly due to physical obstruction of pores rather than the presence of a new, stable precipitate. It also was noted that potential side effects of bacterial treatment must be considered such as the formation of stained patches due to development of fungi (related to the presence of organic nutrients) and the appearance of unwanted products might result from chemical reactions between the stone minerals and by-products of the bacteria [103]. However, although this bio-based technique might not reach the same level of repair effectiveness as synthetic polymeric materials, it could be useful to softly stabilize objects of high aesthetic and artistic value where minimal change in the chemistry of the structure is desired [104]. Nevertheless, there is certainly a need for mild, natural treatments for historical architecture and further research is needed to develop a more thorough understanding of the advantages and disadvantages of bio-based treatments in this regard.

2.2.4 MICCP in cement-based materials

Perhaps the most widely studied application of biogenic calcium carbonate precipitation by microorganisms in recent years is the use of MICCP to improve of properties of portland cement-based systems. MICCP has been shown to improve durability of portland cement concrete by causing a reduction in permeability [44, 45, 53, 105]. Crack remediation [44, 46] and corrosion prevention of steel reinforcement [106] also have been identified as prospective applications of this biomineralization process in concrete. However, the strongest motivation to incorporate MICCP in cement-based systems might be the need for a self-healing material. Formation of microscopic and macroscopic cracks (due to shrinkage, mechanical loads, etc.) is an inevitable occurrence in concrete systems, and these cracks can contribute to severe reductions in strength and durability over the service life of a concrete structure. Bioinspired, self-healing, cement-based materials have received great interest because they could allow for the precipitation of biogenic calcium carbonate by microorganisms embedded in the bulk matrix to seal these cracks [1, 47-50]. (A detailed review of the existing literature on bacterial self-healing concrete is provided in Section 2.6.)

MICCP can be achieved in concrete by either externally or internally introducing microorganisms to the system, and many different methods of inoculation have been used. External incorporation of microorganisms typically involves the application of aqueous bacterial cultures onto concrete as a surface treatment to improve durability [53, 105, 107] or as a repair agent to remediate cracks [46]. Contrastingly, internal inoculation involves incorporating microorganisms to concrete during the mixing process such that they are truly embedded in the cement paste matrix. Perhaps the simplest approach to internal inoculation that has been used in the literature is to suspend the microorganisms in the mixing water of the cement-based material [49, 50, 55, 56]. However, it is also possible to

replace the mixing water with an aqueous bacterial culture comprised of bacteria and growth medium [44, 45, 52, 54, 108, 109], and this method could be considered preferable to suspending bacteria in the mixing water since the cells do not need to be harvested and washed prior to mixing. Natural encapsulation, which involves adding bacterial cells in an endospore (i.e., metabolically inactive or dormant) state [110], is another commonly used approach because endospores are more resilient to harsh conditions than are vegetative (i.e., metabolically active) cells [111]. Finally, a synthetic encapsulation approach, which involves encapsulating or immobilizing cells in a protective carrier, can be employed to provide cells with protection from the harsh environmental conditions that might occur in concrete [47, 50, 112-114].

2.3 CALCIUM CARBONATE MORPOHOLOGY

Biominerals are noted for having unique morphologies that are greatly influenced by the biological processes that stimulate their formation [60]. There are six known polymorphs of calcium carbonate: calcite, aragonite, vaterite, monohydrocalcite, ikaite and amorphous calcium carbonate (ACC) [62]. Among these polymorphs, calcite and aragonite are more thermodynamically stable (less soluble at ambient conditions) than are vaterite and monohydrocalcite; ikaite and ACC are rarely observed in nature. Vaterite and calcite are most commonly observed in biomineralization applications [42, 115].

Despite extensive studies on the mechanism of biogenic calcium carbonate precipitation induced by microorganisms, the polymorph selection process in these systems is not well understood [60]. However, some studies have identified factors that might influence the process. Perhaps the most intuitive of these factors is the type of microorganism used [116-118]; additionally, the rate of microbial growth and/ or urease activity might influence polymorph selection because they directly control the rate of

supply of carbonate for precipitation [116, 119]. Sondi and Salopek-Sondi [120] suggested that the amino acid sequences found in urease might influence the morphology of the precipitate. Kawaguchi and Decho [121] proposed that proteins in the extracellular polymeric substances (EPS) of *Bacillus firmus* and *Lysinibacillus sphaericus* influence the calcium carbonate polymorph selection process, and Lian et al. [122] suggested that the presence of *Bacillus megaterium* cells promoted calcite precipitation while the presence of their EPS promoted vaterite precipitation.

Variation in the growth medium composition and the type of calcium source used (if an exogenous calcium source is added) also have been identified as key factors affecting the morphology of biogenic calcium carbonate [53, 102, 105, 123]. Since the chemical composition of the growth medium has been shown to influence polymorph selection, it would be logical to test if the substrate material might also be of influence; Rodriguez-Navarro et al. [115] demonstrated that the morphology of calcium carbonate precipitated due to *Myxoccocus xanthus* was highly influenced by the mineralogy of the substrate. In this work, calcitic substrates promoted calcite formation while vaterite formation was promoted by siliceous substrates. According to Rodriguez-Navarro et al. [115], pH might be of critical influence to this polymorph selection process, and specifically vaterite formation might be more favorable than calcite in high pH environments.

Understanding the many factors that affect the polymorph selection process of biogenic calcium carbonate in construction materials is important because properties such as solubility [58, 124] and stability [59] of the precipitate are heavily influenced by its crystal structure. Additionally, bonding characteristics of the precipitate to the substrate might be affected by the morphology [52, 115], and strong bonding behavior is imperative in self-healing applications to ensure that the resulting composite material (composed of the precipitate and the substrate) is durable and tough [52]. Although these initial studies

have provided a useful indication of what factors and conditions might affect morphology, it is clear that further research is needed to elucidate the mechanism of the polymorph selection process such that the morphology of biogenic calcium carbonate precipitated by microorganisms can be confidently predicted or controlled in construction materials.

2.4 UREASE ACTIVITY AND ZETA POTENTIAL OF *S. PASTEURII*

S. pasteurii is the most common microorganism used in biomineralization applications [52] because of its alkaliphilic nature and urease enzyme activity. It is well-known that urease activity is a critical parameter influencing ureolytic-driven MICCP since it controls the rate of carbonate production. The urease activity of *S. pasteurii* has been examined in numerous previous studies, and these studies are in agreement that the urease activity exhibited by *S. pasteurii* is considerable [42, 43, 84, 109, 125-129]. Thus, this bacterium is a good candidate for MICCP by the mechanism of urea hydrolysis.

In addition to urease activity, it has been stated that bacterial surface charge could be of substantial importance for MICCP [44, 45, 101, 109, 130]. This surface charge can be approximated using zeta potential [131], which measures the electrokinetic potential in a colloidal dispersion. Although zeta potential has not been previously reported for *S. pasteurii*, it has been assumed in several studies that *S. pasteurii* has a negative net surface charge because most bacterial cells possess a negative zeta potential in neutral and basic environments [132-138]. This was demonstrated in work by Soni et al. [139] where zeta potential was measured for selected bacteria in pH 8.4 drinking water when exposed to different nutrient levels and physiological states. The zeta potential of *Escherichia coli*, green fluorescence protein (GFP)-labeled *Escherichia coli*, *Salmonella* Newport, and *Pseudomonas aeruginosa* were reported as ranging from -34.1 mV to -47.8 mV, -43.7 mV to -45.9 mV, -3.9 mV to -16.6 mV, and -40.0 mV to -46.9 mV, respectively [139].

Similarly, Dick et al. [101] reported zeta potentials at pH 9 ranging from -8.87 mV to -27.78 for five different strains of *Lysinibacillus sphaericus*, and a zeta potential of -13.53 mV for *Bacillus lentus*.

It is possible that this negative charge could attract positively charged calcium ions and induce $CaCO_3$ precipitation on the bacterial cell walls with the bacteria acting as sites for heterogeneous nucleation [42, 46, 86, 109, 116, 122, 140, 141]. Stocks-Fischer et al. [42] observed this nucleation effect in microbial-plugged sand columns using scanning electron microscopy (SEM). Rod-shaped *S. pasteurii* (previously *Bacillus pasteurii*) appeared to be embedded in biogenic calcite crystals, and it was concluded that the intact bacteria acted as nucleation sites for biological precipitation of calcium carbonate. Similarly, Dhami et al. [116] observed bacterial imprints on the surface of carbonate crystals, which suggested that the bacteria might serve as nucleation sites. The precipitation of minerals along the cell wall, or epicellular mineralization, is not only a common occurrence, but a distinctive feature of biologically induced mineralization [62]. Further, the presence of organisms as platforms for precipitation lowers the energy barrier for crystallization, which allows biominerals to form more rapidly, abundantly, and efficiently [4].

2.5 INFLUENCE OF NUTRIENT MEDIUM AND MICROORGANISMS ON CEMENT HYDRATION KINETICS

MICCP has been shown to benefit cement-based systems in numerous ways, but a few detrimental effects have been observed as well. As discussed in Section 2.2.4, one way to introduce microorganisms to concrete is by replacing the mixing water with an aqueous bacterial culture comprised of microorganisms in their nutrient medium. While this inoculation method is the simplest and most cost-effective way to introduce microorganisms to the system, it has been shown to cause severe retardation of cement

hydration kinetics [52]. Specifically, incorporation of *S. pasteurii* in medium containing yeast extract has been shown to retard hydration [54]. Microbial media are designed to provide all of the chemical requirements for cell growth including free water, essential minerals, growth factors, and sources of carbon and nitrogen [142]. The optimal medium recommended by the American Type Culture Collection (ATCC) for 6453 *S. pasteurii* contains 0.13 M Tris base (pH 9), 20 g/L yeast extract (2%), and 10 g/L ammonium sulfate (1%). Urea can be substituted for ammonium sulfate to yield urease activity for MICCP (Reaction 2.1). Tris base controls the pH while yeast extract and ammonium sulfate (or urea) serve as the primary carbon and nitrogen sources for bacterial growth, respectively. While Tris base and urea have been shown to have no adverse effect on cement hydration, a substantial extension of the induction period during hydration has been observed when yeast extract, which might contain sugars and other carbohydrates that are known to be effective retarders, is added to cement paste [47, 54].

Many researchers have added an exogenous calcium source the system to enhance $CaCO_3$ precipitation, and calcium chloride ($CaCl_2$) is commonly used in the literature for this purpose. $CaCl_2$ is a known accelerator [143] and it could be used to counteract the retardation caused by yeast extract, but it is also known to cause severe corrosion of steel reinforcement in reinforced concrete [144]. Thus, this approach is not practical for field use. Calcium nitrate ($Ca(NO_3)_2$) is another accelerator that could be used for the dual purpose of providing additional calcium and counteracting retardation caused by yeast extract, and it does not cause corrosion [145]. However, research has shown that MICCP can occur in concrete using only the intrinsic calcium present in the pore solution (no external calcium source added) [52, 54]. Since a main goal of this research program is to simplify microbial concrete systems such that the overall cost can be reduced, a more effective strategy would be optimize the chemicals that are already present in the system

(growth medium constituents) to mitigate retardation and to avoid the addition of more chemicals (calcium sources and/or accelerators) which will increase cost and complexity.

In general, extension of the induction period corresponds to longer setting times, which could result in longer construction times and increased costs [65]. As such, this is a significant barrier that must be overcome for microbial concrete to be feasible. Although the severe retardation of hydration kinetics observed when vegetative bacterial cultures are added to cement poses a significant threat to the use of microbial concrete in the construction industry, mitigation strategies have not been studied. It is imperative that a solution is identified to mitigate this concern before microbial concrete can be scaled up for widespread use.

2.6 CRACK REMEDIATION IN CEMENT-BASED MATERIALS

Perhaps the most compelling prospective application of MICCP in concrete is the use of biogenic calcium carbonate to seal cracks, either as a repair material or through biologically-induced, autogenous self-healing. Earlier studies on crack-sealing in construction materials focused on the use of bacteria as an external repair material for cracks. For instance, Ramachandran et al. [66] proposed a system where cracks were sealed by filling the cracks with sand, *S. pasteurii* cells, and a solution containing urea and calcium chloride. Similarly, Bang et al. [146] filled glass beads (to protect cells from harsh conditions inside concrete) with *S. pasteurii* cells and injected them into mortar cracks with nutrient medium and calcium chloride. The mortar specimens were monitored for 28 days, and results demonstrated that compressive strength and stiffness increased with time for the samples treated with bacteria as compared to control samples. Van Tittelboom et al. [46] conducted a similar experiment where *L. sphaericus* cells, which were incorporated in a silica gel matrix, were applied to cracked mortar specimens with various calcium

sources and nutrients. It was determined via ultrasonic pulse velocity, visual observations, and water permeability tests that these immobilized bacteria could promote crack healing comparable to that promoted by conventional repair materials.

More recently, interest has shifted towards utilizing MICCP to develop a concrete that is capable of self-healing through autogenous precipitation of calcium carbonate by bacteria embedded in the concrete [1, 48]. Jonkers et al. [50] inoculated *Bacillus cohnii* endospores to cement stone to induce calcium carbonate precipitation with favorable results, and later Wiktor and Jonkers [51] improved the efficacy of this process by using *B. cohnii* endospores to impregnate lightweight coarse aggregates inside concrete which provided additional protection for the microorganisms. Wang et al. [47] incorporated microencapsulated *L. sphaericus* endospores in concrete and observed that the bacterial specimens were able to autogenously seal cracks up to 970 μm, while non-bacterial specimens could only seal cracks up to 250 μm. Additionally, the water permeability of bacterial specimens was approximately 10 times lower than the water permeability of non-bacterial specimens, indicating substantial sealing of cracks in the bacterial specimens.

These studies have produced encouraging results, but more research is needed to develop a reliable, cost-effective, and scalable model for self-healing concrete [57]. Additionally, one important question that remains unanswered in the literature is whether strength recovery can be achieved in bio-based, self-healing concrete. Most previous studies have focused on the self-sealing of cracks as indicated by visual observation, ultrasonic test methods, or water permeability. While the sealing of cracks in concrete is certainly beneficial for durability aspects, a true self-healing concrete should restore structural integrity by providing strength recovery. This strength recovery is dependent upon the mechanical properties of the biogenic calcium carbonate precipitate as well as the

bonding strength of the precipitate to the concrete substrate. Neither of these properties have been fully addressed in the literature, and they are critical areas for future research.

Chapter 3: Microorganism Selection and Growth

3.1 INTRODUCTION

This chapter provides an overview of the microorganism and medium selection process, microbial growth, and metabolic activity during growth as indicated by microbial production of ammonia (NH_3). Monitoring the rate of NH_3 production in the microbial medium during growth provides insight about the metabolic condition of ureolytic bacteria because any substantial increase in NH_3 concentration is likely a direct result of urea hydrolysis catalyzed by the urease enzyme (Section 2.2.1).

3.2 MICROORGANISM SELECTION

Sporosarcina pasteurii, a common ureolytic soil bacterium, was selected to trigger microbial-induced calcium carbonate precipitation (MICCP) by urea hydrolysis in this work. Although many organisms are capable of inducing calcium carbonate precipitation, *S. pasteurii* was chosen because of its resiliency and urease activity. In microbial concrete, the selected bacterium should be able to survive extreme environmental conditions that might occur inside the concrete (e.g., high pH, heat generated by cement hydration, and lack of nutrients). *S. pasteurii* is alkaliphilic [43, 147, 148], meaning that it can resist a high pH environment. In addition, this bacterium can form endospores [149], which are more resistant to harsh conditions including heat and nutrient depletion than are vegetative cells. Finally, it has been reported that the urease activity of *S. pasteurii* is considerable (Section 2.4), which is critical for the production of carbonates in MICCP.

3.3 MICROORGANISM GROWTH

S. pasteurii was grown in a Urea-Yeast Extract (UYE) medium, which is a modified version of the growth medium recommended by the American Type Culture Collection

(ATCC). The medium was modified by replacing ammonium sulfate with urea on an equal mass basis, and the medium contained 15.75 g/L Tris base, 20 g/L yeast extract, and 10 g/L urea. UYE medium was prepared by dissolving Tris base in 1-liter distilled, deionized (DDI) water and adjusting the pH to 9 with hydrochloric acid. The Tris base solution was then divided into two equal aliquots; urea was added to one of these aliquots and yeast extract was added to the other. The mixtures were autoclaved separately per recommendation by ATCC. After sterilization, the solution containing urea and the solution containing the yeast extract were kept at 23°C and combined after cooling.

S. pasteurii cells were grown aerobically at 30°C with shaking. A representative growth profile, displayed in Figure 3.1, was obtained by monitoring the optical density at 600 nm (OD_{600}) for triplicate 100-mL bacterial cultures in 250-mL flasks for 24 hours using a BIO-TEK Synergy HT spectrophotometer (Winooski, VT, United States).

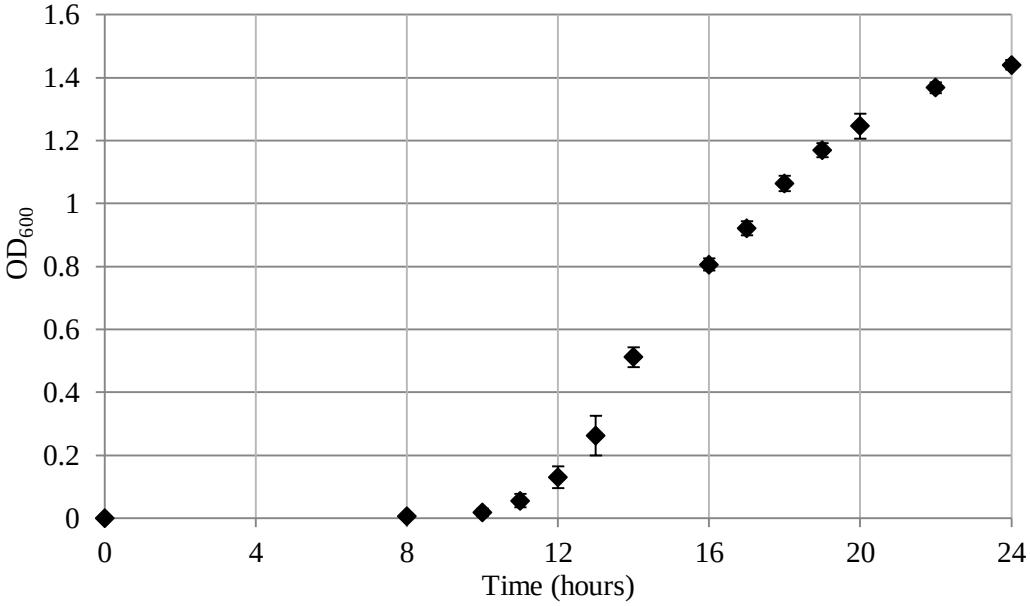

Figure 3.1: Growth curve for *S. pasteurii* (ATCC 6453) in UYE medium at 30°C with shaking. Error bars represent the standard deviation of triplicate cultures.

3.4 UREASE ACTIVITY DURING GROWTH

S. pasteurii is ureolytic, meaning it can catalyze the decomposition of urea into ammonia and carbon dioxide as described in Section 2.2.1. This is a critical step in the MICCP process. Thus, a relationship was established between NH_3 concentration and time, and this relationship was used to estimate the concentration of available carbonates in the culture. NH_3 concentration was monitored for triplicate 100-mL cultures in 250-mL flasks using a Thermo Scientific™ Orion™ High-Performance Ammonia Electrode (Waltham, MA, United States) for 24 hours. The relationship between NH_3 concentration and time is displayed in Figure 3.2. Because the UYE nutrient medium contained 10 g/L urea, or 167 mM urea, the maximum amount of NH_3 that could be produced in this culture (after all of the urea has been hydrolyzed) is 333 mM (Reaction 2.1, Section 2.2.1).

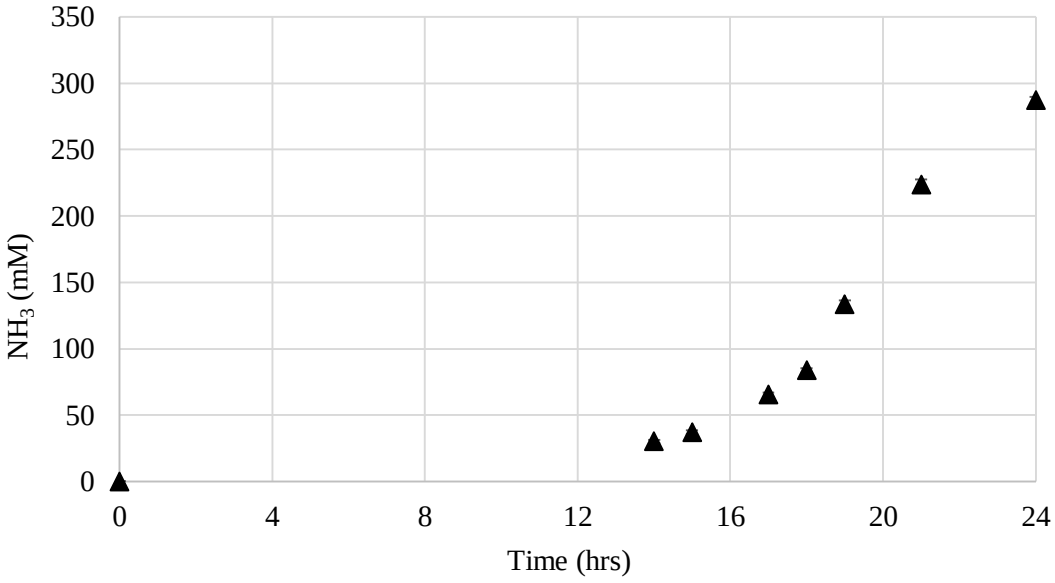

Figure 3.2: NH_3 concentration vs time for *S. pasteurii* (ATCC 6453) in UYE medium at 30°C with shaking. Error bars represent the standard deviation of triplicate cultures.

Chapter 4: Morphology of Calcium Carbonate Precipitated by *S. pasteurii*

4.1 INTRODUCTION

A critical parameter that can be used to characterize the stability of composite materials resulting from microbial-induced calcium carbonate precipitation (MICCP) is the morphology of the biogenic calcium carbonate precipitate. Thermodynamic stability and mechanical strength have been reported to range considerably among the polymorphs of calcium carbonate [58, 59], and factors affecting the polymorph selection process are not well understood. In particular, the effects of various environmental factors on the microorganism-induced precipitate must be examined further so that the morphology of this biogenic calcium carbonate can be predicted or controlled [60, 150]. Calcium carbonate has six known polymorphs: calcite, aragonite, vaterite, monohydrocalcite, ikaite and amorphous calcium carbonate (ACC) [62]. Among these, calcite and aragonite are more thermodynamically stable (less soluble at ambient conditions) than are vaterite and monohydrocalcite; ikaite and ACC are rarely observed in nature.

One key factor that might affect morphology in microbial concrete systems is the calcium ion concentration in the bacterial culture medium. Many researchers add exogenous calcium to the system to maximize precipitation of $CaCO_3$ [45, 146], while others rely only on the intrinsic calcium available in the pore solution [54]. Thus, the calcium concentration, and by extension ionic strength, can vary considerably in microbial concrete, which might impact the polymorph selection process [151]. This effect was observed in work by Evans [152], where it was found that the relative vaterite content increased as ionic strength increased in crystal growth solutions containing varying concentrations of K^+, Na^+, and NH_4^+. The pH also has been shown to influence the

morphology of calcium carbonate [151], and this effect could be important for biogenic calcium carbonate in concrete because it is a high pH environment.

Another factor that could impact the polymorph selection process is substrate mineralogy. While the chemical composition of cement paste is reasonably consistent, the mineralogy of concrete aggregates is rather diverse. Aggregate mineralogy, which can range from highly siliceous to highly calcitic, influences many properties of concrete including thermal expansion [153] and permeability [31], and recent work by Rodriguez-Navarro [115] suggested that it also might impact the morphology of biogenic calcium carbonate precipitated as a result of bacterial activity. In this study, it was reported that the morphology of microbial-induced calcium carbonate was strongly influenced by the chemical composition of the substrate to which it was attached and that siliceous substrates promoted vaterite formation while calcitic substrates promoted calcite formation [115]. Cement paste is calcitic, and will therefore likely promote precipitation of calcite. However, it is unclear how the use of siliceous aggregates in concrete will influence polymorph selection, and particularly whether the mineralogy of the calcitic cement paste matrix or the mineralogy of the siliceous aggregate will govern.

To address these gaps in our understanding of the polymorph selection process, the impact of [Ca^{+2}], substrate mineralogy, and pH on the morphology of microbial-induced calcium carbonate was examined in bacterial cultures, bacterial cement paste samples, and bacterial mortar samples using X-ray Diffraction (XRD).

4.2 MATERIALS AND METHODS

4.2.1 Microorganism and Medium

S. pasteurii was used in this study, and the microorganisms were cultured according to the procedure described in Section 3.3. UYE medium was used, and it contained Tris

base, urea, and yeast extract (Section 3.3). Tris base and urea do not contain calcium while yeast extract often contains a negligible amount of calcium. Sherwood [154] reported that calcium contents in yeast extract ranged from 0.14 - 0.21% by mass, and Abelovska et al. [155] determined that a 2% solution of yeast extract (the concentration used in UYE medium) contained only 0.0004 M of calcium.

4.2.2 Cement

A Texas Lehigh Type I/II (Buda, TX) portland cement was used in this study, and the mass composition of oxides, which was obtained using X-ray fluorescence, is presented in Table 4.1.

Table 4.1: Mass composition of oxides. LOI: Loss on ignition.

Oxides	**% (w/w) composition**
CaO	63.63
SiO_2	20.14
Al_2O_3	5.42
Fe_2O_3	2.47
MgO	1.32
SO_3	3.09
Na_2O	0.17
K_2O	0.95
LOI	2.82

4.2.3 Fine Aggregate

Mortar samples were prepared with three different types of fine aggregate: Colorado River sand, limestone sand, and silica sand. The aggregates were passed through a No. 4 sieve such that the particles were smaller than 4.75 mm. XRD was used to confirm the mineralogy of these sands, and the XRD patterns are displayed in Figure 4.1.

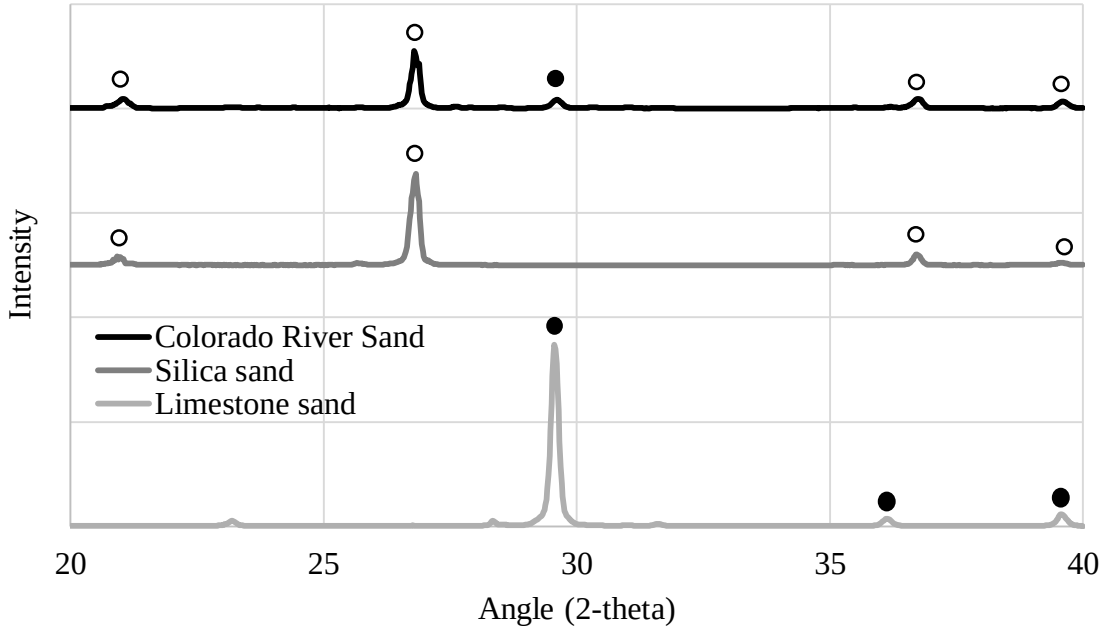

Figure 4.1: Mineralogy of fine aggregates determined by XRD. Curves are averages of triplicate samples; open circles represent SiO_2 peaks and solid circles represent calcite peaks.

4.2.4 Sample Preparation

The morphology of calcium carbonate precipitated due to *S. pasteurii* was examined in three different environments: bacterial cultures (suspended bacteria grown in a liquid nutrient medium), portland cement paste, and mortar. Table 4.2 summarizes the experimental conditions tested. As discussed in Section 4.2.1, UYE medium might already contain a small amount of calcium due to the presence of yeast extract in the medium. However, this was considered negligible since the added calcium dosage (0.03 M or 0.167 M) was always considerably greater than the intrinsic calcium present in the medium (~0.0004 M) [155].

Table 4.2: Summary of samples.

Sample Set	**Type**	**pH**	**[Ca^{+2}] Added**
Culture-9-LowCa	Bacterial culture	9	0.03 M
Culture-12-LowCa	Bacterial culture	12	0.03 M
Culture-9-HighCa	Bacterial culture	9	0.167 M
Culture-12-HighCa	Bacterial culture	12	0.167 M
Paste-Neat	Neat cement paste	-	0.03 M
Paste-Bac	Bacterial cement paste	-	0.03 M
Mortar-CRS-Neat	Neat mortar- Colorado river sand (CRS)	-	0.03 M
Mortar-CRS-Bac	Bacterial mortar- Colorado river sand (CRS)	-	0.03 M
Mortar-S-Neat	Neat mortar- Silica sand (S)	-	0.03 M
Mortar-S-Bac	Bacterial mortar- Silica sand (S)	-	0.03 M
Mortar-C-Neat	Neat mortar- Limestone sand (C)	-	0.03 M
Mortar-C-Bac	Bacterial mortar- Limestone sand (C)	-	0.03 M

Four types of bacterial culture experiments were prepared. For each set of experiments, cultures were grown in 100 mL UYE medium in 250-mL flasks. Culture-9-HighCa was prepared at pH 9 (recommended by the ATCC for *S. pasteurii* growth) with the addition of 0.167 M $CaCl_2$, which was added at the time of inoculation. As stated in Section 2.2.1, the urea concentration in UYE medium is 0.167 M, and *S. pasteurii* urease can hydrolyze this urea to produce carbonate. Thus, the concentration of 0.167 M of $CaCl_2$ was used to induce the maximum amount of $CaCO_3$ precipitation (Reactions 2.1-2.4). Culture-12-HighCa cultures was prepared at pH 12 (to simulate the alkalinity of cement paste pore solution) also with the addition of 0.167 M $CaCl_2$. The remaining cultures (Culture-9-LowCa and Culture-12-LowCa) were prepared with only 0.03 M $CaCl_2$ to simulate the amount of calcium available in fresh cement paste [156, 157].

In the bacterial culture experiments (Culture-9-HighCa, Culture-12-HighCa, Culture-9-LowCa, Culture-12-LowCa), pH and calcium ion concentration were varied. However, variation in calcium concentration also impacts ionic strength of the medium, which might also influence the polymorph selection process. Conductivity was measured

for UYE medium at pH 9 and pH 12 with calcium additions of 0 M, 0.03 M, and 0.167 M to assess this (Figure 4.2). Conductivity is often used to approximate the ionic strength of liquid media, and as conductivity increases so does ionic strength.

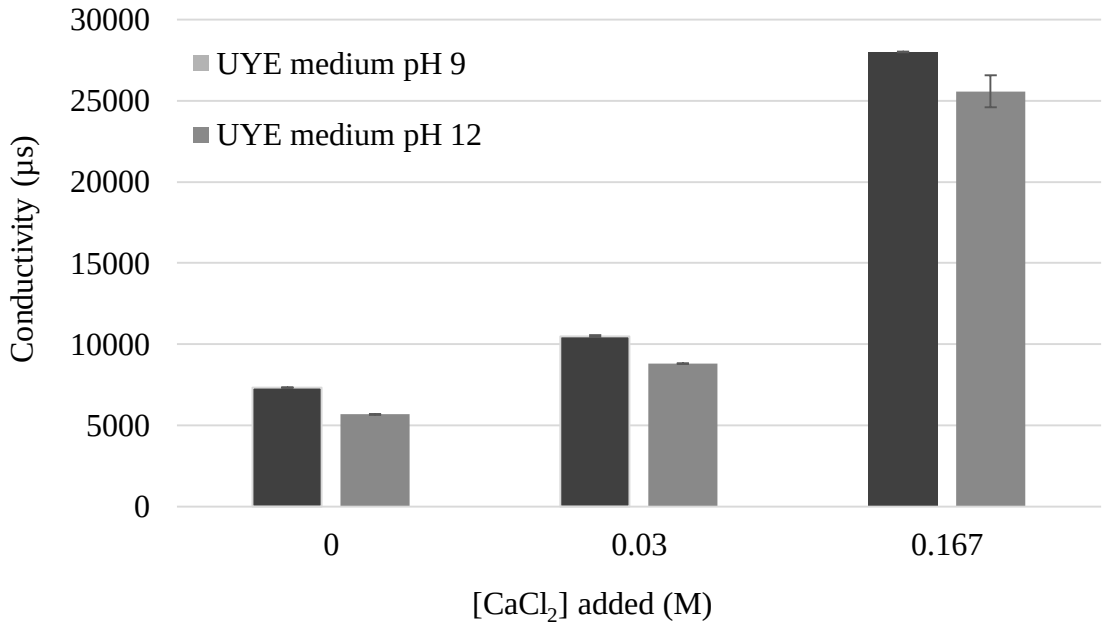

Figure 4.2: Conductivity of UYE medium at pH 9 and pH 12 with $CaCl_2$ additions of 0 M, 0.03 M, and 0.167M. Error bars represent the standard deviation of triplicate samples.

Cement paste samples were prepared by stirring 14 g of cement and 7 g of solution (distilled water for Paste-Neat and bacterial culture for Paste-Bac) by hand for 2 minutes; then the samples were cast into 3 x 3 cm cylindrical molds. The solution-to-cement ratio (s/c) for all pastes was 0.50 by mass. Both cement paste samples were prepared with the addition of 0.03 M $CaCl_2$, which was added during mixing. Mortar samples were prepared using the same procedure described for cement paste, but fine aggregate was added such that the ratio of cement to sand was 1:4. The s/c ratio was kept at 0.50.

4.2.5 XRD

XRD was performed using a Siemens Bruker X-ray Diffractometer (Madison, WI, United States) to determine the morphology of $CaCO_3$ precipitated in each sample. Generally, samples were placed and compacted into a sample holder, and analysis was conducted at angles from 20-60° 2θ with 6 seconds dwell time. The diffractometer was operated at 40 keV and 30 mA, with a step size of 0.02° 2θ. The precipitates from the bacterial cultures were collected 24 hours after the addition of the inoculum and $CaCl_2$ by centrifugation at 2720 x g for 15 minutes. The supernatant was removed with a transfer pipet, and the pellets were directly placed in the XRD sample holder. Triplicate specimens were prepared for each sample set.

Cement paste and mortar samples were cured in a 100% relative humidity room at 25 °C for 24 hours directly after mixing. Then the molds were removed, and the samples were prepared for XRD testing. First, the sample was crushed with a pestle and an aliquot was obtained from the core of each specimen. The aliquots were ground with a mortar and pestle, such that the particles were finer than 53 μm. Then, the aliquots were ground with ethanol to stop hydration [158]. The prepared samples were kept in a vacuum desiccator until they were tested. Triplicate specimens were prepared for each sample set.

4.3 RESULTS AND DISCUSSION

4.3.1 Bacterial Cultures

Bacterial cultures Culture-9-LowCa and Culture-12-LowCa showed $CaCO_3$ precipitation, and XRD analysis demonstrated that vaterite and calcite were present in both cultures (Figure 4.3).

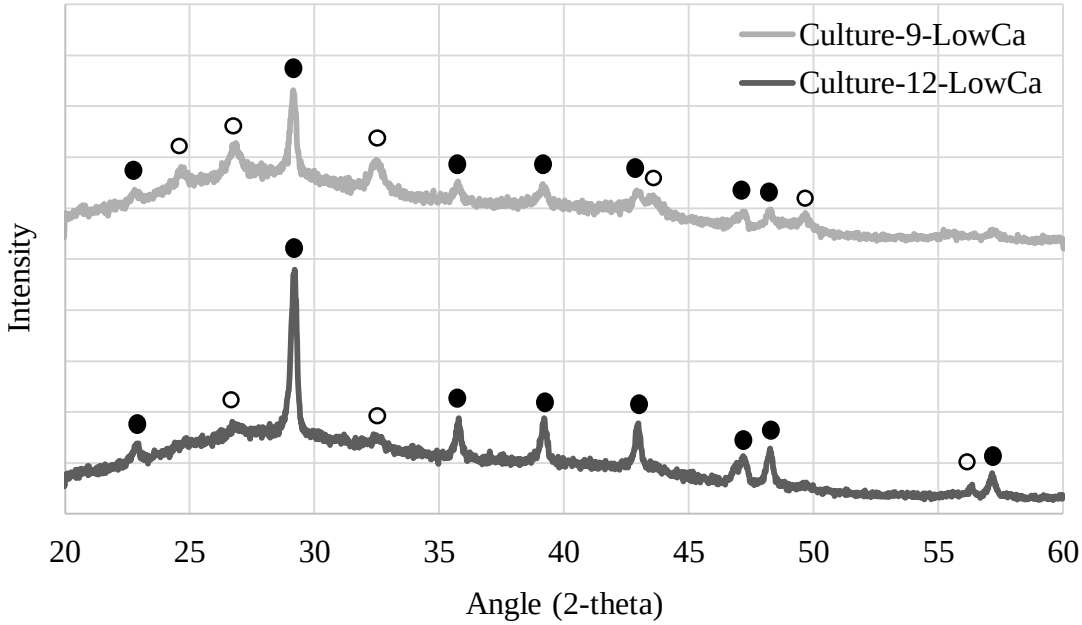

Figure 4.3: XRD patterns for Culture-9-LowCa and Culture-12-LowCa at 1 day. Curves are averages of triplicate samples; open circles represent vaterite peaks and solid circles represent calcite peaks.

$CaCO_3$ precipitation was observed in both Culture-9-HighCa and Culture-12-HighCa. XRD analysis demonstrated the presence of vaterite and calcite in Culture-9-HighCa, but only vaterite was observed in Culture-12-HighCa (Figure 4.4).

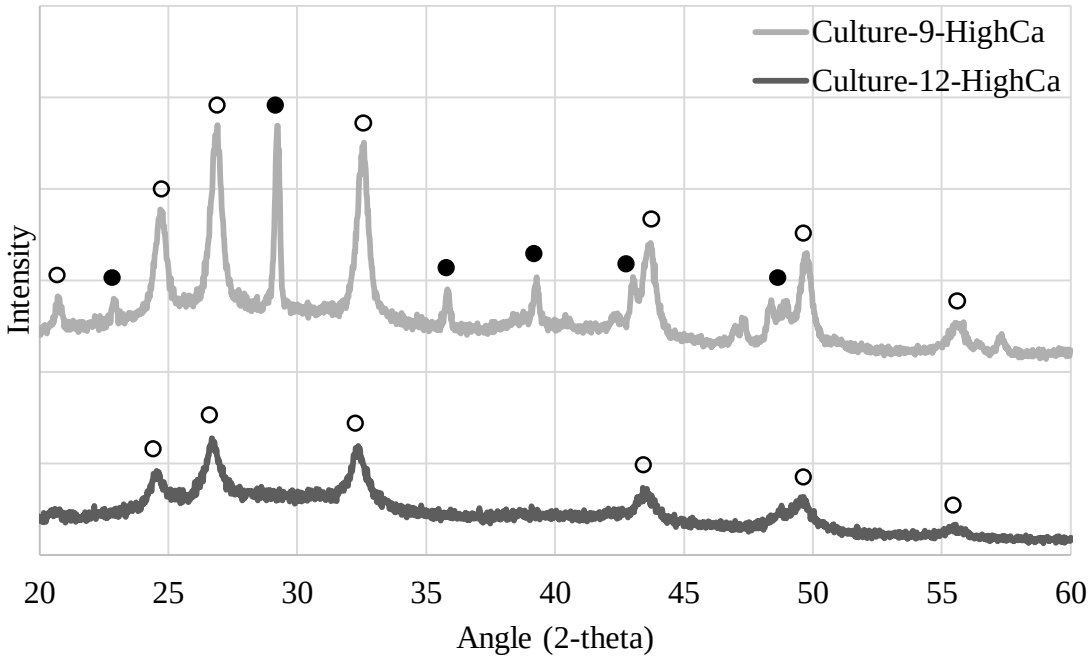

Figure 4.4: XRD patterns for Culture-9-HighCa and Culture-12-HighCa at 1 day. Curves are averages of triplicate samples; open circles represent vaterite peaks and solid circles represent calcite peaks.

As previously stated, calcite is the most stable polymorph of calcium carbonate. In bacterial cultures, $CaCO_3$ precipitates according to Oswald's rule, which defines the order of crystallization wherein the least stable polymorph precipitates first [115]. Relatedly, it should be noted that the least stable polymorph has the highest solubility index while the most stable polymorph has the lowest solubility index. For $CaCO_3$, ACC has the highest solubility index, followed by vaterite, aragonite, and calcite. Thus, the crystallization order for $CaCO_3$ is from the least thermodynamically stable polymorph (ACC) to the most thermodynamically stable polymorph (calcite) [151]. However, reaction kinetics can be influenced by parameters such as pH, ionic strength, and chemical composition of the surrounding environment.

XRD patterns presented in Figures 4.3 and 4.4 showed that increasing [Ca^{+2}] affected $CaCO_3$ precipitation in bacterial cultures at both pH 9 and pH 12, and this could be attributed specifically to the additional calcium present or the overall increase in ionic strength caused by the increased calcium concentration. Increasing [Ca^{+2}] from 0.03 M to 0.167 M at pH 9 resulted in a less prominent calcite peaks and more prominent vaterite peaks (*compare* Figures 4.3 and 4.4). This suggested that cultures with a higher [Ca^{+2}], and a correspondingly higher ionic strength, contained more vaterite and less calcite than did cultures supplemented with a lower concentration. Further, increasing [Ca^{+2}] at pH 12 resulted in the disappearance of calcite entirely (*compare* Figures 4.3 and 4.4). This could indicate that the overall ionic strength, and possibly the concentration of calcium ions specifically, has a noticeable influence of nucleation of calcite crystals and transformation of vaterite to calcite. A similar effect has been observed in abiogenic systems that did not contain bacteria. Ogino et al. [159] found that the relative concentration of vaterite increased with increasing [Ca^{+2}] and [CO_3^{-2}], and the vaterite crystals were found to remain stable for extended periods which was attributed to the lack of calcite seeds within the vaterite crystals [159]. Similarly, Evans [152] reported that vaterite content increased as ionic strength increased in calcium carbonate crystal growth solutions.

From Figures 4.3 and 4.4, it appeared that pH also played a role in the polymorph formation of biologically-induced calcium carbonate. At the higher [Ca^{+2}], both calcite and vaterite were precipitated at pH 9, while only vaterite was precipitated at pH 12. However, biological systems are notably complex, and there are other factors that must be considered when comparing these cultures. For example, the behavior of the microorganisms, and particularly the amount of carbonate produced by urease, might vary in the pH 9 and pH 12 cultures. Thus, it cannot be definitively concluded that the increase in pH alone promoted vaterite precipitation. However, it can be stated that increasing the calcium

concentration, and therefore also increasing the ionic strength, of a culture at a constant pH resulted in a greater relative concentration of vaterite as did increasing the pH of a culture with a constant calcium concentration. This might indicate that high [Ca^{+2}] (and correspondingly high ionic strength) and high pH affected the reaction kinetics and promoted an increase in vaterite precipitation.

4.3.2 Cement Paste and Mortar

Cement paste samples Paste-Neat and Paste-Bac showed $CaCO_3$ precipitation. XRD analysis demonstrated that calcite was the only resulting polymorph in both samples (Figure 4.5).

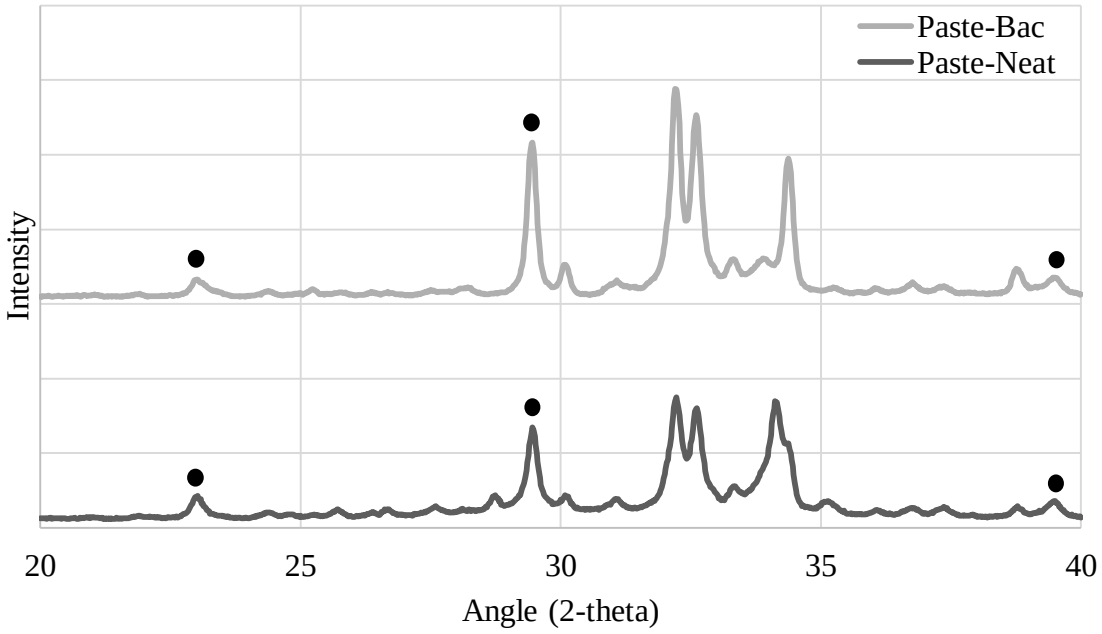

Figure 4.5: XRD patterns for Paste-Bac and Paste-Neat at 1 day. Curves are averages of triplicate samples; solid circles represent calcite peaks.

Mortar samples Mortar-CRS-Neat and Mortar-CRS-Bac, which were prepared with Colorado River sand, exhibited $CaCO_3$ precipitation. XRD analysis demonstrated that calcite was the only resulting polymorph in both samples (Figure 4.6).

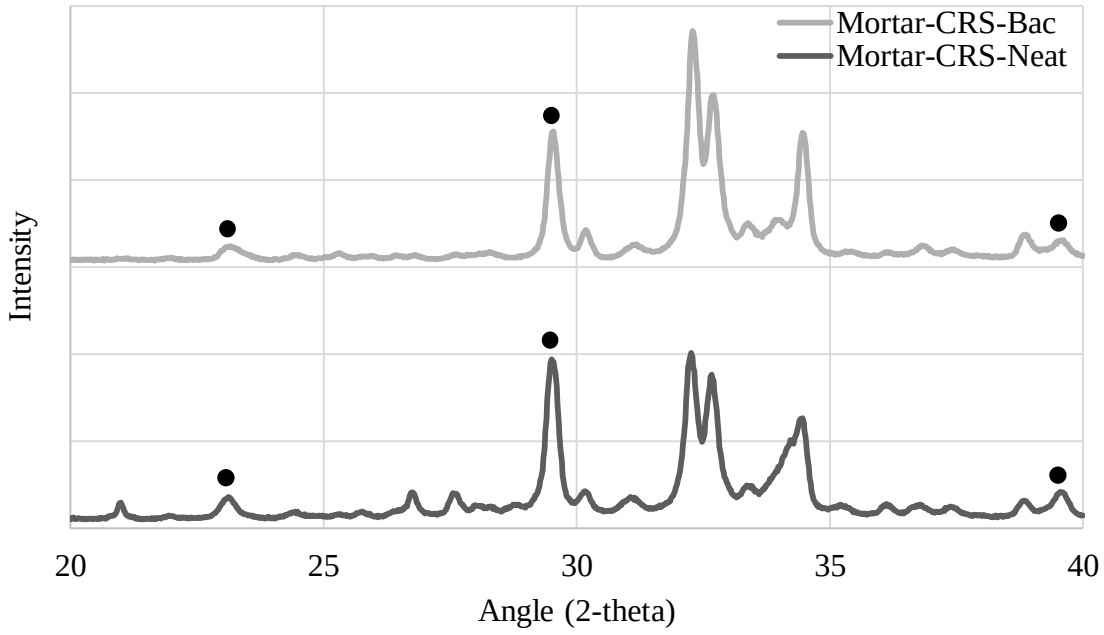

Figure 4.6: XRD patterns for Mortar-CRS-Bac and Mortar-CRS-Neat at 1 day. Curves are averages of triplicate samples; solid circles represent calcite peaks. CRS: Colorado River sand.

$CaCO_3$ precipitation was observed in mortar samples Mortar-C-Neat and Mortar-C-Bac, which were prepared with limestone sand. XRD analysis demonstrated that calcite was the only resulting polymorph in both samples (Figure 4.7).

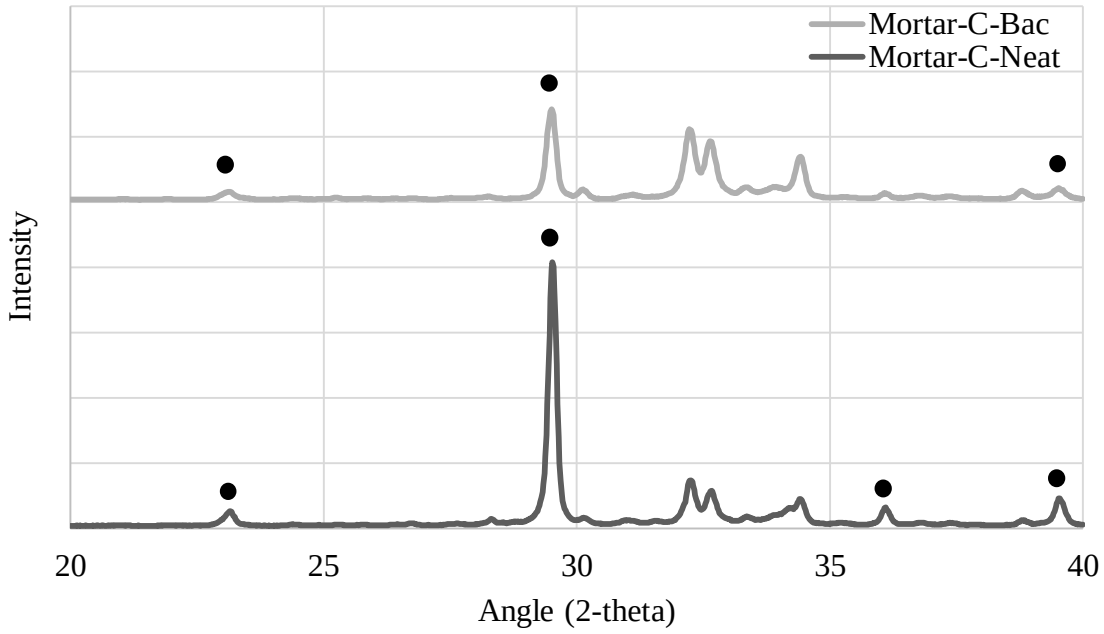

Figure 4.7: XRD patterns for Mortar-C-Bac and Mortar-C-Neat at 1 day. Curves are averages of triplicate samples; solid circles represent calcite peaks. C: Limestone sand.

Mortar samples Mortar-S-Neat and Mortar-S-Bac, which were prepared with silica sand, showed $CaCO_3$ precipitation. XRD analysis demonstrated that calcite was the only resulting polymorph in both samples (Figure 4.8).

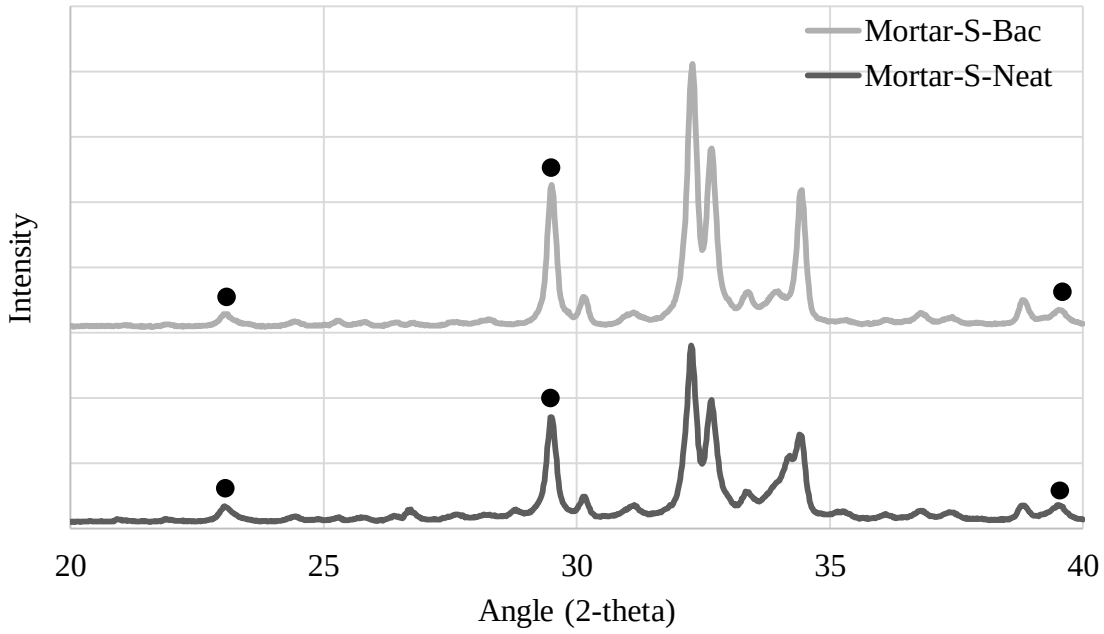

Figure 4.8: XRD patterns for Mortar-S-Bac and Mortar-S-Neat at 1 day. Curves are averages of triplicate samples; solid circles represent calcite peaks. S: Silica sand.

Analysis conducted on bacterial cultures in Section 4.3.1 indicated that variation in $[Ca^{+2}]$ and pH influenced the morphology of $CaCO_3$ obtained via MICCP. However, when a substrate was introduced to the system, the resulting precipitates differed from those obtained in the bacterial cultures under the same conditions. Culture-12-LowCa (prepared at pH 12 with 0.03 M $CaCl_2$) exhibited both vaterite and calcite precipitation, but only calcite was present in Paste-Bac, Mortar-CRS-Bac, Mortar-C-Bac, and Mortar-S-Bac, which also were prepared with an added calcium concentration of 0.03 M. This suggested that the influence of substrate mineralogy on MICCP is important for biomineralization in cement-based materials, and might be more influential as compared to other factors such as $[Ca^{+2}]$ and pH.

Rodriguez-Navarro et al. [115] previously suggested that the morphology of $CaCO_3$ induced by microorganisms is mainly governed by mineralogy of the substrate to which

the bacteria were attached. When *Myxococcus xanthus* cells were exposed to silicate-based substrates (various glasses and sandstone), only vaterite production was observed. However, when the cells were introduced to a calcitic substrate (Iceland spar crystals and various stones), calcite was the only polymorph observed. The mechanical quality of $CaCO_3$ precipitation also was influenced greatly by substrate mineralogy; uniform, coherent formation of calcite was observed on calcitic substrates while incoherent formation of vaterite on silicate substrates was observed. This suggests that calcite might be preferable to vaterite for biomineralization applications because it is more thermodynamically and mechanically stable [115]. This also is in accordance with work conducted by De Muynck et al. [105] who determined that when a calcitic substrate was used, mainly calcite precipitation was observed, even in a high pH environment. Relatedly, Wiktor and Jonkers [51] observed mainly calcite crystals in bacterial cement paste with an addition of 0.4M calcium lactate.

Although the morphology of $CaCO_3$ precipitated by microorganisms in cement paste has been studied previously, it was unclear how morphology would be affected when aggregates, particularly siliceous aggregates, were introduced to the system. Only calcite was observed in all mortar samples regardless of the type of aggregate used in this study. Although it was suspected that the addition of silica sand might promote vaterite precipitation due to its siliceous nature, even the Mortar-S-Bac and Mortar-S-Neat samples contained only calcite (Figure 4.8). Thus, it appeared that the influence of the calcitic cement paste matrix might have governed the $CaCO_3$ morphology. This is an important distinction, and a step towards improving the understanding of the $CaCO_3$ polymorph selection process in microbial concrete.

Chapter 5: Dissolution Kinetics, Solubility, and Stability of Biogenic Calcium Carbonate

5.1 INTRODUCTION

Biominerals are noted for having unique structures and morphologies as well as excellent mechanical properties that in some cases exceed those of their synthetic counterparts [61-64]. Additionally, biological systems can form minerals with hierarchal structures through self-assembly at moderate temperatures and pressures [74]. This capability has generated substantial interest in inducing biomineralization processes to produce materials for human use.

In addition to mechanical properties, the thermodynamic stability and morphology of biominerals can differ substantially from their synthetic counterparts. Calcium carbonate is one of the most widely studied biominerals [62, 160], but little work has been done to compare the properties of biogenic calcium carbonate to abiogenic (not produced by the action of living organisms) calcium carbonate. The bacteria in microbial-induced calcium carbonate (MICCP) systems essentially act as vehicles for carbonate production and biogenic calcium carbonate precipitation, but there are simpler ways to introduce carbonate to the system to trigger precipitation of calcium carbonate; therefore, comparing the properties of biogenic calcium carbonate as compared to abiogenic calcium carbonate could be useful to justify the use of MICCP in concrete. For example, Amidi and Wang [161] proposed a method for surface treatment of concrete bricks using calcium carbonate precipitation induced by a solution containing dimethyl carbonate and calcium chloride where the dimethyl carbonate hydrolyzes slowly to form carbonate. The authors stated that this abiogenic system, which substantially reduced the water absorption and increased the compressive strength of concrete bricks, was purposefully developed without bacteria to

avoid some concerns associated with bacterial systems such as high material costs and the need for extensive quality control and a highly skilled labor force [161]. However, it is possible that the properties of biologically-induced calcium carbonate might be different than the properties of synthetic calcium carbonate. To increase understanding in this area, the morphology, dissolution kinetics, and thermodynamic solubility of biogenic calcium carbonate was compared to that of abiogenic calcium carbonate. Dissolution kinetics provided an indication of kinetic solubility, which is concerned with the rate at which these minerals dissolve, while thermodynamic solubility was measured at equilibrium and is independent of the pathway between reactants and products. Thus, both kinetic and thermodynamic solubility measurements were needed to fully characterize the stability of the biogenic and abiogenic calcium carbonates.

5.2 MATERIALS AND METHODS

5.2.1 Microorganism and Medium

S. pasteurii was used in this study, and the microorganisms were cultured according to the procedure described in Section 3.3.

5.2.2 Cement

Texas Lehigh Type I/II (Buda, TX) portland cement was used in this study, and the mass composition of oxides was presented in Table 4.1 (Section 4.2.2).

5.2.3 Sample Preparation

Biogenic (B) calcium carbonates, commercial (C) calcium carbonates, and synthetic (S) calcium carbonates were compared in this study; a summary of these *ex situ* calcium carbonate samples is presented in Table 5.1.

Table 5.1: Summary of *ex situ* samples.

Sample Set Name	Description
B-CC	Biogenic $CaCO_3$ precipitated in an *S. pasteurii* culture with $CaCl_2$ as the calcium source
B-CA	Biogenic $CaCO_3$ precipitated in an *S. pasteurii* culture with $Ca(C_2H_3O_2)_2$ as the calcium source
A-C-FS	Abiogenic $CaCO_3$ obtained commercially (Fisher Scientific)
A-C-AO	Abiogenic $CaCO_3$ obtained commercially (Acros Organics)
A-S-CC	Abiogenic $CaCO_3$ synthesized from Na_2CO_3 and $CaCl_2$
A-S-CA	Abiogenic $CaCO_3$ synthesized from Na_2CO_3 and $Ca(C_2H_3O_2)_2$

Biogenic calcium carbonate was produced using either calcium chloride ($CaCl_2$) or calcium acetate ($Ca(C_2H_3O_2)_2$) as the calcium source; B-CC and B-CA were precipitated in 600-mL *S. pasteurii* cultures in 1-L flasks, where the calcium source was added at the time of inoculation. After 24 hours of incubation at 30°C with shaking, the precipitates were collected by vacuum filtration through a 0.2-µm filter. A-C-FS and A-C-AO were obtained from commercial sources. A-S-CC and A-S-CA were synthesized by combining solutions of 0.5 M sodium carbonate (Na_2CO_3) and 0.5 M calcium chloride ($CaCl_2$) or calcium acetate ($Ca(C_2H_3O_2)_2$) and stirring the solution for 1 hour at 23°C. Then, the resulting $CaCO_3$ precipitates were collected by vacuum filtration through a 0.2-µm filter.

5.2.4 XRD

XRD was conducted using a Siemens Bruker X-ray Diffractometer (Madison, WI, United States) to determine the morphology of the $CaCO_3$ in each *ex situ* sample set. The calcium carbonate samples were passed through a No. 100 sieve such that the particles were finer than 149 µm. Then, the powder material was compacted into a sample holder and prepared for testing. Analysis was conducted from 20-60° 2θ with 6 seconds dwell time. The diffractometer was operated at 40 keV and 30 mA, at a step size of 0.02° 2θ. Triplicate specimens were prepared for each sample set. Following analysis, the patterns were analyzed using commercial software and a whole-pattern fit [162, 163] was

performed to provide a quantitative estimate for the mineralogical composition of each *ex situ* calcium carbonate sample.

The ability of biogenic and abiogenic calcium carbonate to nucleate and precipitate in cement paste was compared using XRD. Four types of cement pastes were prepared:

- Neat paste: prepared with distilled water and cement;
- Neat + Sodium Carbonate (SC) paste: prepared with a 0.167 M Na_2CO_3 solution and cement;
- UYE Nutrient paste: prepared with UYE medium and cement;
- UYE Bacterial paste: prepared with *S. pasteurii* cells grown in UYE medium to OD_{600}=0.6 and cement;

The UYE medium contained Tris base, urea, and yeast extract (Section 3.3); Tris base and urea do not contain calcium while yeast extract often contains a negligible amount of calcium. Sherwood [154] reported that calcium contents in yeast extract ranged from 0.14 - 0.21% by mass, and Abelovska et al. [155] determined that a 2% solution of yeast extract (the concentration used in UYE medium) contained only 0.0004 M of calcium. However, the calcium ion concentration in cement paste pore solutions has been reported to range from 0.02 to 0.1 M in fresh samples. Thus, the amount of calcium added due to the presence of yeast extract in UYE Nutrient paste and UYE Bacterial paste could be considered trivial compared to the amount of calcium available in the pore solution.

For all pastes, the solution-to-cement ratio (s/c) was 0.50 by mass. Pastes were prepared by mixing 40 g of cement with 20 g of either distilled water (for neat pastes), 0.167 M Na_2CO_3 solution (for neat + SC pastes), UYE medium (for UYE nutrient pastes), or bacterial cultures (for UYE bacterial pastes) by hand stirring for 2 minutes. Then, the samples were cast into 3 x 3 cm cylindrical molds and cured at 100% relative humidity at 25°C for 24 hours. After curing, the molds were removed, and the samples were prepared

for testing. The cement paste sample was crushed with a pestle, and a representative aliquot was obtained from the core. Representative aliquots were pulverized with a mortar and pestle, such that the resulting powder was finer than 53 μm. Then, the sample was ground with ethanol to stop hydration [158], and 10% (w/w) zincite was added as an internal standard. The sample was mixed well to ensure homogeneity. Samples were stored in a vacuum desiccator until the time of testing. Analysis was conducted from 25-40° 2θ with 6 seconds dwell time. The diffractometer was operated at 40 keV and 30 mA, at a step size of 0.02° 2θ. Triplicate specimens were prepared for each sample set.

Calcite was quantified in each sample using the Reference Intensity Ratio (RIR) method [164]. The remaining $CaCO_3$ polymorphs were not quantified because results presented in Chapter 4 indicated that calcite was the only $CaCO_3$ polymorph detected in our bacterial cement paste and mortar samples. However, morphology was qualitatively assessed for each sample to ensure that only calcite was present. A ratio was established between the intensities of the primary zincite (internal standard) and calcite peaks by creating samples with known mass proportions and plotting the results on a standard curve. Calcite content was varied from 2% to 18% while zincite was maintained at 10%. NaCl was selected as a filler material because it is crystalline and its peaks do not overlap with calcite or zincite. The proportions for each sample representing a point on the standard curve are presented in Table 5.2, and the RIR standard curve is displayed in Figure 5.1.

Table 5.2: Mass composition of samples representing points on the RIR standard curve.

Point	Calcite (%)	Zincite (%)	NaCl filler (%)
1	2	10	88
2	4	10	86
3	6	10	84
4	8	10	82
5	10	10	80
6	12	10	78
7	14	10	76
8	16	10	74
9	18	10	72

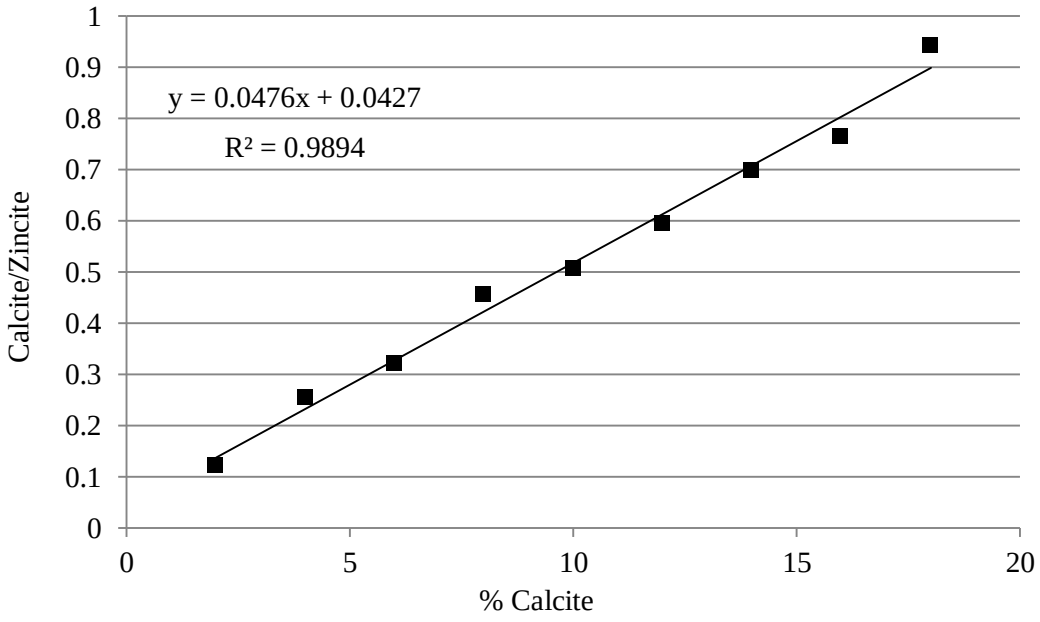

Figure 5.1: RIR standard curve.

Calcite was quantified in each sample using the equation Y = 0.0476X + 0.0427, where Y is the intensity of the primary calcite peak divided by the intensity of the primary zincite peak and X is wt. % calcite.

5.2.5 Dissolution Kinetics

Dissolution kinetics were examined by dissolving 20 mg of $CaCO_3$ from each *ex situ* sample set in 10 mL of continuously stirred 0.01 M phosphoric acid and monitoring the pH for 300 seconds at 23°C [124]. As described in Section 5.2.4, each calcium carbonate sample was passed through a No. 100 sieve prior to the dissolution experiments such that the particles were finer than 149 μm. The pH was monitored using a Thermo-Scientific™ Orion™ 720A pH probe (Waltham, MA, United States), and measurements were recorded in 15-second intervals for 300 seconds. Triplicate experiments were performed for each sample set.

5.2.6 Thermodynamic Solubility

Thermodynamic solubility (i.e., equilibrium) was evaluated by dissolving 20 mg of $CaCO_3$ in distilled, deionized (DDI) water which possessed an initial pH of 5.76. The solution was then continuously stirred at 23°C for 24 hours after the addition of $CaCO_3$, and the final pH was measured to provide a relative indication of the amount of dissolved $CaCO_3$ among the six *ex situ* sample sets. The final pH measurements were used to calculate final [H+] using the equation $[H+] = 10^{-pH}$. Triplicate experiments were performed for each sample set.

5.3 RESULTS AND DISCUSSION

5.3.1 Morphology of $CaCO_3$

XRD patterns for B-CA and B-CC are displayed in Figure 5.2; B-CA contained only vaterite while B-CC contained vaterite, calcite, and aragonite.

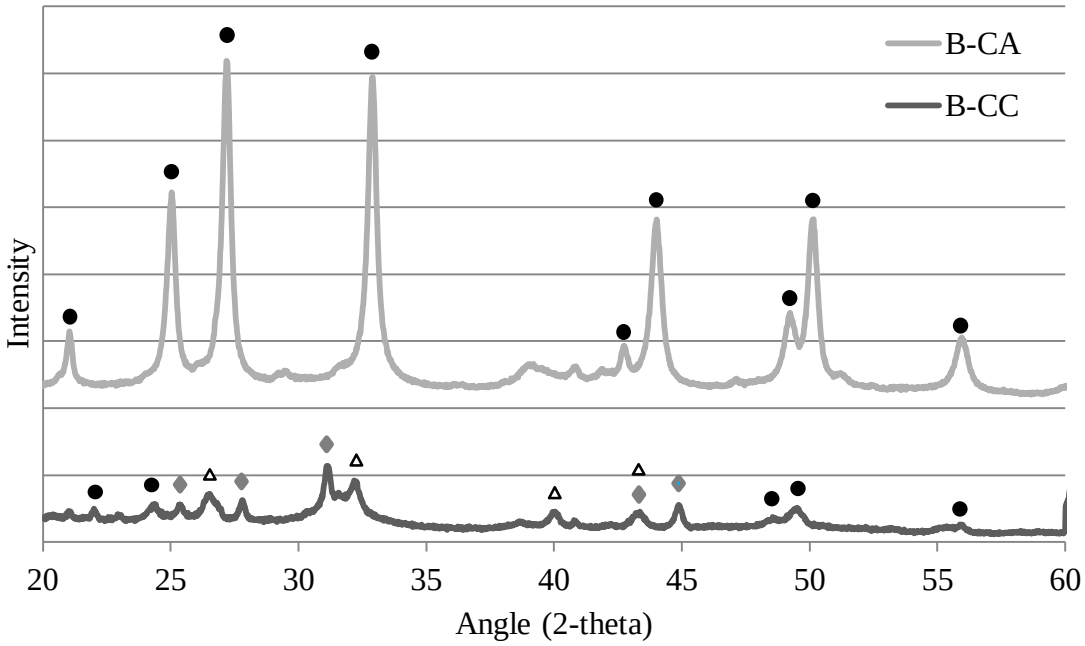

Figure 5.2: XRD patterns for B-CA and B-CC. Curves are averages of triplicate samples. Solid circles represent vaterite peaks, diamonds represent aragonite peaks, and open triangles represent calcite peaks.

XRD patterns for A-C-FS and A-C-AO are presented in Figure 5.3, and both of these samples contained only calcite.

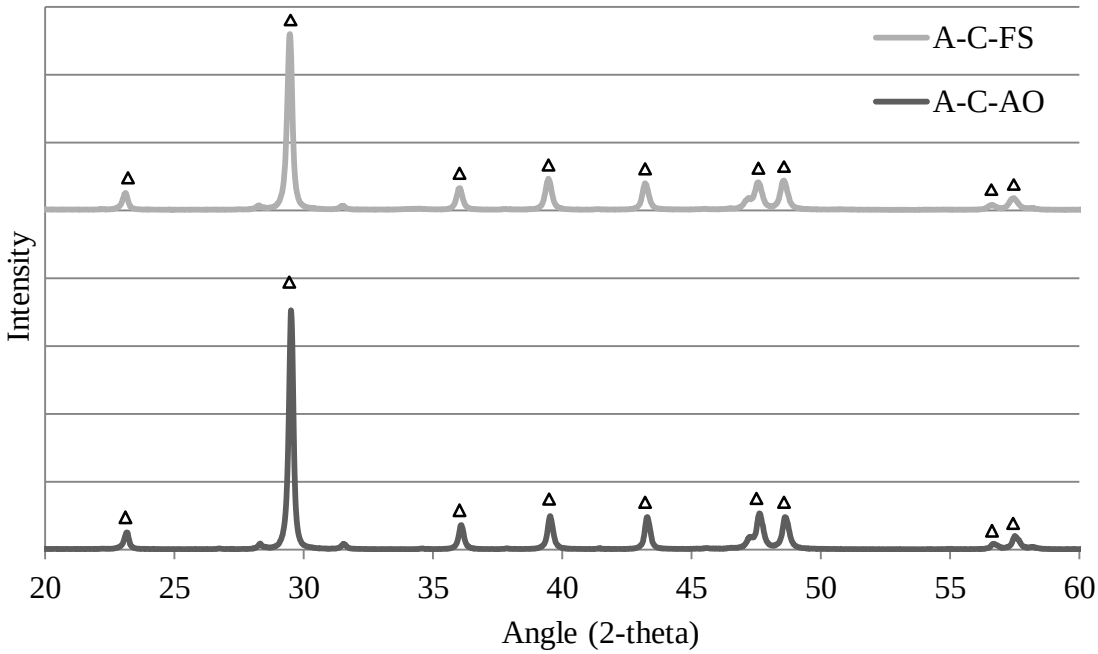

Figure 5.3: XRD patterns for A-C-FS and A-C-AO. Curves are averages of triplicate samples. Open triangles represent calcite peaks.

XRD patterns for A-S-CA and A-S-CC are displayed in Figure 5.4; A-S-CA contained only calcite while A-S-CC contained mostly calcite with some small vaterite peaks.

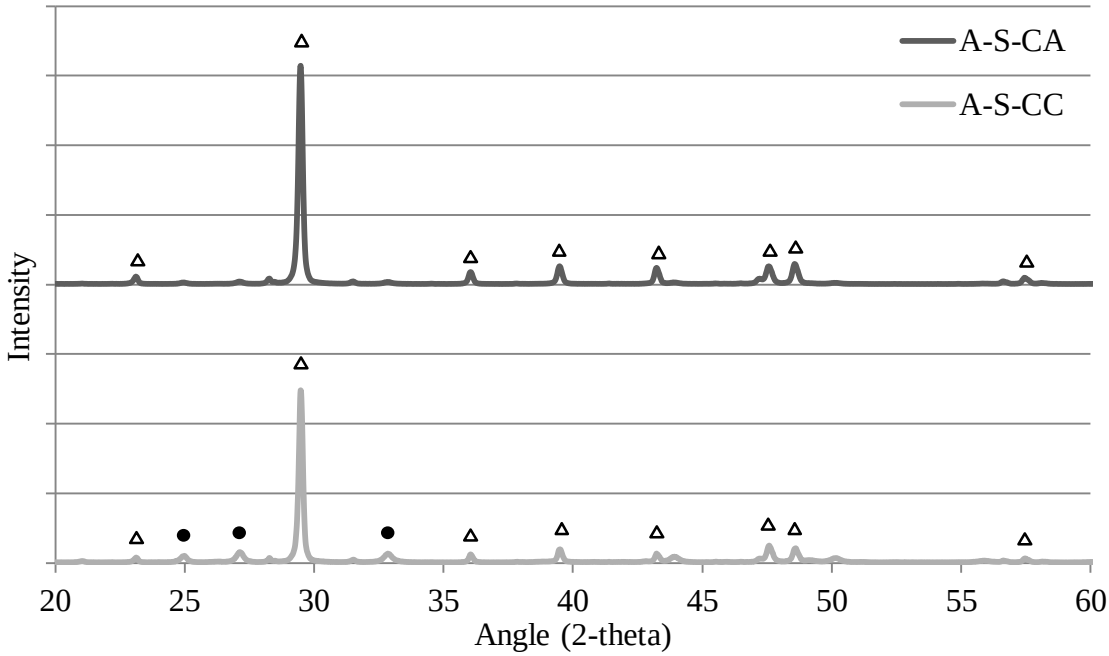

Figure 5.4: XRD patterns for A-S-CA and A-S-CC. Curves are averages of triplicate samples. Solid circles represent vaterite peaks and open triangles represent calcite peaks.

As discussed in Section 5.2.4, a whole pattern fit [162, 163] was performed on triplicate sets of XRD data for each of the six *ex situ* samples to provide a quantitative estimate of the morphology of each calcium carbonate specimen. Results of this estimation are presented in Table 5.3, and detailed phase ID reports for each sample can be found in Appendix A: Whole-Pattern Fits of *Ex Situ* Biogenic and Abiogenic $CaCO_3$. From these data, it was apparent that each of the abiogenic $CaCO_3$ samples consisted almost exclusively of calcite, although A-S-CC contained slight percentages of vaterite and aragonite. However, the morphology of the biogenic $CaCO_3$ samples differed substantially from the abiogenic samples; B-CC contained aragonite, calcite, and vaterite while only vaterite was detected in B-CA.

Table 5.3: Morphology of $CaCO_3$ in each sample set by mass. Error represents the standard deviation of triplicate samples.

Sample Set	Aragonite (%)	Calcite (%)	Vaterite (%)
B-CC	35.47 ± 5.78	36.97 ± 5.20	27.60 ± 6.61
B-CA	0.00 ± 0.00	0.00 ± 0.00	100.00 ± 0.00
A-S-CC	2.20 ± 3.30	91.37 ± 4.74	6.77 ± 2.02
A-S-CA	0.05 ± 0.07	98.17 ± 0.23	1.83 ± 0.23
A-C-FS	0.00 ± 0.00	99.97 ± 0.06	0.00 ± 0.00
A-C-AO	0.00 ± 0.00	100.07 ± 0.06	0.00 ± 0.00

5.3.2 Dissolution Kinetics

Results of the dissolution assay are presented in Figure 5.5, where a greater rate of pH increase indicates a greater rate of dissolution.

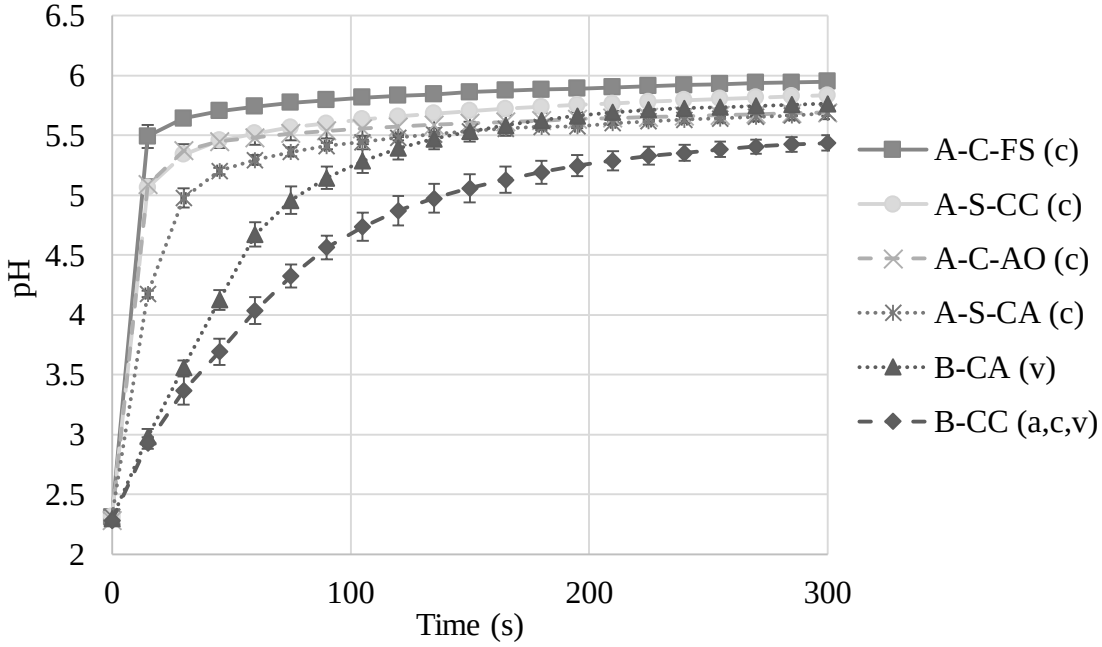

Figure 5.5: Change in pH of a 0.01 M phosphoric acid solution at 23°C following addition of $CaCO_3$ over 300 seconds. Error bars represent the standard deviation of triplicate samples. c: calcite. v: vaterite. a: aragonite.

Since calcite is traditionally the least soluble $CaCO_3$ polymorph followed by aragonite and vaterite [58], it was expected that the abiogenic $CaCO_3$ samples would

exhibit slower dissolution rates than would the biogenic samples because the abiogenic samples contained mostly calcite. However, from Figure 5.5, the opposite trend occurred. Biogenic vaterite (B-CA) exhibited a slower dissolution rate than the commercial calcites (A-C-FS and A-C-AO) and the calcites produced synthetically in our laboratory (A-S-CA and A-S-CC); a mixed morphology biogenic calcium carbonate that contained calcite, aragonite, and vaterite (B-CC) exhibited the slowest dissolution and had a lower final pH (pH = 5.44) at t = 300 seconds. This indicated that the biogenic calcium carbonates examined in this study were more kinetically stable than the abiogenic calcium carbonates, and this might be due to the biological mechanisms by which they were formed.

5.3.3 Thermodynamic Solubility

Results presented in Section 5.3.2 indicated that the biogenic calcium carbonates in this study were more kinetically stable than the abiogenic calcium carbonates, but it remained unclear how thermodynamic stability differed among these samples. Thus, a thermodynamic solubility experiment was performed, and the results of this experiment are presented in Figure 5.6. It should be noted that a lesser final $[H^+]$ indicates greater thermodynamic solubility, which in turn corresponds to reduced thermodynamic stability.

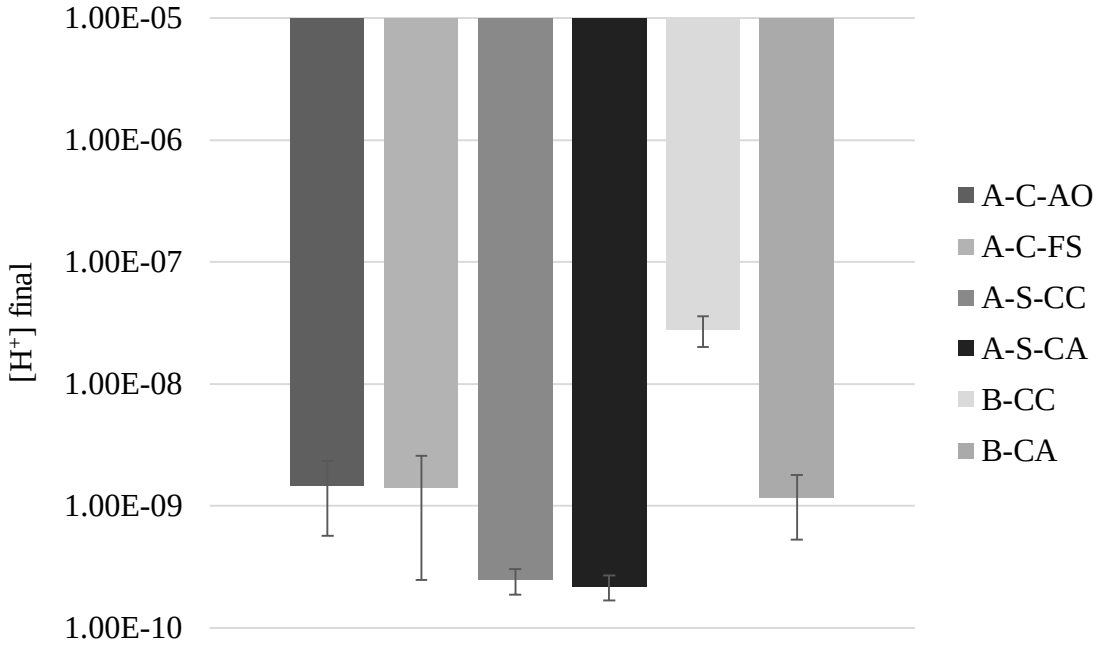

Figure 5.6: $[H^+]$ in DDI water at 23°C following 24 hours of continuous stirring with $CaCO_3$. Error bars represent the standard deviation of triplicate samples.

Results presented in Figure 5.6 indicated that B-CC (biogenic calcium carbonate with a mixed morphology) exhibited reduced solubility as compared to abiogenic calcites (A-C-AO, A-C-FS, A-S-CC, A-S-CA) and biogenic vaterite (B-CA). These data are in agreement with results of the kinetic dissolution experiment presented in Figure 5.5, where B-CC reached the lowest final pH at t=300 seconds. As previously stated, calcite is the least soluble $CaCO_3$ polymorph followed by aragonite and then vaterite [58]. Thus, it was expected that B-CA (100% vaterite) would exhibit a higher thermodynamic solubility as compared to B-CC (calcite, aragonite, and vaterite), and this expectation was confirmed. However, the abiogenic calcites exhibited a higher solubility as compared to the mixed morphology B-CC, and this observation deviates from the laws of thermodynamics, which dictate that calcite is less soluble than aragonite and vaterite. Thus, it appeared that the

mechanism of formation had a great impact on the stability of $CaCO_3$ in this study, and that biogenic $CaCO_3$ was more stable than abiogenic $CaCO_3$.

5.3.4 Calcite Precipitation in Cement Paste

Ex situ studies in Sections 5.3.1-5.3.3 provided useful information about the differences in morphology, kinetic stability, and thermodynamic stability in abiogenic calcium carbonate as compared to biogenic calcium carbonate. However, it remained unclear how abiogenic $CaCO_3$ and biogenic $CaCO_3$ would nucleate and form differently in a cement-based system *in situ*. As such, XRD was used to quantify the amount of $CaCO_3$ precipitated in neat cement paste, neat cement paste where 0.167 M sodium carbonate was added, UYE nutrient paste, and UYE bacterial paste at 1 day.

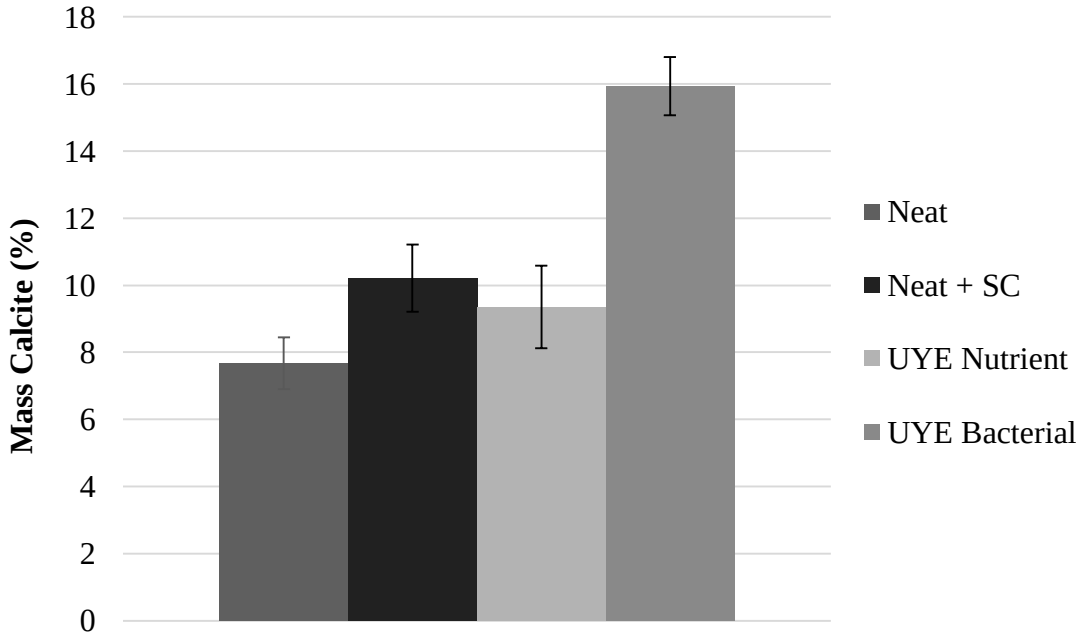

Figure 5.7: Mass percentages of calcite at 1 day. Error bars represent the standard deviation of triplicate samples. SC: sodium carbonate. UYE: Urea-Yeast Extract medium.

From Figure 5.7, calcite content increased in neat + SC paste as compared to neat paste at 1 day, which suggested that some calcium carbonate precipitation occurred due to the addition of sodium carbonate. However, the increase in calcite content was far greater for UYE bacterial paste, which indicated that the simple addition of an exogenous, synthetic carbonate source to cement paste could not induce $CaCO_3$ precipitation comparable to that induced by the addition of bacterial cultures.

Chapter 6: Characterization of Vegetative *S. pasteurii* Exposed to Heat, Nutrient Depletion, and High pH

6.1 INTRODUCTION

A critical challenge for long-term use of microbial-induced calcium carbonate precipitation (MICCP) in concrete is ensuring that the bacteria can remain metabolically active (i.e., vegetative) throughout the service life. In bacterial cement paste, where vegetative cells of *S. pasteurii* were added to the cement paste, Basaran [52] reported that only 0.4% of inoculated cells remained viable after 28 days. Similarly, Jonkers and Schlangen [49] found that just 2% of *Bacillus cohnii* and *Bacillus halodurnas* endospores and 7% *Bacillus pseudofirmus* endospores survived 10 days after inoculation to cement stone. The death of microorganisms in cement-based systems is likely attributable to sudden environmental changes during the mixing process, including an increase in temperature (due to heat generated by cement hydration), depletion of nutrients, and a rapid increase in pH. Previous studies have explored ways to prolong the viability of microorganisms in these systems such as encapsulating or immobilizing cells [50, 47, 112-114], but little attention has been focused on understanding how vegetative cells are affected by environmental conditions specific to cement-based systems. Furthermore, the role of dead cells and endospores (i.e., metabolically inactive cells) is uncertain. Specifically, it is unclear how urease activity and zeta potential are different in dead cells and endospores as compared to live, vegetative cells. For instance, even though dead cells are no longer metabolically active, it might be possible that urease can persist even after the microorganisms die, and this urease could continue to induce calcium carbonate precipitation [126]. It also is unclear if dead cells might aid in MICCP by serving as nucleation sites for calcium carbonate precipitation [54]. To address these uncertainties and provide insight about the ability of live, vegetative *S. pasteurii* to persist inside concrete,

the effects of conditions designed to mimic those present in cement based systems (heat, nutrient depletion, and high pH) on the viability, urease activity and zeta potential of vegetative *S. pasteurii* were investigated.

6.2 MATERIALS

6.2.1 Microorganism and Medium

S. pasteurii was used in this study, and the microorganisms were cultured according to the procedure described in Section 3.3.

6.2.2 Cement

Texas Lehigh Type I/II (Buda, TX) portland cement was used in this study, and the mass composition of oxides was presented in Table 4.1 (Section 4.2.2).

6.2.3 High Alkalinity Solution (HAS)

The HAS in this study was used to simulate the high alkalinity environment that is inherent to the pore solution of cement paste, and it contained 17.94 g/L KOH and 5.24 g/L NaOH [165]. This solution possessed a pH of approximately 13.6. The actual pH of fresh cement pastes have been reported as ranging from approximately 12.5 to 13.5 [166], so HAS was used to represent the high end of the pH spectrum for a fresh paste.

6.2.4 Cement Extract (CE) Solution

To serve as a complement to the HAS, CE solution was developed by mixing 350 g of Type I/II cement with 2L of deionized water and continuously stirring the suspension for one hour [167, 168]. At this time, the solution was filtered, and the resulting CE solution possessed a pH of approximately 12.9. CE was used to examine the effects of a more realistic, milder pH as compared to that of HAS, and it also provided a more accurate depiction of the chemical composition of a cement paste pore solution.

6.2.5 Sample Matrix

Nine sample sets were explored in this study, and a summary of these sample sets is presented in Table 6.1. An untreated sample set was chosen to represent live, vegetative cells and serve as the control. Then, eight other sample sets were chosen to examine how conditions designed to mimic those that might occur in cement-based materials would affect the viability, urease activity, and zeta potential of vegetative *S. pasteurii* cells.

Table 6.1: Summary of samples.

Name	**Sample treatment**	**Viability?**	**Urea hydrolysis?**	**Zeta potential?**	**XRD?**
U	None	Y	Y	Y	Y
HT-45	Heat-treated at 45 °C for 4 hrs	Y	Y	Y	N
HT-55	Heat-treated at 55 °C for 4 hrs	Y	Y	Y	Y
S	Resuspended in H_2O for 4 hrs	Y	Y	Y	N
HAS	Resuspended in HAS for 4 hrs	Y	Y	Y	N
HAS+N	Resuspended in HAS + 20 g/L yeast extract + 10 g/L urea for 4 hrs	Y	Y	Y	N
CE	Resuspended in CE for 4 hrs	Y	Y	N	N
CE+N	Resuspended in CE + 20 g/L yeast extract + 10 g/L urea for 4 hrs	Y	Y	N	N
A	Autoclaved	Y	Y	Y	Y

Heat treatment was employed to elucidate the effect of heat generated by cement hydration. The maximum allowable concrete temperature is commonly specified as 57 °C,

and typical temperature rise for concrete using Type I/II cement can range up to 30°C above the placement temperature [169]. Thus, the HT-55 sample set in this study was exposed to 55°C for four hours to simulate heat in concrete designed to meet the conventional maximum allowable concrete temperature of 57 °C. HT-45 was then defined to represent a milder temperature increase, and this sample set was exposed to 45°C for four hours.

The starved (S) sample set was used to evaluate the effect of nutrient depletion on vegetative *S. pasteurii* cells, and HAS was employed to evaluate the effect of exposure to a high pH coupled with nutrient depletion. For the HAS sample set, the cultured cells were centrifuged and resuspended in HAS (no carbon source and electron donor); on the other hand, cells in bacterial cement paste are typically inoculated with their nutrients. As a result, the degree of nutrient depletion and pH shock endured by the cells in the HAS sample set might be more severe than what is actually present in bacterial concrete. Thus, HAS+N (containing 17.94 g/L KOH, 5.24 g/L NaOH, 20 g/L yeast extract, and 10 g/L urea) was prepared to investigate the effect of high pH without nutrient depletion. CE and CE+N were prepared to serve as milder complements to HAS and HAS+N. Finally, the autoclaved (A) sample set was employed to investigate the behavior of dead cells. The cells were classified as dead based on their inability to grow in liquid or solid UYE medium.

6.3 METHODS

6.3.1 Viability

The total number of viable cells was estimated in each sample set immediately after treatment using the Most Probable Number (MPN) method. The sample inoculum was serially diluted by a factor of 10 (10^{0}-10^{-4}) in pH 9 UYE medium in 10-mL test tubes. The tenfold serial dilutions were performed in triplicate for each sample set, and the test tubes were incubated at 30°C with shaking for 96 hours. Then, the number of positive growth

responses (indicated by visible turbidity) at each dilution was recorded for each sample set, and this information was used to obtain the MPN index and upper and lower 95% confidence limits from standard tables [170].

6.3.2 Urea Hydrolysis

Urease activity was examined for *S. pasteurii* sample sets by monitoring ammonia (NH_3) production from urea hydrolysis. After growth in UYE medium (Section 3.3) to OD_{600}=0.8, cells in each sample set were treated according to Table 6.1. Then, cells were harvested by centrifugation at 7500 x g for 10 minutes, resuspended in fresh UYE medium, and incubated at 30°C with shaking. Ammonia concentrations were measured using a Thermo Scientific™ Orion™ High-Performance Ammonia Electrode (Waltham, MA, United States) for 24 hours. To correct for the small amount of NH_3 present in fresh UYE medium at t = 0 (primarily due to decomposition of urea during autoclaving), the NH_3 concentration was measured immediately after cell resuspension (t=0), and this value was subtracted from all subsequent measurements. The cumulative percentage of urea consumed was calculated according to the stoichiometry of Reaction 2.1, which shows that 1 mole of urea is hydrolyzed to form two moles of NH_3 and one mole of carbon dioxide. Because each medium contains 10 g/L urea, or 167 mM urea, the maximum amount of NH_3 that can be produced in each culture is 333 mM. The amount of NH_3 present at t=0 was subtracted from both the concentration at the time of interest and the maximum possible ammonia concentration, and the percent urea consumed was calculated using Equation 6.1.

$$\%\ \text{urea consumed}_{(t=x)} = \frac{[NH_{3\,(t=x)}] - [NH_{3\,(t=0)}]}{[NH_{3\,(max)}] - [NH_{3\,(t=0)}]} \times 100\% \qquad (6.1)$$

6.3.3 Electrophoretic Mobility and Zeta Potential

S. pasteurii cells in select sample sets were grown in UYE medium (Section 3.3) to OD_{600}=0.8 and treated according to Table 6.1. Then, cells were harvested by centrifugation at 4000 x g for 6 minutes, washed, and resuspended in sterile 20 mM Tris buffer at pH 9 for testing. A Malvern Zetasizer Nano ZS (Malvern, Worcestershire, United Kingdom) was used to measure electrophoretic mobility, and the Henry equation (Equation 6.2) was used to calculate zeta potential [171].

$$U_E = \frac{2\varepsilon z f(Ka)}{3\eta} \qquad (6.2)$$

where U_E is the electrophoretic mobility, ε is the dielectric constant, z is the zeta potential, f(Ka) is Henry's function, and η is viscosity.

For Henry's function, f(Ka) = 1.5, or the Smoluchowski approximation, was used. Electrophoretic mobility was measured immediately after treatment, and samples were then stored at room temperature (23 °C) for 28 days. Electrophoretic mobility was measured again at 3, 7, and 28 days after treatment to assess whether untreated, heat treated, starved, and autoclaved cells could maintain their surface charge over time. Triplicate specimens were prepared for each sample set, and three runs were performed on each specimen.

6.3.4 XRD

XRD was conducted to quantify calcite in select samples according to the Reference Intensity Ratio (RIR) procedure described in Section 5.2.4. In general, four types of pastes were prepared:

- Neat paste: prepared with distilled water and cement;
- Nutrient paste: prepared with UYE medium and cement;

- Spent Nutrient paste: prepared with spent UYE nutrient medium (obtained by growing *S. pasteurii* in UYE medium to OD_{600}=0.8 and then retaining the spent medium after filtering the bacterial culture through a 0.2-μm filter to remove the bacterial cells) and cement;
- Bacterial paste: prepared for untreated and autoclaved sample sets with *S. pasteurii* cells grown in UYE medium to OD_{600}=0.8 and treated according to Table 6.1 (in their original UYE nutrient media) and cement;

The paste samples were prepared according to the procedure described in Section 5.2.4. Calcite was quantified in each sample using the equation Y = 0.0476X + 0.0427, which was obtained from the RIR standard curve (Figure 5.1), where Y is the intensity of the primary calcite peak divided by the intensity of the primary zincite peak and X is wt. % calcite.

6.4 RESULTS AND DISCUSSION

6.4.1 Viability

The concentrations of total viable cells in each sample set, which was evaluated immediately after treatment using the MPN method, are displayed in Figure 6.1.

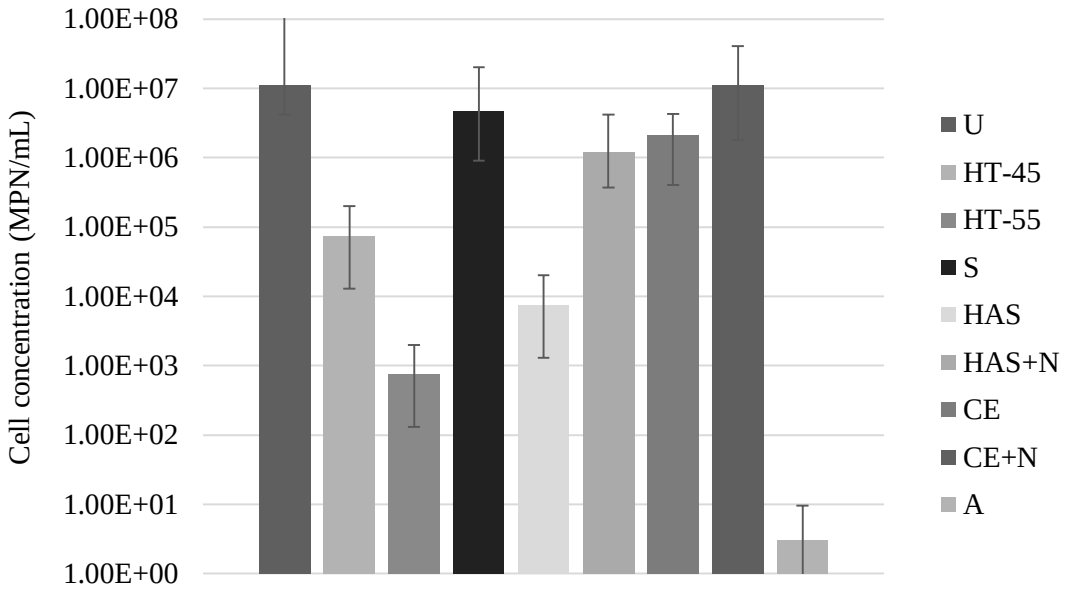

Figure 6.1: Total viable cell concentration in each sample set estimated by Most Probable Number (MPN). Error bars represent the upper and lower 95% confidence limits.

It is apparent from Figure 6.1 that most treated sample sets contained a lower concentration of viable cells (as measured by MPN) as compared to the untreated sample set. The autoclaved cells (A sample set) did not yield any detectable turbidity, which indicated that if there were any microorganisms present, the concentration was lower than the detectable limit [170]. Of the remaining sample sets, HT-55 and HAS exhibited the most noticeable reductions in total viable cell concentration, while HT-45, S, HAS+N, CE, and CE+N retained a greater cell concentration.

6.4.2 Urea Hydrolysis

Percentages of urea consumed, which were calculated from NH_3 measurements as described in Section 6.3.2, for the each of the sample sets described in Table 6.1 are presented in Figure 6.2.

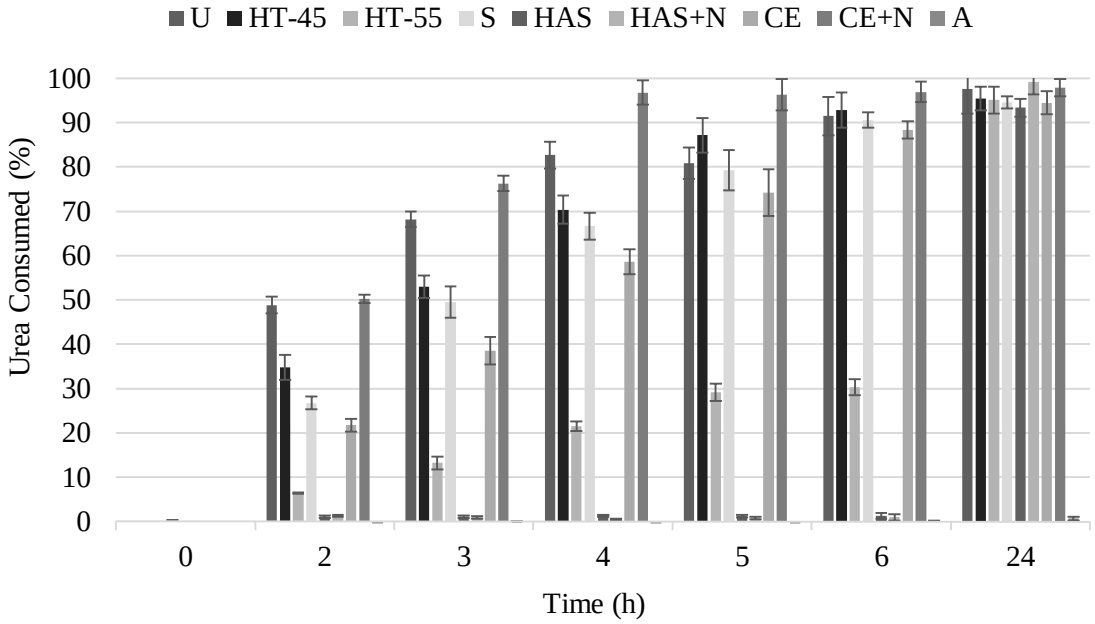

Figure 6.2: Urea consumed in UYE medium at 30°C with shaking by *S. pasteurii* for each sample set (obtained by calculation). Error bars represent the standard deviation of triplicate cultures.

From Figure 6.2, it is evident that urea hydrolysis by *S. pasteurii* cells was kinetically impeded in all treated sample sets as compared to the untreated sample set with the exception of CE+N, and these results are in good agreement with the viability results presented in Figure 6.1. After U and CE+N sample sets; S, HT-45, and CE exhibited the strongest urease activity and these samples were able to match the NH_3 concentration in the untreated sample set within 5 hours of incubation. Contrastingly, HT-55 cultures induced urea hydrolysis at a noticeably reduced rate for the first 6 hours of incubation, while HAS, HAS+N, and A did not exhibit any increase in NH_3 concentration during the first 6 hours. However, after 24 hours of incubation, all of the sample sets except A were able to recover and decompose close to 100% of the urea available in their medium.

Results in Figure 6.2 showed that the treatment employed in the CE+N sample set did not inhibit the rate of urea hydrolysis by *S. pasteurii*, and treatments employed in the S, HT-45, and CE sample sets caused a slight reduction in the rate of urea hydrolysis. For the heat-treated samples, reduction in the rate of urea hydrolysis became much more pronounced when the temperature was increased from 45°C (HT-45) to 55°C (HT-55). However, with the exception of autoclaved cells, which did not exhibit any urease activity for the entire 24-hour period, the rate of urea hydrolysis was most dramatically impacted in the HAS and HAS+N sample sets. These samples, which were exposed to pH 13.6 for four hours, did not show any increase in NH_3 concentration during the first 6 hours of incubation in fresh medium, which might be due to pH shock. However, the cells in these samples were able to recover and hydrolyze nearly 100% of the urea available in their medium after 24 hours of incubation.

These observations provided useful information about the potential for vegetative bacterial cells to produce carbonates *in situ* in bacterial concrete. It appears that concrete might be a suitable environment for these microorganisms to inhabit, but it is essential that care is taken to mitigate heat generation since the increase of heat exposure from 45°C to 55°C resulted in a marked decrease in viability and the rate of urea hydrolysis by *S. pasteurii* cells. This could be achieved through the use of low heat cements and/ or supplementary cementing materials such as fly ash [172]. Further, the increase of pH from 12.9 (CE and CE+N; generated by mixing cement and water) to 13.6 (HAS and HAS+N; a solution containing KOH and NaOH) temporarily halted urease activity. Thus, in microbial concrete applications where the concrete will contain vegetative microorganisms, care should be taken to avoid use of cements with high alkali contents and/or high gypsum contents that tend to increase the pH [173].

6.4.3 Electrophoretic Mobility and Zeta Potential

Results of electrophoretic mobility measurements are presented in Table 6.2, and corresponding zeta potential values are presented in Figure 6.3.

Table 6.2: Electrophoretic mobility of *S. pasteurii* (in pH 9 Tris buffer at 23°C) at 0, 3, 7, and 28 days after treatment. Error represents the standard deviation of triplicate cultures.

Sample Set	**Electrophoretic Mobility (µm-cm/V-s)**			
	0 days	**3 days**	**7 days**	**28 days**
U	-2.79 ± 0.22	-2.77 ± 0.07	-2.60 ± 0.13	-2.81 ± 0.09
HT-45	-2.41 ± 0.11	-2.20 ± 0.22	-2.61 ± 0.11	-2.29 ± 0.10
HT-55	-2.43 ± 0.22	-2.18 ± 0.15	-2.30 ± 0.13	-2.55 ± 0.17
S	-2.23 ± 0.11	-2.52 ± 0.20	-2.38 ± 0.23	-2.55 ± 0.11
HAS	-2.65 ± 0.06	-2.65 ± 0.22	-2.61 ± 0.07	-2.51 ± 0.07
HAS+N	-2.15 ± 0.08	-2.57 ± 0.22	-2.51 ± 0.12	-2.33 ± 0.09
A	-2.64 ± 0.05	-2.61 ± 0.12	-2.48 ± 0.19	-2.54 ± 0.15

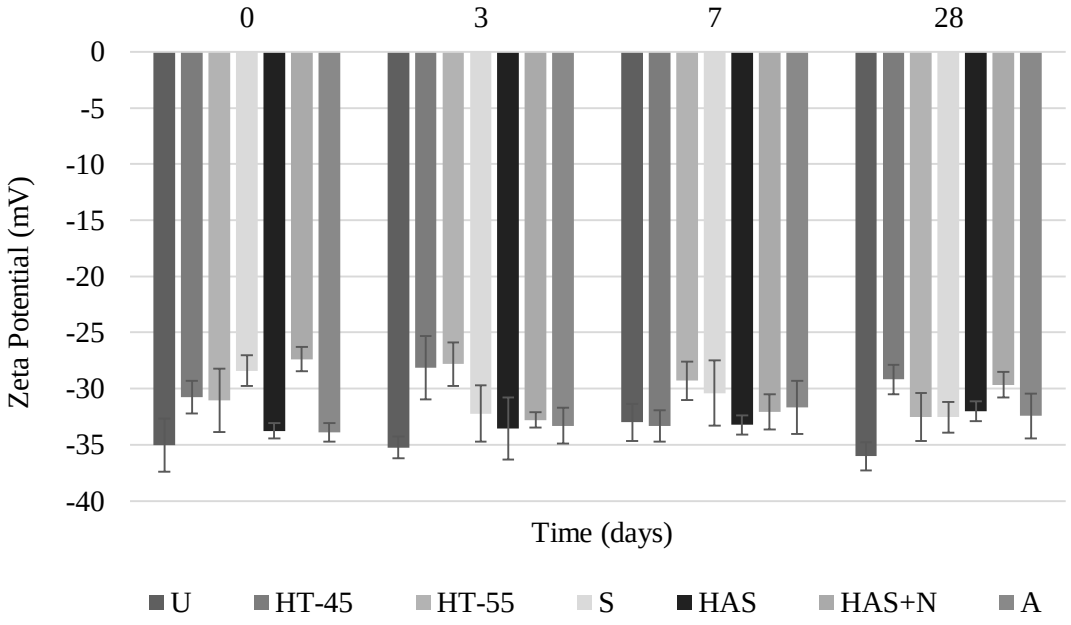

Figure 6.3: Zeta potential of *S. pasteurii* (in pH 9 Tris buffer at 23°C) at 0, 3, 7, and 28 days after treatment. Error bars represent the standard deviation of triplicate cultures.

S. pasteurii cells harvested from each sample set exhibited similar zeta potential values, indicating that cells exposed to heat, lack of nutrients, high pH, and autoclaving maintained a robust negative surface charge similar to that of the untreated cells. The zeta potential of *S. pasteurii* cells also was reasonably constant for up to 28 days in each sample set, indicating that even stressed or dead cells could sustain a negative surface charge over time. Surface charge is considered to be an influential parameter in the nucleation process of minerals, and it has been proposed that bacterial cells in cement paste could promote calcium carbonate precipitation by serving as nucleation sites [46, 109, 140]. Interestingly, if this mechanism can occur, it seems that all cells, even weakened or dead cells, could contribute to calcium carbonate formation by providing sites for heterogeneous nucleation to occur.

6.4.4 XRD

Using the primary calcite and primary zincite intensity data in Table 6.3, the mass percentages of calcite were calculated for select samples (Figure 6.4).

Table 6.3: Intensities of primary calcite and zincite peaks, and calcite intensity divided by zincite intensity at 1 day. Error represents the standard deviation of triplicate samples.

Paste sample	**Primary calcite peak intensity**	**Primary zincite peak intensity**	**Primary calcite intensity/ primary zincite intensity**
Neat	2627 ± 174	6443 ± 154	0.408 ± 0.037
Nutrient	3253 ± 255	6687 ± 263	0.488 ± 0.058
Spent Nutrient	2926 ± 61	6738 ± 267	0.434 ± 0.024
Bacterial- U	4287 ± 138	5305 ± 263	0.810 ± 0.051
Bacterial- A	3611 ± 872	5640 ± 770	0.634 ± 0.080

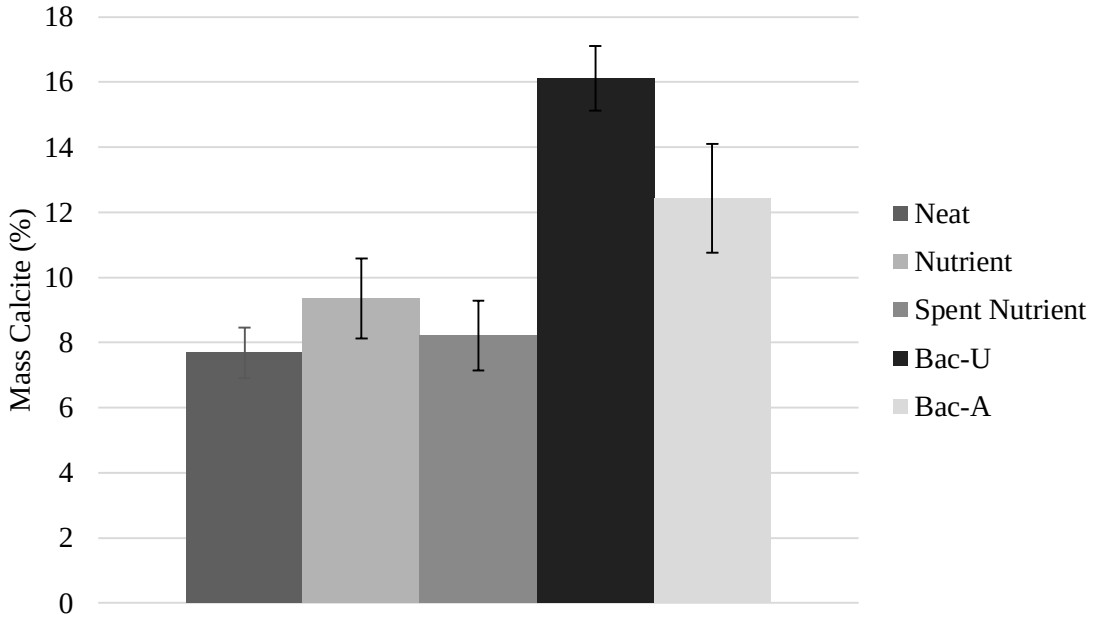

Figure 6.4: Mass percentages of calcite at 1 day. Error bars represent the standard deviation of triplicate samples. Bac-U: Bacterial- untreated. Bac-A: Bacterial- Autoclaved.

From Figure 6.4, calcite content increased considerably in the bacterial pastes as compared to neat, nutrient, and spent nutrient pastes at 1 day, and this increase could be attributed to MICCP by *S. pasteurii* cells. As compared to neat paste, untreated bacterial paste and autoclaved bacterial paste contained 110% and 62% more calcite, respectively. Interestingly, calcite content increased in the autoclaved paste relative to the neat paste despite the fact that autoclaved sample sets showed no urease activity when resuspended in fresh UYE medium after autoclaving (Section 6.4.2). Because the autoclaved cells could not continue urea hydrolysis after the autoclaving process, this increase in calcite is likely attributable to carbonate production by urease that occurred prior to autoclaving. However, no substantial increase in calcite concentration was observed in spent nutrient paste even though it theoretically contained the same concentration of carbonate as the

autoclaved paste. This suggests that the presence of dead cells, which maintained a negative surface charge as indicated by zeta potential measurements, might have promoted the formation of calcite by serving as nucleation sites.

Chapter 7: Optimization of Nutrient Medium for *S. pasteurii* in Microbial Concrete

7.1 INTRODUCTION

To mitigate the delay in cement hydration kinetics caused by addition of vegetative microorganisms and growth medium described in Section 2.5, alternative carbon sources were explored to replace yeast extract as an electron donor in the growth medium because yeast extract has been shown specifically to retard cement hydration [47, 54]. Previous studies have addressed identifying alternative nutrient sources for bacteria in microbial concrete [108, 109], but none of these studies have examined the effects of these nutrients on hydration kinetics. Instead, attention has focused primarily on the use of waste materials as nutrients. This approach is advantageous from an environmental standpoint, and it also has been postulated that the use of waste materials to replace commercial nutrients could alleviate the substantial costs associated with these commercial nutrients [108, 109]. However, further cost analysis must be carried out to support this claim. While using waste materials for nutrients might reduce the material costs for microbial concrete, other drawbacks associated with the use of waste materials must be considered. For instance, the chemical composition and physical properties of waste materials tend to vary considerably due to irregularities and variations in processing [174]. As such, extensive quality control and/ or processing of waste materials might be required prior to use in microbial concrete since growth behavior of the microorganisms and fresh state properties of the concrete could be heavily influenced by variation of the waste materials.

To address this concern, which might limit the use of microbial concrete in the construction industry, the influence of alternative carbon sources on cement hydration was explored, and the chemical constituents of the growth medium were optimized to minimize retardation of hydration. Results were used to develop an improved medium for *S. pasteurii*

that is less impactful on hydration while maintaining similar bacterial growth behavior, urease activity, and zeta potential.

7.2 MATERIALS

7.2.1 Microorganism

S. pasteurii was used in this study, and the microorganisms were cultured according to the procedure described in Section 3.3.

7.2.2 Cement

Texas Lehigh Type I/II (Buda, TX) portland cement was used in this study, and the mass composition of oxides was presented in Table 4.1 (Section 4.2.2).

7.2.3 Carbon Sources

In addition to yeast extract, six alternative carbon sources were examined: lactose mother liquor, corn steep liquor, meat extract, glucose, L-arginine, and sodium acetate. This group of potential carbon sources was selected to provide substantial variety, including both complex and defined carbon sources. Lactose mother liquor, corn steep liquor, and meat extract are complex carbon sources, meaning that their exact chemical composition is unknown; glucose, L-arginine, and sodium acetate are defined carbon sources because they are of known composition.

7.3 EVALUATION OF CARBON SOURCES

7.3.1 Growth Tests

The effects of each of the six compounds (Section 7.2.3) on microbial growth were examined by replacing yeast extract in *S. pasteurii* growth medium with each prospective carbon source on an equal mass basis. Therefore, each medium contained 20 g/L of the carbon source, 10 g/L of urea, and 15.75 g/L of Tris base (pH 9). *S. pasteurii* was grown

in 200 μL of each medium in a 96-well plate at 30°C with shaking. Five wells were inoculated for each medium, and absorbance at 600 nm (OD_{600}) was recorded hourly using a BIO-TEK Synergy HT spectrophotometer (Winooski, VT, United States). The growth profiles, averaged from the five replicates, are presented in Figure 7.1.

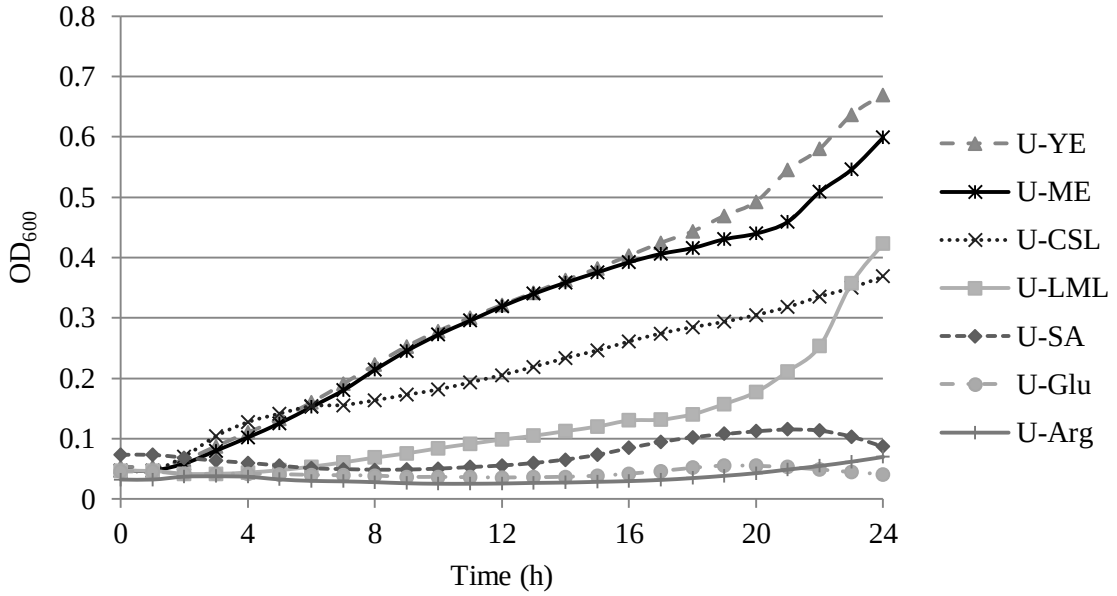

Figure 7.1: Growth of *S. pasteurii* (averaged from five replicates) at 30°C in media containing 15.75 g/L Tris base (pH 9), 10 g/L urea, and 20 g/L of a carbon source; U: urea, YE: yeast extract, ME: meat extract, CSL: corn steep liquor, LML: lactose mother liquor, SA: sodium acetate, Glu: glucose, Arg: L-arginine.

As compared to the media with yeast extract, meat extract, corn steep liquor, or lactose mother liquor, the media with sodium acetate, glucose, or arginine did not produce substantial bacterial growth as measured by OD_{600}. This indicated that while each of the complex carbon sources were good sources of nutrients that could support growth, substantial growth could not occur in a buffered solution with urea and a defined carbon source. Although *S. pasteurii* might have the ability to use these defined sources, the

buffered medium might be missing an essential element or vitamin that is present in the complex carbon sources [175].

7.3.2 Isothermal Calorimetry

To examine the effects of the alternative carbon sources on hydration, isothermal calorimetry was performed on a neat paste and carbon source pastes. Neat paste refers to a mixture that is prepared with distilled water and cement; carbon source pastes are prepared with the carbon source solution (20 g/L of carbon source dissolved in water) and cement. Pastes were prepared by mixing 16 g of cement with either 8 g of distilled water (for neat pastes) or 8 g of the carbon source solution by hand for 2 min. Thus, the solution-to-cement ratio (s/c) for all pastes was 0.50 by mass. Immediately after a paste sample was prepared, 20 g of the sample were placed in a 3114/3236 TAM Air Thermal, Thermometric AB Isothermal Calorimeter (Sweden) for 45 hours. The temperature was maintained at 23°C during the testing. Triplicate specimens were prepared for neat paste and for each carbon source paste.

At the initial tested carbon source concentration of 20 g/L (2%), lactose mother liquor and glucose did not exhibit any increase in the rate of heat generated during the 45-hour testing period, which indicated that hydration was severely retarded by these substances. As such, isothermal calorimetry was repeated for lactose mother liquor and glucose at a lower concentration of 10 g/L (1%) to produce useful data for comparative purposes. These results are presented in Figure 7.2, and the degree of retardation varied considerably among the carbon sources.

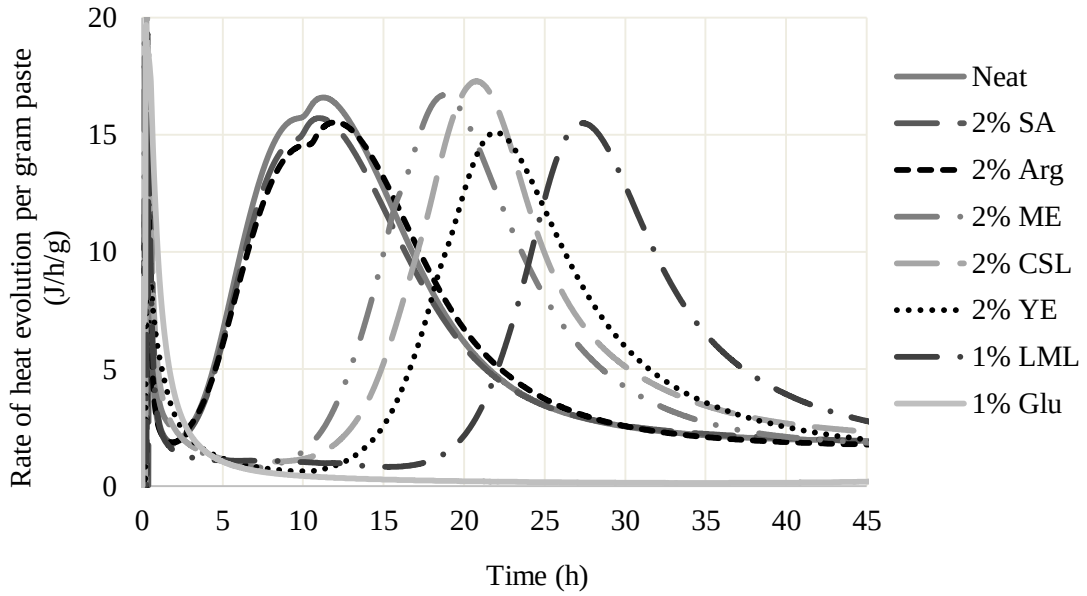

Figure 7.2: Rate of heat evolution (averaged from duplicate samples) for carbon source pastes with an s/c of 0.50; YE: yeast extract, ME: meat extract, CSL: corn steep liquor, LML: lactose mother liquor (tested at reduced concentration of 1%), SA: sodium acetate, Glu: glucose (tested at reduced concentration of 1%), Arg: L-arginine.

From Figure 7.2, cement paste mixed with sodium acetate and L-arginine additions did not exhibit any substantial retardation as compared to neat paste. However, the addition of glucose caused severe retardation even at a 1% (w/w) concentration, which was expected because sugars are effective retarders [176]. As such, glucose was removed from consideration at this time. Although L-arginine did not have any negative effects on hydration, it also was removed from consideration because Figure 7.1 showed that L-arginine did not lead to bacterial growth in the defined medium tested.

In contrast to the defined carbon sources, each of the complex carbon sources caused substantial retardation, particularly lactose mother liquor. However, substantial bacterial growth was observed when yeast extract was replaced with 2% (w/w) of meat extract, corn steep liquor, or lactose mother liquor (Figure 7.1). As such, reducing the

concentration of these substances might be possible, which could lessen the impact on hydration.

7.3.3 Chemical Oxygen Demand (COD)

COD was measured for prospective carbon sources. The reactor digestion method [177] was used, and potassium hydrogen phthalate (KHP) was used as the standard. Table 7.1 displays the measured COD of each carbon source.

Table 7.1: COD of yeast extract, meat extract, corn steep liquor, lactose mother liquor, and sodium acetate. Error represents the standard deviation of triplicate measurements.

Carbon Source	**COD (mg O_2/ mg substance)**
Yeast Extract	0.584 ± 0.005
Meat Extract	0.660 ± 0.010
CSL	0.274 ± 0.005
LML	0.200 ± 0.022
Sodium Acetate	0.397 ± 0.001

Both corn steep liquor and lactose mother liquor exhibited a lower COD per mg than did yeast extract. As an electron donor, a higher mass concentration of corn steep liquor or lactose mother liquor would be needed to be equivalent to 2% (w/w) yeast extract. This is reflected in work by Achal [109] where 10% (w/w) lactose mother liquor was used when it served as the sole carbon source. Because increasing the concentration of corn steep liquor and lactose mother liquor in the growth medium would likely exacerbate the substantial retardation that these substances caused at a concentration of 2% (w/w), corn steep liquor and lactose mother liquor were removed from consideration. On the other hand, the meat extract contains 13% more COD per unit mass as compared to the yeast extract, such that 17.7 g/L meat extract provides equivalent COD to the 20 g/L yeast extract specified in the ATCC recommended medium for 6453 *S. pasteurii*.

7.4 GROWTH MEDIA SELECTION

Based on results presented in Section 7.3, two alternative media were developed for exploration in this study to compare with Urea-Yeast Extract (UYE) medium (Table 7.2). UYE medium is a modified version of the optimal medium recommended by ATCC, and it was created by replacing ammonium sulfate with urea on an equal mass basis. Urea-Meat Extract (UME) medium was developed on the basis of providing equal COD as the UYE medium, and the yeast extract was replaced with 17.7 g/L meat extract. Finally, a hybrid medium, Urea-Meat Extract-Sodium Acetate (UME-SA) medium, was developed from UME medium by reducing meat extract content by half (to 8.85 g/L) and adding 15 g/L sodium acetate.

All media (i.e., UYE, UME and UME-SA) were prepared by dissolving Tris base in 1-liter distilled, deionized (DDI) water and adjusting the pH to 9 with hydrochloric acid. The Tris base solution was then divided into two aliquots, and urea was added to one aliquot. Yeast extract, meat extract, or meat extract and sodium acetate were added to the other aliquot, and the mixtures were autoclaved separately per recommendation by ATCC. After sterilization, the solution containing urea and the solution containing the carbon source and electron donor (yeast extract, meat extract, or meat extract and sodium acetate) were kept at room temperature (23°C) and combined after cooling.

Table 7.2: Compositions of UYE, UME, and UME-SA media per liter DDI water.

Medium	**pH**	**Tris base (g)**	**Urea (g)**	**Yeast Extract (g)**	**Meat Extract (g)**	**Sodium Acetate (g)**
UYE	9	15.75	10	20	-	-
UME	9	15.75	10	-	17.7	-
UME-SA	9	15.75	10	-	8.85	15

7.5 METHODS TO EXAMINE PERFORMANCE OF GROWTH MEDIA

Following the analysis of carbon sources and media selection, each media was examined using the following experimental methods: isothermal calorimetry, growth tests, urease activity, zeta potential, and quantitative X-ray diffraction (XRD). An overview of these methods is provided in Sections 7.5.1–7.5.5. Isothermal calorimetry was carried out to determine how each medium (Table 7.2) would impact cement hydration. Then, growth curves were obtained to verify growth in each medium; urease activity and zeta potential were used to gain insight to the metabolic activity and surface charge, respectively, of the cells in each medium. Finally, quantitative XRD was employed to assess the amount of calcite precipitated in bacterial cement pastes with each medium and neat cement paste.

7.5.1 Isothermal Calorimetry

Isothermal calorimetry was performed according to the procedure described in Section 7.3.2; in addition to neat paste, nutrient pastes also were examined. Nutrient paste refers to a mixture that was prepared with nutrient medium and cement. The solution-to-cement ratio (s/c) for all pastes was 0.50 by mass, and triplicate specimens were prepared for each sample type.

7.5.2 Growth Profiles

To examine growth of *S. pasteurii* in each medium, OD_{600} for triplicate 100-mL bacterial cultures in 250-mL flasks was recorded for 24 hours.

7.5.3 Urea Hydrolysis

S. pasteurii cells were grown in each medium until the stationary growth period was reached, and the urease activity in each culture was examined according to the procedure described in Section 6.3.2.

7.5.4 Electrophoretic Mobility and Zeta Potential

Electrophoretic mobility and zeta potential of *S. pasteurii* cells grown in each medium were determined according to the procedure described in Section 6.3.3.

7.5.5 XRD

XRD was conducted to quantify calcite in select samples according to the Reference Intensity Ratio (RIR) procedure described in Section 5.2.4. Three types of pastes were prepared:

- Neat paste: prepared with distilled water and cement;
- Nutrient paste: prepared with UYE, UME, or UME-SA medium and cement;
- Bacterial paste: prepared with *S. pasteurii* cells grown in UYE, UME, or UME-SA medium to OD_{600}=0.6 and cement;

The paste samples were prepared according to the procedure described in Section 5.2.4. Calcite was quantified in each sample using the equation Y = 0.0476X + 0.0427, which was obtained from the RIR standard curve (Figure 5.1), where Y is the intensity of the primary calcite peak divided by the intensity of the primary zincite peak and X is wt. % calcite.

7.5.6 Statistical Analysis

A two-sample t-test with one-tailed distribution [178] was carried out to determine whether the mean value of calcite content in bacterial pastes was greater than the mean value of calcite content in nutrient (non-bacterial) pastes. Thus, the hypothesis for this t-test was that the mean mass % calcite content was higher in bacterial cement paste samples than the mean mass % content in nutrient cement paste samples, and the null hypothesis was that there was no difference between the mean mass % calcite content in bacterial

cement paste samples and nutrient cement paste samples. An alpha of 0.01 was used for all t-tests, and critical values of t were obtained from standard tables [179].

7.6 RESULTS AND DISCUSSION

7.6.1 Isothermal Calorimetry

Results of isothermal calorimetry for neat cement paste, UYE nutrient paste, UME nutrient paste, and UME-SA nutrient paste are presented in Figure 7.3, where the curves are averages of triplicate samples.

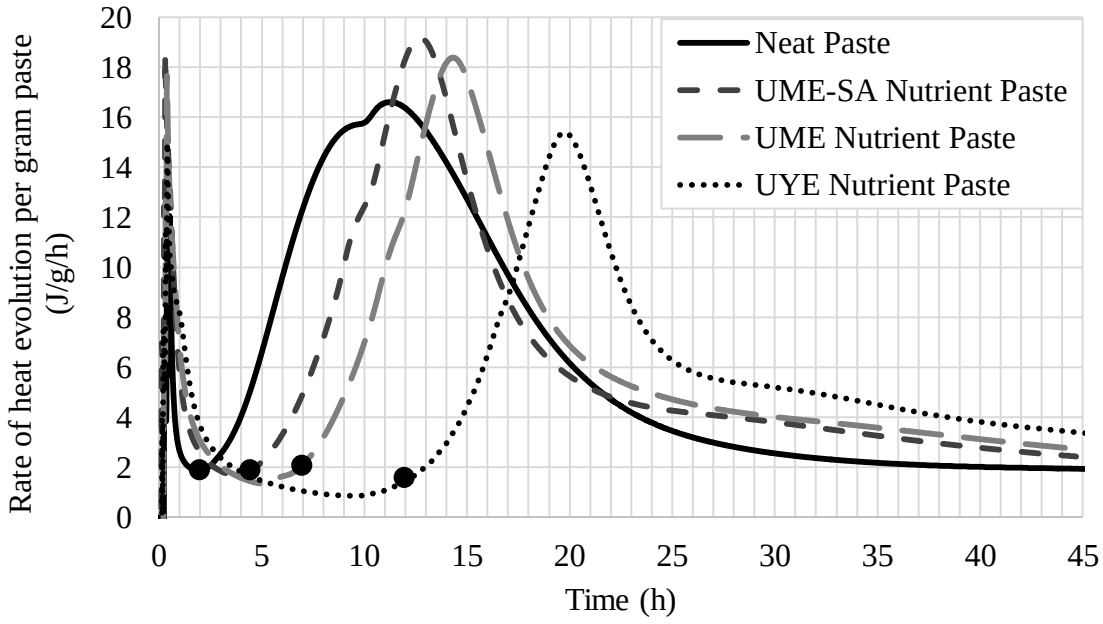

Figure 7.3: Rate of heat evolution (averaged from triplicate samples) for neat, UYE nutrient, UME nutrient, and UME-SA nutrient pastes with an s/c of 0.50. Solid circles represent the end of the induction period for each paste.

From Figure 7.3, the beginning of the acceleratory period (or similarly, the end of the induction period) occurred at approximately 2 hours for neat paste, 4.5 hours for UME-SA nutrient paste, 7 hours for UME nutrient paste, and 12 hours for UYE nutrient paste. Therefore, compared to neat paste, the induction periods for UME-SA, UME, and UYE

nutrient pastes were extended by 2.5, 5, and 10 hours, respectively. Thus, the use of UME-SA medium in nutrient paste reduced the extension in the induction period by 75% compared to standard UYE medium and the use of UME medium in nutrient paste reduced the extension in the induction period by 50% compared to standard UYE medium.

These data indicate that UME-SA medium and, to a lesser extent, UME medium are more desirable than is UYE medium with respect to the criterion of hydration. However, further experimentation was necessary to determine whether UME-SA and UME cultures could effectively induce $CaCO_3$ precipitation in cement paste; these concerns are addressed in Sections 7.6.2 - 7.6.5.

7.6.2 Growth Profiles

Figure 7.4 shows the growth curves for *S. pasteurii* in UYE, UME, and UME-SA media, and substantial growth occurred in all media. Therefore, from a bacterial growth standpoint, these three media are viable options for biomineralization applications. However, it should be noted that the rate and magnitude of growth appeared to be lesser in UME medium as compared to UYE medium and UME-SA medium, and that UME-SA cultures reached a higher final optical density than did UYE and UME cultures at 24 hours.

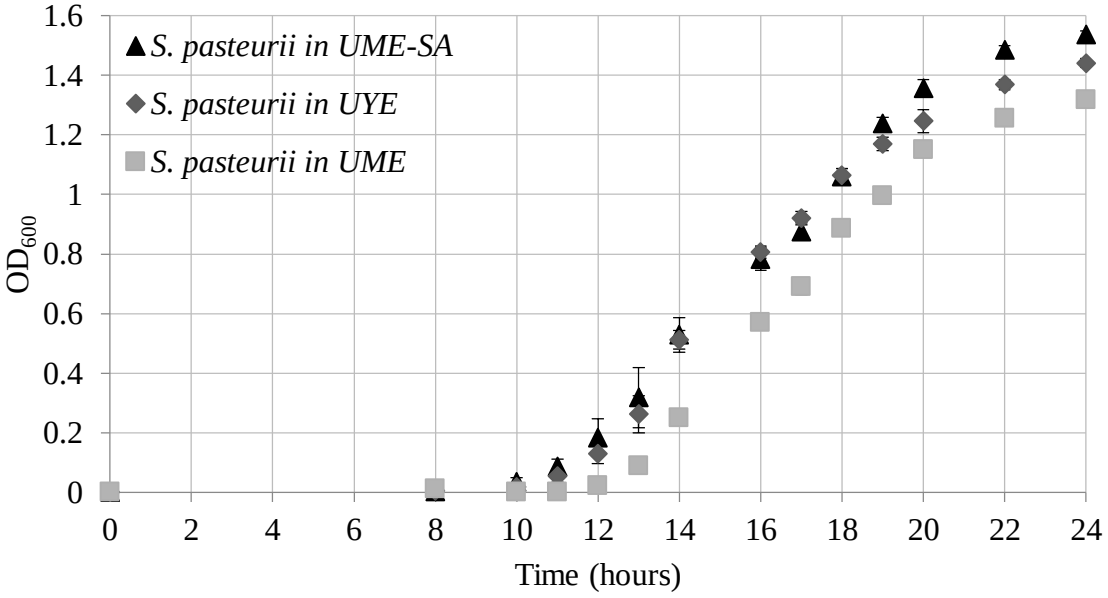

Figure 7.4: Growth profiles for *S. pasteurii* at 30°C in UME-SA, UYE and UME media. Error bars represent the standard deviation of triplicate cultures.

7.6.3 Urea Hydrolysis

The amounts of urea consumed by *S. pasteurii* urease in each medium, which was calculated from measured NH_3 concentrations as described in Section 6.3.2, are presented in Figure 7.5.

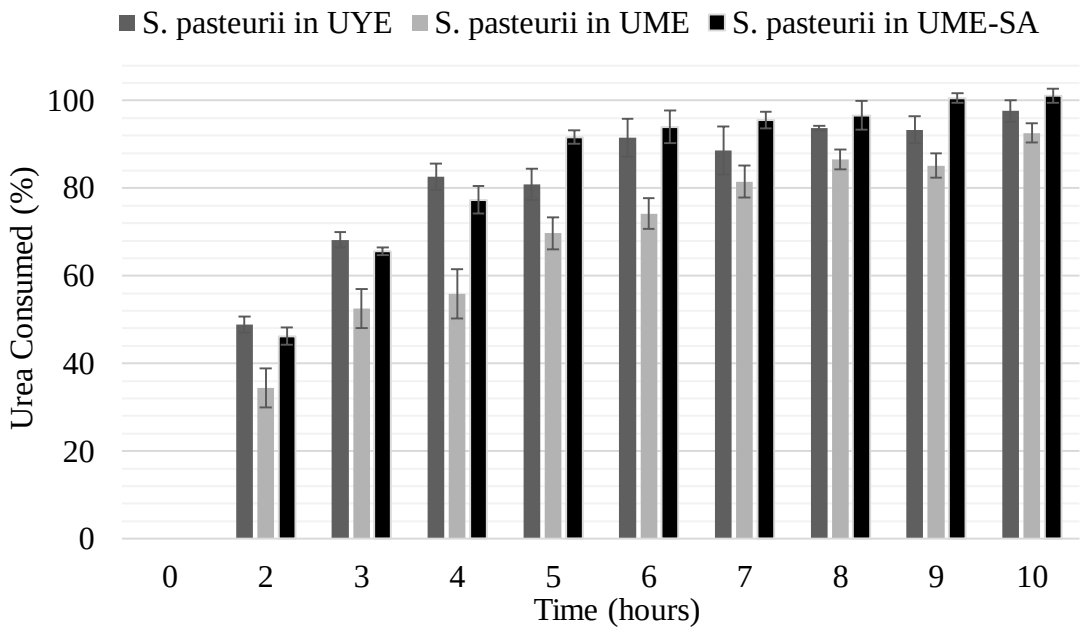

Figure 7.5: Percent urea consumed by *S. pasteurii* in at 30°C UYE, UME, and UME-SA media (obtained by calculation). Error bars represent the standard deviation of triplicate cultures.

From Figure 7.5, *S. pasteurii* behaved similarly in each medium, but the ammonia concentration increased more rapidly in the UYE and UME-SA cultures as compared to the UME culture. This suggests that urease activity in the UYE and UME-SA cultures was generally greater than that in the UME culture. However, since substantial urease activity was present in all three cultures, all three media are viable for biomineralization applications from a urease activity standpoint.

7.6.4 Electrophoretic Mobility and Zeta Potential

S. pasteurii has been assumed to possess a negative surface charge [45], and it has been suggested that this charge can attract positively charged calcium ions and induce $CaCO_3$ precipitation through heterogeneous nucleation on the bacterial cell walls [42, 46, 86, 109, 140]. Results of electrophoretic mobility and zeta potential measurements are

presented in Table 7.3. *S. pasteurii* exhibited a similar zeta potential in UYE, UME, and UME-SA media. *S. pasteurii* cells exhibited a substantially more negative zeta potential as compared to cement particles, which supports the idea that bacterial cells are good sites for heterogeneous nucleation of $CaCO_3$. Another factor that might positively influence the nucleation process is the small size of the bacteria cells. Rod-shaped *S. pasteurii* cells have been reported as ranging from 1.3 to 4.0 μm in length and 0.5 to 1.2 μm in diameter [111]. In general, the heterogeneous nucleation process is accelerated in the presence of smaller particles because of their greater surface area for attachment [180, 181].

Table 7.3: Electrophoretic mobility and zeta potential for *S. pasteurii* grown in UYE, UME, or UME-SA media and for cement particles in pH 9 Tris buffer at 23°C. Error represents the standard deviation of triplicate samples.

Sample Type	**Electrophoretic Mobility (μm-cm/V-s)**	**Zeta Potential (mV)**
S. pasteurii grown in UYE	-2.79 ± 0.22	-35.6 ± 2.8
S. pasteurii grown in UME	-2.56 ± 0.30	-32.7 ± 3.8
S. pasteurii grown in UME-SA	-2.55 ± 0.11	-32.5 ± 1.3
Cement	-0.08 ± 0.02	-1.0 ± 0.3

7.6.5 XRD and Statistical Analysis

Calcite was the only calcium carbonate polymorph observed in each of the pastes, and intensities of the primary calcite and zincite peaks in each sample as well as the primary calcite intensity divided by the primary zincite intensity are presented in Table 7.4. For all samples, the primary calcite and zincite peaks were observed within the range of 29.4-29.8 °2θ and 36.2-36.6 °2θ, respectively. As previously stated, the equation $Y = 0.0476X + 0.0427$, where Y is the intensity of the primary calcite peak divided by the intensity of the primary zincite peak and X is wt. % calcite, was used to quantify the mass percentage of calcite in each sample. Figure 7.6 displays the calculated mass percentages of calcite.

Table 7.4: Intensities of primary calcite and zincite peaks, and primary calcite intensity divided by primary zincite intensity at 1 day. Error represents the standard deviation of triplicate samples.

Sample Type	**Primary Calcite Peak Intensity**	**Primary Zincite Peak Intensity**	**Primary Calcite Intensity/ Primary Zincite Intensity**
Neat Paste	2627 ± 174	6443 ± 154	0.408 ± 0.037
Nutrient Paste: UME	2369 ± 702	5028 ± 701	0.464 ± 0.073
Nutrient Paste: UYE	3253 ± 255	6687 ± 263	0.488 ± 0.058
Nutrient Paste: UME-SA	2116 ± 387	4751 ± 606	0.444 ± 0.043
Bacterial Paste: *S. pasteurii* in UME	3780 ± 221	5327 ± 223	0.712 ± 0.072
Bacterial Paste: *S. pasteurii* in UYE	4287 ± 138	5304 ± 262	0.810 ± 0.051
Bacterial Paste: *S. pasteurii* in UME-SA	3794 ± 49	5950 ± 611	0.642 ± 0.058

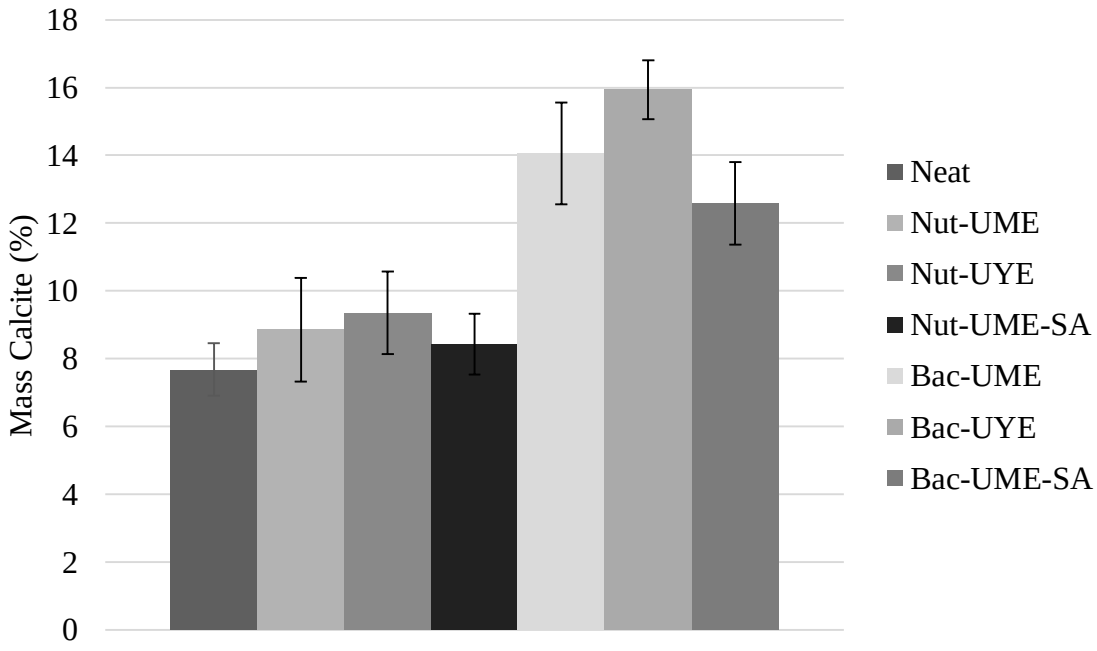

Figure 7.6: Mass percentages of calcite at 1 day. Error bars represent the standard deviation of triplicate samples. Neat: Neat paste. Nut: Nutrient paste. Bac: Bacterial paste.

From Figure 7.6, calcite content increased substantially in all three of the bacterial pastes as compared to neat and nutrient pastes at 1 day. In fact, the bacterial pastes with UME, UYE, and UME-SA media increased their average calcite content by 58.6%, 70.4%, and 49.3%, respectively, as compared to their corresponding nutrient pastes at 1 day. Taken together, the results presented in Sections 7.6.2-7.6.5 suggest that *S. pasteurii* can utilize the nutrients provided in UME, UYE, and UME-SA media to produce carbonate and induce calcite precipitation.

A t-test was performed to determine whether the mean mass % calcite content was higher in bacterial paste samples as compared to nutrient paste samples using the data presented in Table 7.5. Prior to performing the t-tests, the normality of these data was analyzed using the Shapiro-Wilk test [182], and it was determined that each data set was normally distributed.

Table 7.5: Mass % calcite in nutrient pastes and bacterial pastes.

	Nutrient pastes	**Bacterial pastes**
Number of samples	9	9
Mean (% calcite)	8.88	14.19
Standard deviation	1.15	1.80
Variance	1.32	3.25

A value of 7.02 was calculated for t, and a value of 2.92 was obtain for $t_{critical}$ from standard tables [179] using the chosen alpha and the total calculated degrees of freedom (alpha = 0.01, df = 16). Since $t > t_{critical}$, the null hypothesis was rejected and it was determined that the mean mass % calcite for all bacterial pastes was greater than the mean mass % calcite for all nutrient pastes.

Chapter 8: Evaluation of Vegetative *S. pasteurii* as a Repair Material and Self-Healing Agent for Flexural Cracks in Mortar

8.1 INTRODUCTION

It has been widely recognized that microbial-induced calcium carbonate precipitation (MICCP) can be used to seal cracks in cement-based materials by externally or internally introducing bacteria to the system, but little attention has been aimed at investigating the capacity of this process to provide strength recovery. An important distinction exists between the processes of crack-sealing and crack-healing that has been often overlooked in the literature. Crack-sealing refers to the recovery of transport properties such as permeability and diffusivity, while crack-healing refers to the recovery of mechanical properties such as strength and stiffness in addition to transport properties [1].

Ramachandran et al. [66] and Basaran [52] investigated the ability of *S. pasteurii* to provide compressive strength recovery by remediating saw-cut cracks and internal cracks, respectively, in mortar cubes with promising results. Ramachandran et al. [66] also cut cracks with a width of 3.175 mm in mortar beams and subsequently filled the cracks with a mixture of sand and *S. pasteurii*. After 28 days, a greater stiffness was observed in beams treated with bacteria and sand then beams that were not treated and instead left exposed to air. However, information about strength recovery was not reported.

In this study, to provide information about the efficacy of vegetative *S. pasteurii* as a repair material and self-healing agent for flexural cracks in mortar, neat mortar beams and bacterial mortar beams were loaded in a three-point bending configuration until failure. Then, the beams were subjected to various bacteria-based treatments and crack sealing was monitored for 28 days using ultrasonic pulse velocity. Finally, 28 days after treatment, the

beams were tested in flexure again to assess strength recovery due to the bacterial treatments.

8.2 MATERIALS AND METHODS

8.2.1 Cement

Texas Lehigh Type I/II (Buda, TX) portland cement was used in this study, and the mass composition of oxides was presented in Table 4.1 (Section 4.2.2).

8.2.2 Fine Aggregate

Colorado River sand was used as the fine aggregate in this study, and the mineralogical properties of this sand were described in Section 4.2.3. The sand was passed through a No. 4 sieve prior to mixing such that the particles were finer than 4.75 mm.

8.2.3 Sample Matrix

Three types of 1 in. x 1 in. x 8 in. mortar beams were prepared: neat beams, UYE bacterial beams, and UME-SA bacterial beams. The mixture proportions for these beams are described in Table 8.1. The solution-to-cement (s/c) ratio was 0.50 by mass, and the cement-to-sand ratio was 1:4 by mass.

Table 8.1: Mortar bar mix proportions.

Sample Set	**Cement (g)**	**Sand (g)**	**Water (g)**	***S. pasteurii* in UYE (g)**	***S. pasteurii* in UME-SA (g)**
Neat mortar	1200	4800	600	0	0
UYE bacterial mortar	1200	4800	0	600	0
UME-SA bacterial mortar	1200	4800	0	0	600

Ten different treatment groups were used to evaluate the ability of bacterial beams to self-heal after flexural cracks were induced and to evaluate a wide range of bacteria-based repair treatments for these cracks; these groups are summarized in Table 8.2. Each

type of treatment was performed using standard UYE medium and the optimized UME-SA medium developed in Chapter 7. $CaCl_2$ was used as the calcium source based on results presented in Chapter 5, where bacterial cultures with inoculated with $CaCl_2$ yielded more stale (less soluble) calcium carbonate than bacterial cultures inoculated with $Ca(C_2H_3O_2)_2$.

Table 8.2: Summary of samples.

Group	**Treatment description**
Neat beams (A)	
A1	Spray with UYE bacterial solution + 0.167 M $CaCl_2$
A2	Spray with UME-SA bacterial solution + 0.167 M $CaCl_2$
A3	Apply paste of pelleted cells and spray with UYE nutrient solution + 0.167 M $CaCl_2$
A4	Apply paste of pelleted cells and spray with UME-SA nutrient solution + 0.167 M $CaCl_2$
UYE bacterial beams (B)	
B1	Spray with UYE nutrient solution + 0.167 M $CaCl_2$
B2	Spray with UYE bacterial solution + 0.167 M $CaCl_2$
B3	Apply paste of pelleted cells and spray with UYE nutrient solution + 0.167 M $CaCl_2$
UME-SA bacterial beams (C)	
C1	Spray with UME-SA nutrient solution + 0.167 M $CaCl_2$
C2	Spray with UME-SA bacterial solution + 0.167 M $CaCl_2$
C3	Apply paste of pelleted cells and spray with UME-SA nutrient solution + 0.167 M $CaCl_2$

Self-healing ability was evaluated in groups B1 and C1, where only nutrient solution and $CaCl_2$ were applied to the cracked area of the bacterial beam with the idea that vegetative microorganisms that were embedded in the cement paste matrix during mixing would be able to induce $CaCO_3$ precipitation by urea hydrolysis. For groups A1, A2, B2, and C2, bacteria were provided externally by spraying a 1-day old stock bacterial culture

(OD_{600}=1.6) on the cracked area along with $CaCl_2$. For groups A3, A4, B3, and C3, cells were pelleted from the same 1-day old stock culture by centrifugation at 7500 x g for 10 minutes, and the paste of pelleted cells was applied with a metal spatula to the cracked area. Following the application of the paste of cells, nutrient solution and $CaCl_2$ were applied to the damaged area. After treatment, nutrient solution with $CaCl_2$ was applied to all beams every 2-3 days. Figure 8.1 shows beams from group A3 at different stages of treatment.

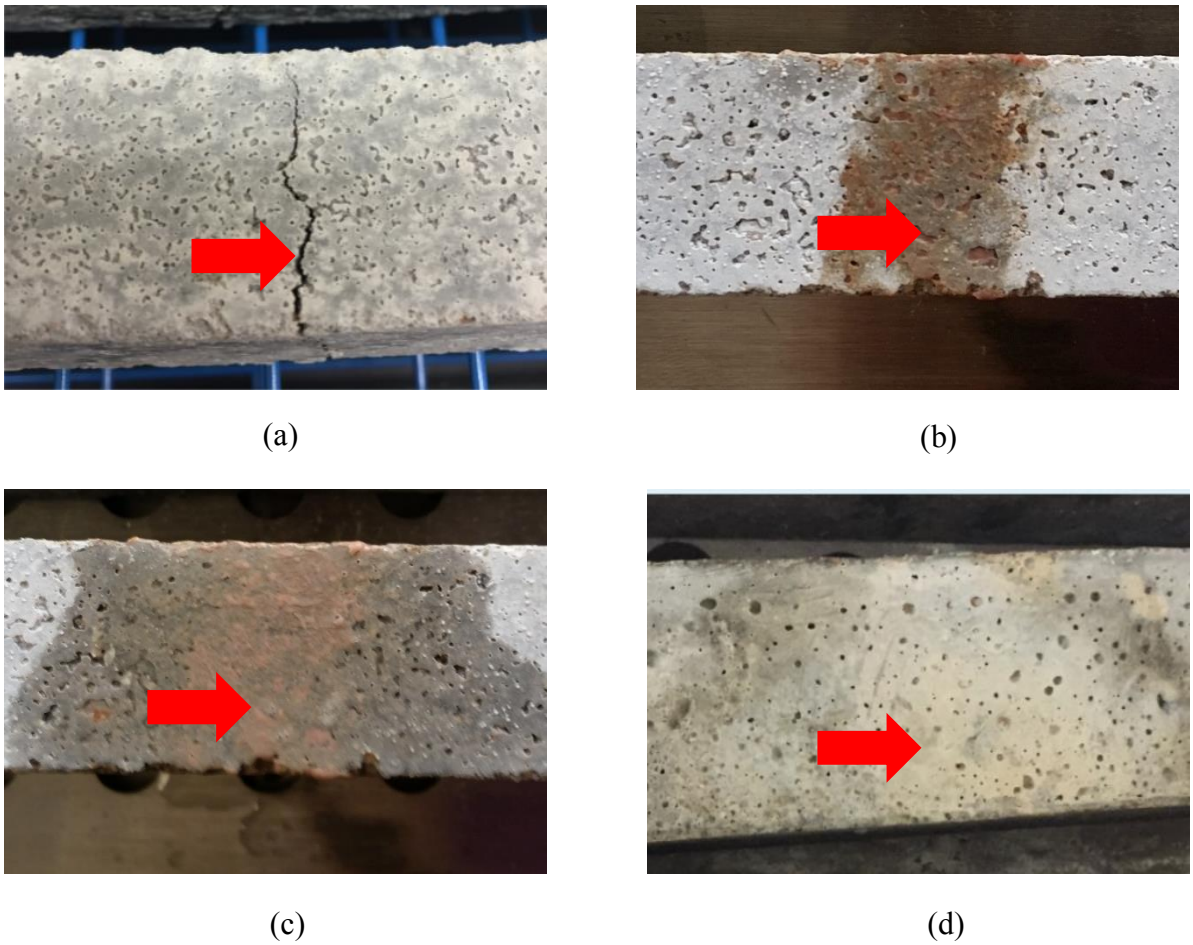

(a) (b)

(c) (d)

Figure 8.1: Beams from group A3 (a) immediately after cracking and before treatment, (b) immediately after the paste of pelleted cells were applied during treatment, (c) after nutrient solution and $CaCl_2$ were ponded on top of the pelleted cells during treatment, and (d) 16 days after treatment. Arrows indicate the approximate location of the crack.

8.2.4 Initial Cracking

Realistic flexural cracks were induced in each beam by loading the specimens to failure in a three-point bending configuration using an Instron 8872 servohydraulic testing system (Norwood, MA, United States). A strain controlled loading rate of 0.4 mm/ minute was used, and care was taken to remove the beams immediately after failure such that the beam specimens remained intact. The peak load was recorded for each beam during this

process. The peak loads were used to calculate flexural stress at midspan, which was then used to evaluate strength recovery of treated beams.

8.2.5 Ultrasonic Pulse Velocity (UPV)

UPV was used to detect crack-sealing in each sample group for up to 28 days after treatment. Ultrasonic waves travel faster in concrete (4000-5000 m/s) than in water (1480 m/s) or in air (350 m/s). Thus, when a crack occurs, the transmission time will be increased because the waves will travel around the crack. Then, as sealing occurs, the transmission time will gradually decrease since the waves can travel through the sealant and reestablish a direct transmission path [46]. This method was ideal to detect sealing since it allowed for frequent monitoring of the specimens without causing damage.

UPV transmission time was measured immediately before and after cracking (0 days) and then again at 1, 7, 14, 21, and 28 days after treatment. The transducers were positioned at either end of the 1 in. x 1 in. x 8 in. beams such that the ultrasonic wave would travel across the length of each specimen. The transducers possessed planar surfaces, and the end surface of the mortar beams were filed until smooth to ensure good coupling with the transducers. Some samples were coupled to the planar transducers with marine grease, while other samples were air coupled. UPV transmission time was measured on several samples with grease and without grease, and these measurements were used to establish a relationship between transmission time with grease and transmission time without grease as the coupling agent. This relationship is displayed in Figure 8.2.

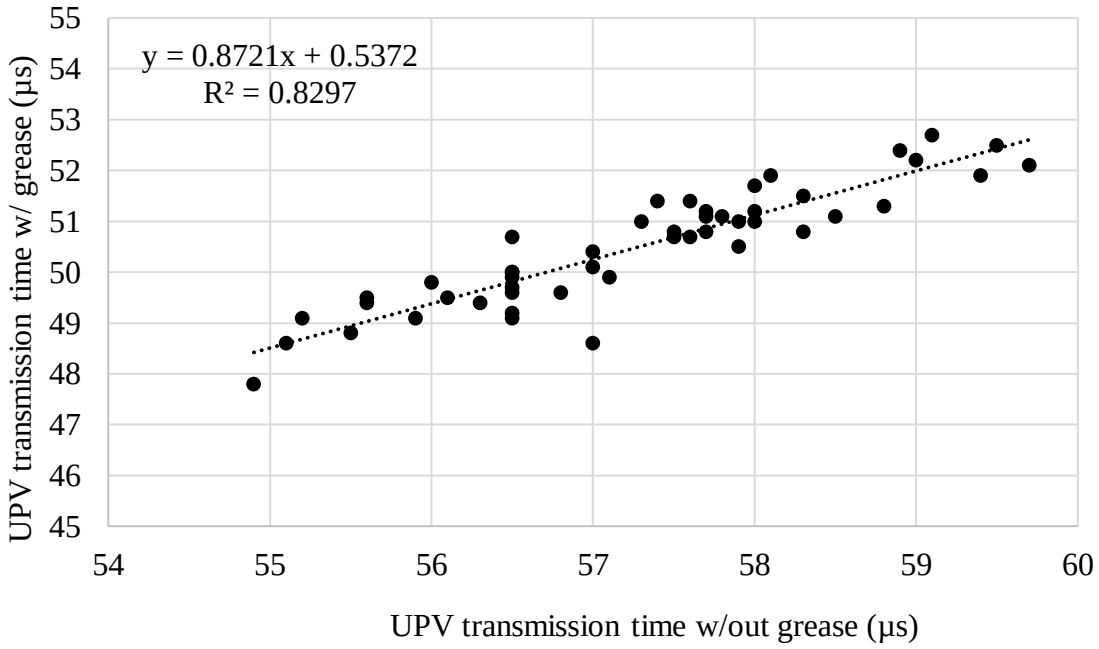

Figure 8.2: Correlation between UPV transmission time with grease and without grease.

The equation Y = 0.8721X + 0.5372 where Y is UPV transmission time with grease and X is UPV transmission time without grease was used as a correction factor for the measurements taken without grease such that the data could be compared.

8.2.6 Strength Recovery

The three-point bending tests described in Section 8.2.4 were repeated for each beam 28 days after treatment. The same loading rate of 0.4 mm/ minute was used, and the beams were loaded such that tension was applied to the treated face of the specimen where the initial crack occurred. The peak loads were recorded and used to calculate the flexural stress. A ratio of the peak stress of each treated beam to the initial peak stress of that same beam determined during initial cracking was calculated to evaluate flexural strength recovery (Equation 8.1).

$$\text{Flexural strength recovery (\%)} = \frac{\text{peak stress of treated beam}}{\text{peak stress of pristine beam}} \times 100\% \qquad (8.1)$$

8.3 RESULTS AND DISCUSSION

8.3.1 Initial Cracking

The average peak flexural stress obtained for beams in groups A, B, and C are displayed in Figure 8.3, and a representative load deflection curve for each group is displayed in Figure 8.4.

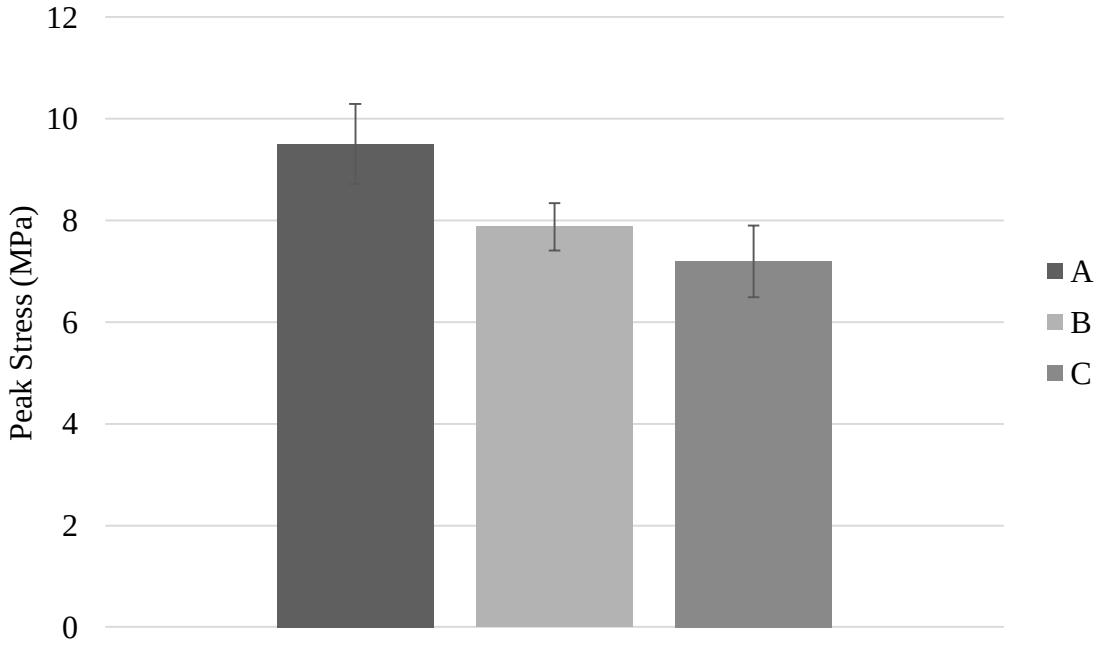

Figure 8.3: Average peak flexural stress for 1 in. x 1 in. x 8 in. mortar beams in groups A (neat beams), B (UYE bacterial beams), and C (UME-SA bacterial beams). Error bars represent the standard deviation.

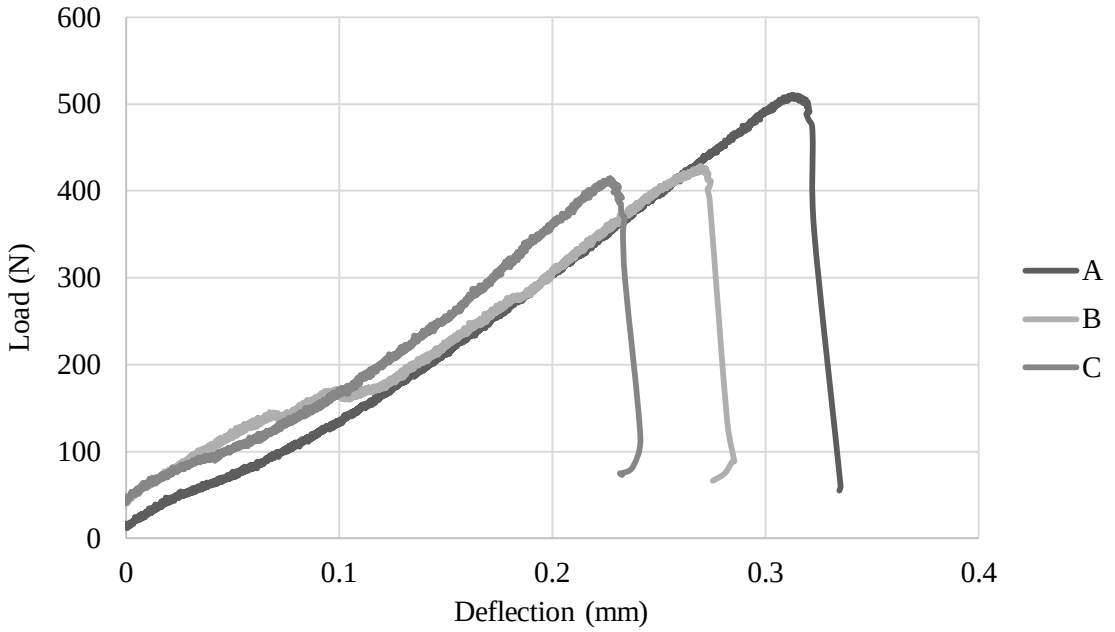

Figure 8.4: Representative load vs. deflection behavior for sample groups A (neat beams), B (UYE bacterial beams), and C (UME-SA bacterial beams) loaded to failure.

Beams in groups A, B, and C exhibited similar flexural strength (Figure 8.3), although the neat beams in group A appeared slightly stronger than the bacterial beams in groups B and C. Beams from each group also exhibited a similar stiffness, which is defined as the slope of the elastic portion of the load vs. deflection curves (Figure 8.4). The initial cracks were examined using optical microscopy, and the crack generally ranged from 200 - 400 µm in width. However, it is important to note that the cracks in this study were non-uniform since they were realistic structural cracks induced by flexural loading. Optical images depicting the initial cracking as well as beams from each sample group 28 days after treatment are included in Appendix B: Optical Images of Crack Sealing.

8.3.2 UPV

Results of the UPV measurements for each treatment group are displayed in Figure 8.5. UPV transmission time increased for all groups at 0 days (immediately after precracking), and this increase in transmission time indicated that beams in each treatment group exhibited a similar amount of damage.

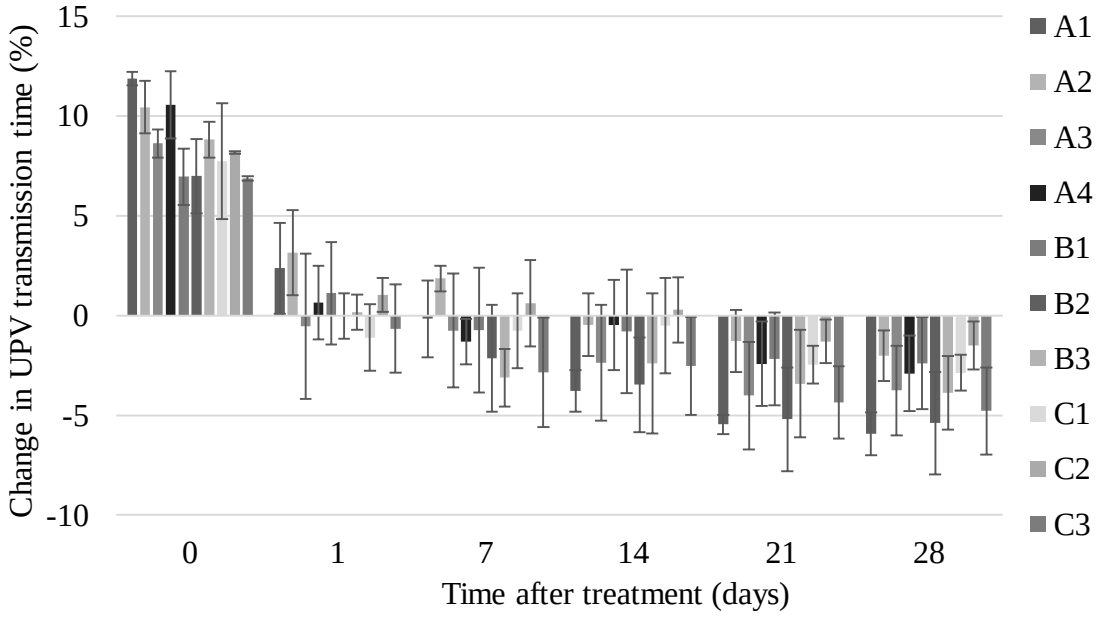

Figure 8.5: Change in ultrasonic pulse velocity transmission time at 0, 1, 7, 14, 21, and 28 days after treatment. Measurements for day 0 were taken after the cracks were induced and immediately before the treatments were applied. Error bars represent the standard deviation of triplicate samples.

From Figure 8.5, a substantial reduction in ultrasonic transmission time occurred just 1 day after treatment for all sample groups such that the transmission times were close to their original values obtained in pristine beams before cracking. Then, transmission time continued to decrease throughout the entire 28-day period, which indicated that the crack-sealing process was still occurring. In fact, 28 days after treatment mortar beams in all

groups were able to transmit ultrasonic waves in even less time than the waves were transmitted in pristine beams at 0 days prior to cracking.

8.3.3 Strength Recovery

UPV data presented in Section 8.3.2 provided evidence of crack-sealing in mortar beams in this study, but the cracks cannot be considered truly "healed" unless recovery of mechanical properties such as strength is achieved [1]. Thus, three-point bending tests were repeated on the treated mortar beams 28 days after treatment, and a ratio was calculated between the peak flexural stress of the treated beams and the initial peak flexural stress of the pristine beams to assess strength recovery. The initial peak flexural loads of each pristine beam and the peak flexural loads of the same beam tested 28 days after treatment are included in Appendix C: Flexural Loads and Stresses, and the percentages of strength recovery for each sample group are displayed in Figure 8.6.

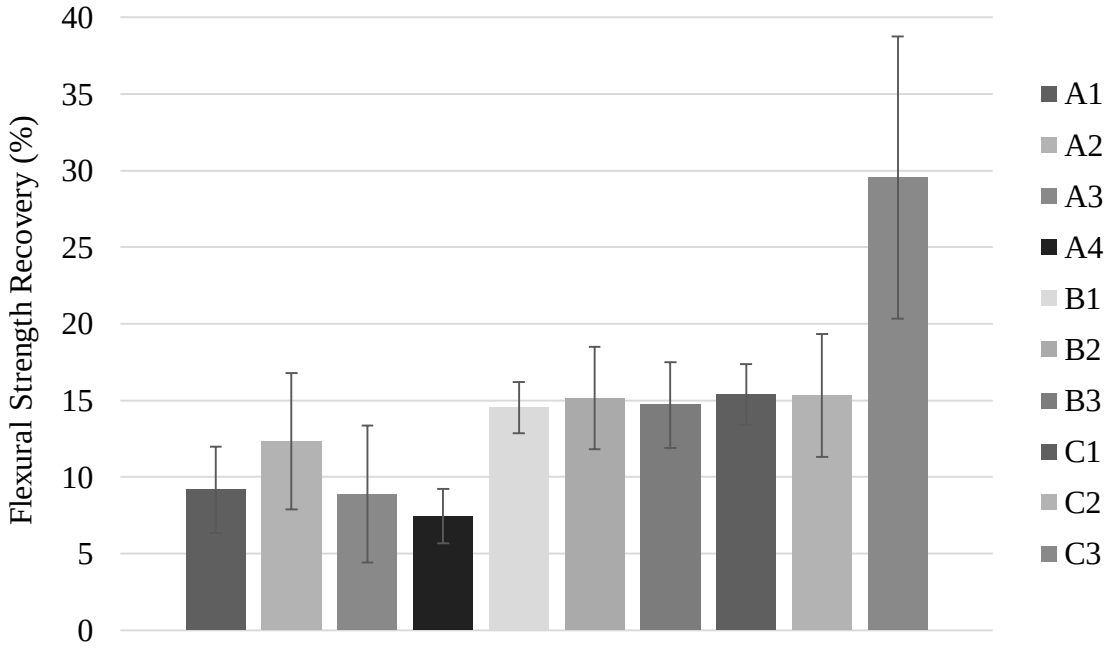

Figure 8.6: Flexural strength recovery for each sample set 28 days after treatment. Error bars represent the standard deviation of triplicate samples.

Ideally, self-healing should lead to full recovery of strength, and the *quality* of the healing can be characterized by the percentage of recovery at a given damage level. Thus, healing is concerned not only with materials that fill the cracks, but materials that act as a binding agent to hold the crack faces together [1]. From Figure 8.6, all of the treatments employed in this study resulted in flexural strength recovery, and recovery up to 29.6% was seen in group C3. However, visual observations and ultrasonic measurements indicated that the cracks were sealed, so the lesser degree of strength recovery might have been due to a lack of binding between the calcium carbonate precipitate and the mortar substrate. Further research is needed to assess this bonding strength. Additionally, the degree of damage enacted upon the beams in this study was rather high since the beams were preloaded to failure, and this might also explain why a greater degree of strength recovery could not be obtained. Basaran [52] initiated internal microcracks in bacterial mortar cubes by loading the specimens to 70% of their compressive strength and evaluating strength recovery after 28 days. The degree of recovery observed was dependent upon the curing method used, and a full recovery of compressive strength was seen in bacterial mortar cubes cured by periodically spraying nutrient medium on the cubes. This could indicate that the degree of initial damage might have an impact on strength recovery. Further, the bonding strength of the precipitate to the mortar substrate might be more critical in specimens subjected to flexural loading (which imparts tension on the cracked face) as compared to specimens subjected to compressive loading.

In general, the bacterial beams (groups B and C) exhibited a higher degree of strength recovery than the neat beams that were simply treated with bacteria. Further, beams in groups B1 and C1 were able to recover approximately 15% of their flexural strength even though no bacteria were applied externally to the cracked area during treatment; therefore, this healing likely occurred due to metabolic activity of vegetative *S.*

pasteurii that were already present in the cement paste matrix. Beams in group C3 exhibited the highest degree of strength recovery at close to 30%, but this group also possessed a high standard deviation, which is cause for concern regarding the robustness criterion of *reliability*. This high standard deviation could be explained by the use of non-uniform, realistic cracks in this study.

Chapter 9: Conclusions and Suggestions for Future Research

9.1 CONCLUSIONS

This study investigated several key factors related to the robustness and the feasibility of microbial concrete where the goal is to have microbial-induced calcium carbonate precipitation (MICCP) within the cement paste matrix by activity of vegetative *S. pasteurii* cells. Results presented herein led to a better understanding of biomineralization in cement-based materials and provided suggestions to improve the process. Thus, this research advances the practicality of microbial concrete as a reliable material for use in industry. Section 9.1.1 provides a summary of the important results of this research.

9.1.1 Key Results

- The morphology of microbial-induced calcium carbonate precipitates was influenced by ionic strength/calcium ion concentration, pH, and substrate mineralogy.
- Biogenic calcium carbonate, which was produced due to activity of vegetative *S. pasteurii,* exhibited superior kinetic and thermodynamic stability as compared to abiogenic calcium carbonate.
- The viability and urease activity of vegetative *S. pasteurii* cells were substantially impacted by exposure to conditions designed to mimic those present in cement-based systems including heat, high pH, and nutrient depletion. However, zeta potential was minimally affected by these conditions and urease activity was recovered for all sample sets after 24 hours of incubation at 30°C.
- A 75% improvement in the observed retardation of cement hydration kinetics caused by the addition of vegetative *S. pasteurii* in a urea-yeast extract (UYE)

medium was achieved by replacing yeast extract in the growth medium with a combination of meat extract and sodium acetate (to an equivalent chemical oxygen demand as the yeast extract).

- Ultrasonic measurements revealed that vegetative *S. pasteurii* can be used to achieve crack-sealing in mortar, but a low degree of strength recovery was exhibited in these systems; this might have been due to insufficient bonding strength between the microorganism-induced precipitate and the mortar substrate.

9.2 FUTURE WORK

The research presented in this thesis provides useful information about the robustness and feasibility of microbial concrete. However, several areas for further research are recommended:

- The influence of calcium concentration on the morphology of biogenic calcium carbonate was investigated in this study, and it was found that varying the calcium concentration did have an effect on morphology. However, increasing the calcium concentration also increased the ionic strength, which also might influence the polymorph selection process. Thus, future work should examine whether overall ionic strength or calcium concentration is influencing the morphology, or if they both play a role. This could be assessed by examining the morphology of the samples with different calcium additions but a constant ionic strength.
- It was proposed in this work that insufficient bonding strength of microbial-induced calcium carbonate to the mortar substrate might have prevented higher degrees of strength recovery in damaged mortar beams. However, this bonding strength has not yet been investigated in the literature. It is imperative that the durability of the bond between the microorganism-induced precipitate and mortar be characterized.

- Although it was determined in this work that biogenic calcium carbonate exhibited superior kinetic and thermodynamic stability as compared to abiogenic calcium carbonate, mechanical properties (e.g., strength and stiffness) of these minerals were not investigated. These properties should be compared to provide further information about the differences in the quality of calcium carbonate precipitated in biogenic and abiogenic systems.
- Li and Herbert [1] stated that robust self-healing concrete should possess a long shelf life that is comparable to the service life of the structure. According to this idea, bacteria should remain viable and metabolically active in microbial concrete throughout the entire service life, which can be as long as 50-100 years. This presents an extraordinary challenge, particularly for microorganisms inoculated to concrete in a vegetative state. Thus, more long-term viability studies are needed to investigate if this is feasible. Furthermore, it is still unclear whether vegetative microorganisms can produce carbonates and induce $CaCO_3$ formation in concrete *in situ*; thus, additional investigation is needed in this area.
- *S. pasteurii* growth medium was optimized in this work to mitigate retardation of cement hydration kinetics, which could in turn reduce construction costs. However, even in the optimized medium, the addition of microorganisms and nutrients exhibited some retardation as compared to neat cement paste. Thus, future work should be aimed at minimizing or ideally eliminating the delay entirely. Additionally, based on recent research [57], further measures to reduce cost must be explored. Some examples of methods to reduce cost that should be investigated include identification of less expensive nutrient sources and the use of non-sterile materials and equipment.

Appendix A: Whole-Pattern Fits of *Ex Situ* Biogenic and Abiogenic $CaCO_3$

Whole-pattern fits, which were performed to quantitatively estimate the crystal structure of each *ex situ* calcium carbonate described in Section 5.2.3, are presented in Figures A.1 – A.36.

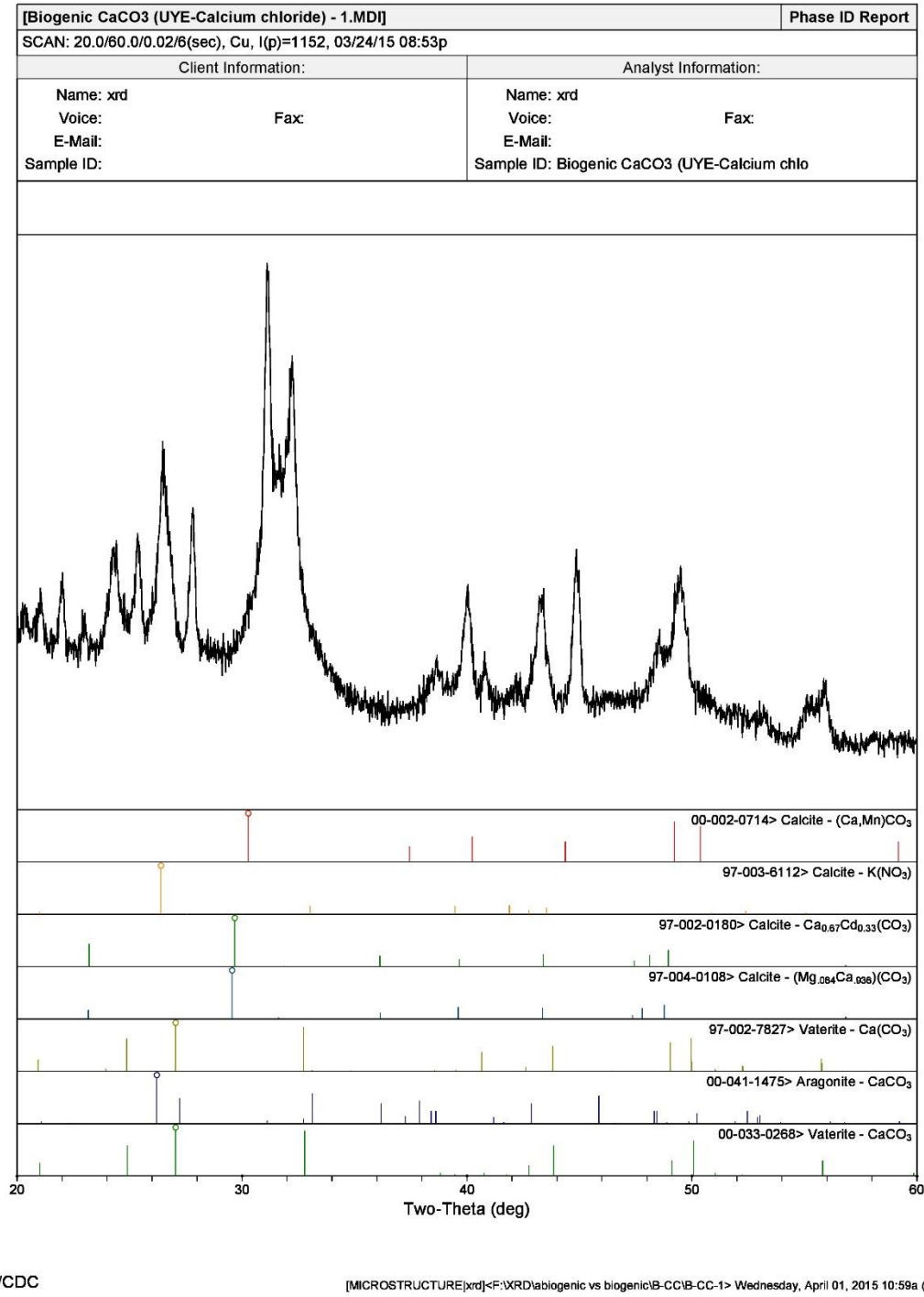

Figure A.1: B-CC-1 phase ID report showing peaks.

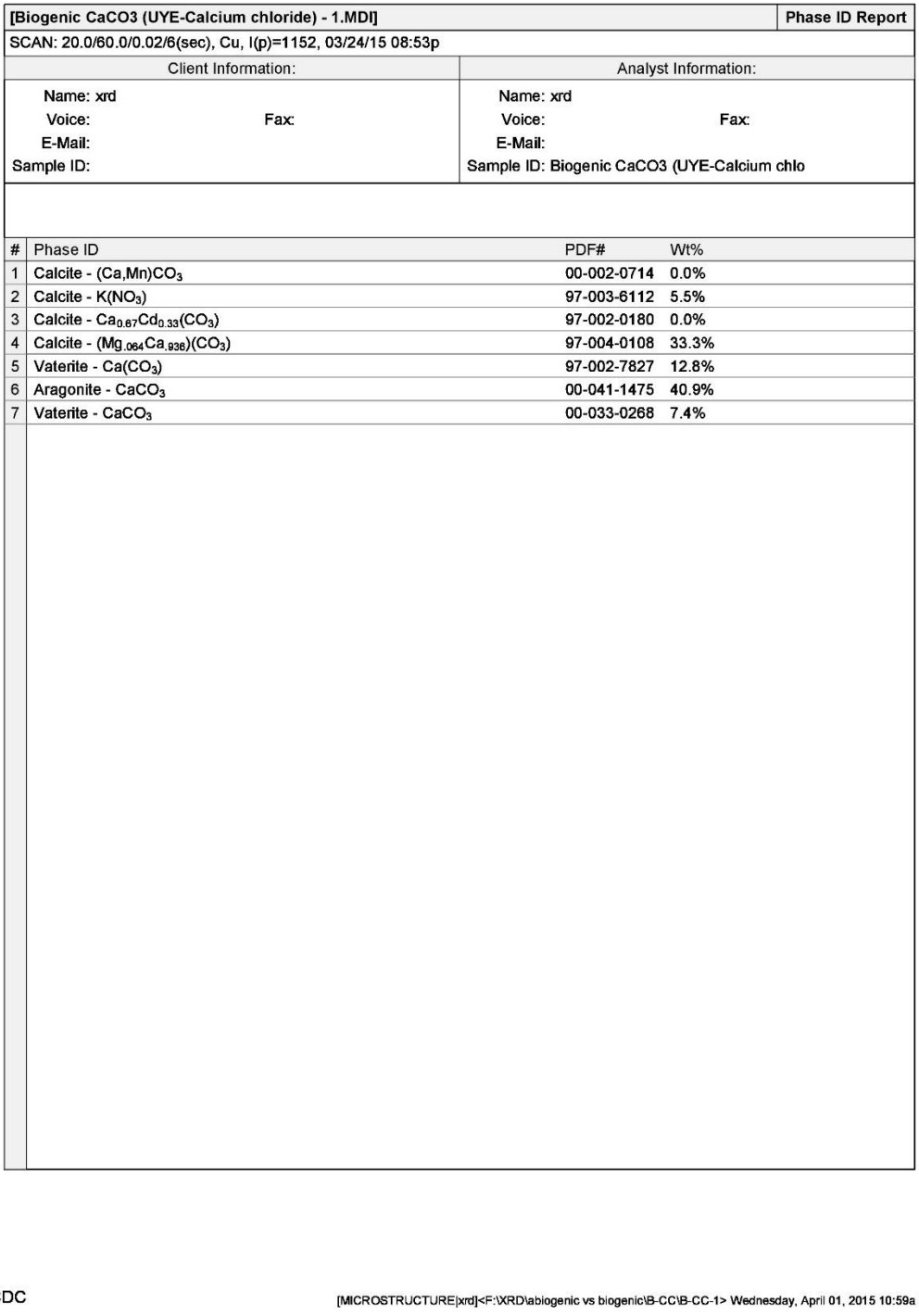

[Biogenic CaCO3 (UYE-Calcium chloride) - 1.MDI] — Phase ID Report

SCAN: 20.0/60.0/0.02/6(sec), Cu, I(p)=1152, 03/24/15 08:53p

Client Information:	Analyst Information:
Name: xrd	Name: xrd
Voice: Fax:	Voice: Fax:
E-Mail:	E-Mail:
Sample ID:	Sample ID: Biogenic CaCO3 (UYE-Calcium chlo

#	Phase ID	PDF#	Wt%
1	Calcite - $(Ca,Mn)CO_3$	00-002-0714	0.0%
2	Calcite - $K(NO_3)$	97-003-6112	5.5%
3	Calcite - $Ca_{0.67}Cd_{0.33}(CO_3)$	97-002-0180	0.0%
4	Calcite - $(Mg_{.064}Ca_{.936})(CO_3)$	97-004-0108	33.3%
5	Vaterite - $Ca(CO_3)$	97-002-7827	12.8%
6	Aragonite - $CaCO_3$	00-041-1475	40.9%
7	Vaterite - $CaCO_3$	00-033-0268	7.4%

CMRG/CDC

[MICROSTRUCTURE|xrd]<F:\XRD\abiogenic vs biogenic\B-CC\B-CC-1> Wednesday, April 01, 2015 10:59a (MDI/JADE9)

Figure A.2: B-CC-1 phase ID report showing mineralogical composition by weight.

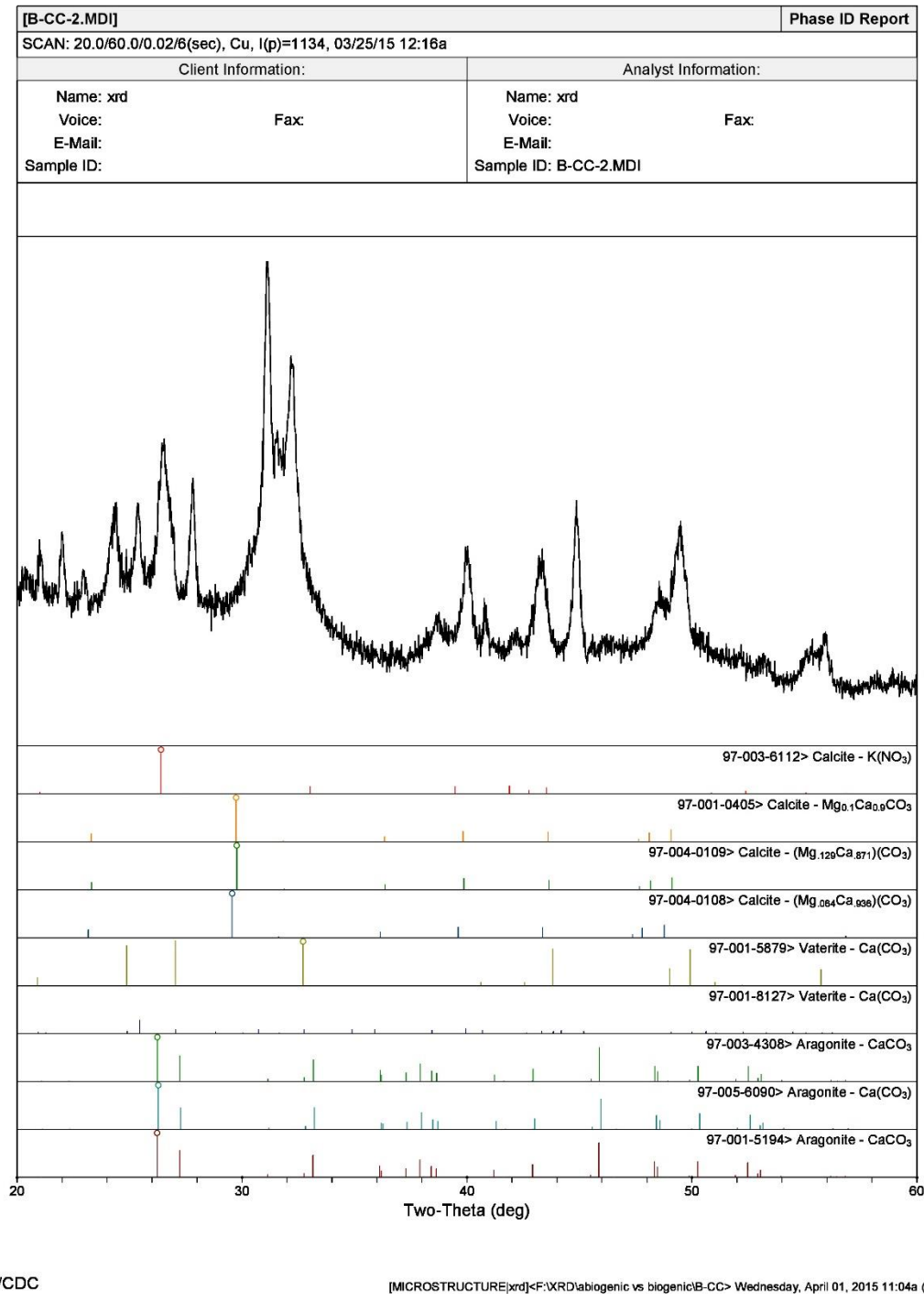

Figure A.3: B-CC-2 phase ID report showing peaks.

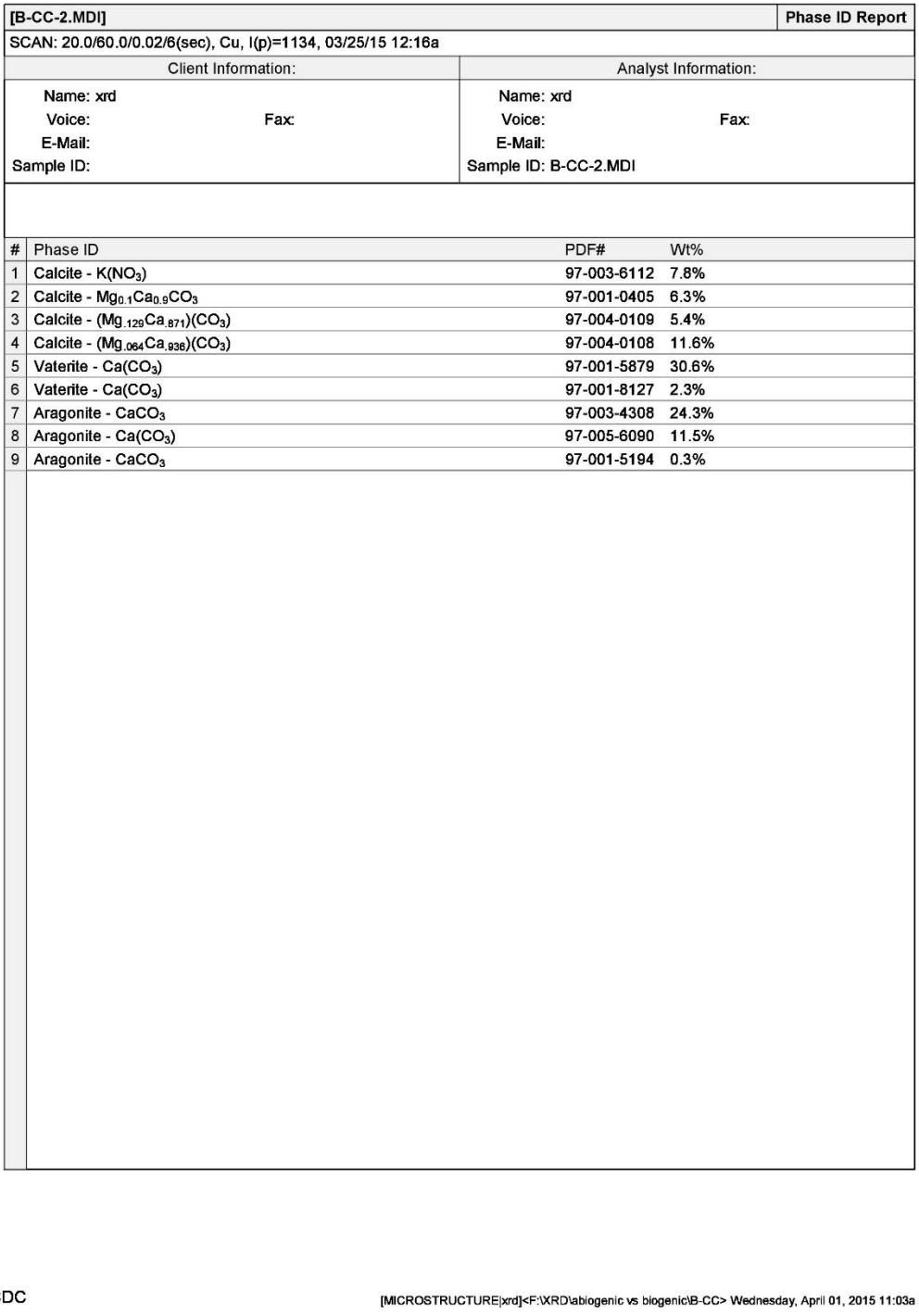

[B-CC-2.MDI] Phase ID Report

SCAN: 20.0/60.0/0.02/6(sec), Cu, I(p)=1134, 03/25/15 12:16a

Client Information:	Analyst Information:
Name: xrd	Name: xrd
Voice: Fax:	Voice: Fax:
E-Mail:	E-Mail:
Sample ID:	Sample ID: B-CC-2.MDI

#	Phase ID	PDF#	Wt%
1	Calcite - $K(NO_3)$	97-003-6112	7.8%
2	Calcite - $Mg_{0.1}Ca_{0.9}CO_3$	97-001-0405	6.3%
3	Calcite - $(Mg_{.129}Ca_{.871})(CO_3)$	97-004-0109	5.4%
4	Calcite - $(Mg_{.064}Ca_{.936})(CO_3)$	97-004-0108	11.6%
5	Vaterite - $Ca(CO_3)$	97-001-5879	30.6%
6	Vaterite - $Ca(CO_3)$	97-001-8127	2.3%
7	Aragonite - $CaCO_3$	97-003-4308	24.3%
8	Aragonite - $Ca(CO_3)$	97-005-6090	11.5%
9	Aragonite - $CaCO_3$	97-001-5194	0.3%

CMRG/CDC

[MICROSTRUCTURE|xrd]<F:\XRD\abiogenic vs biogenic\B-CC> Wednesday, April 01, 2015 11:03a (MDI/JADE9)

Figure A.4: B-CC-2 phase ID report showing mineralogical composition by weight.

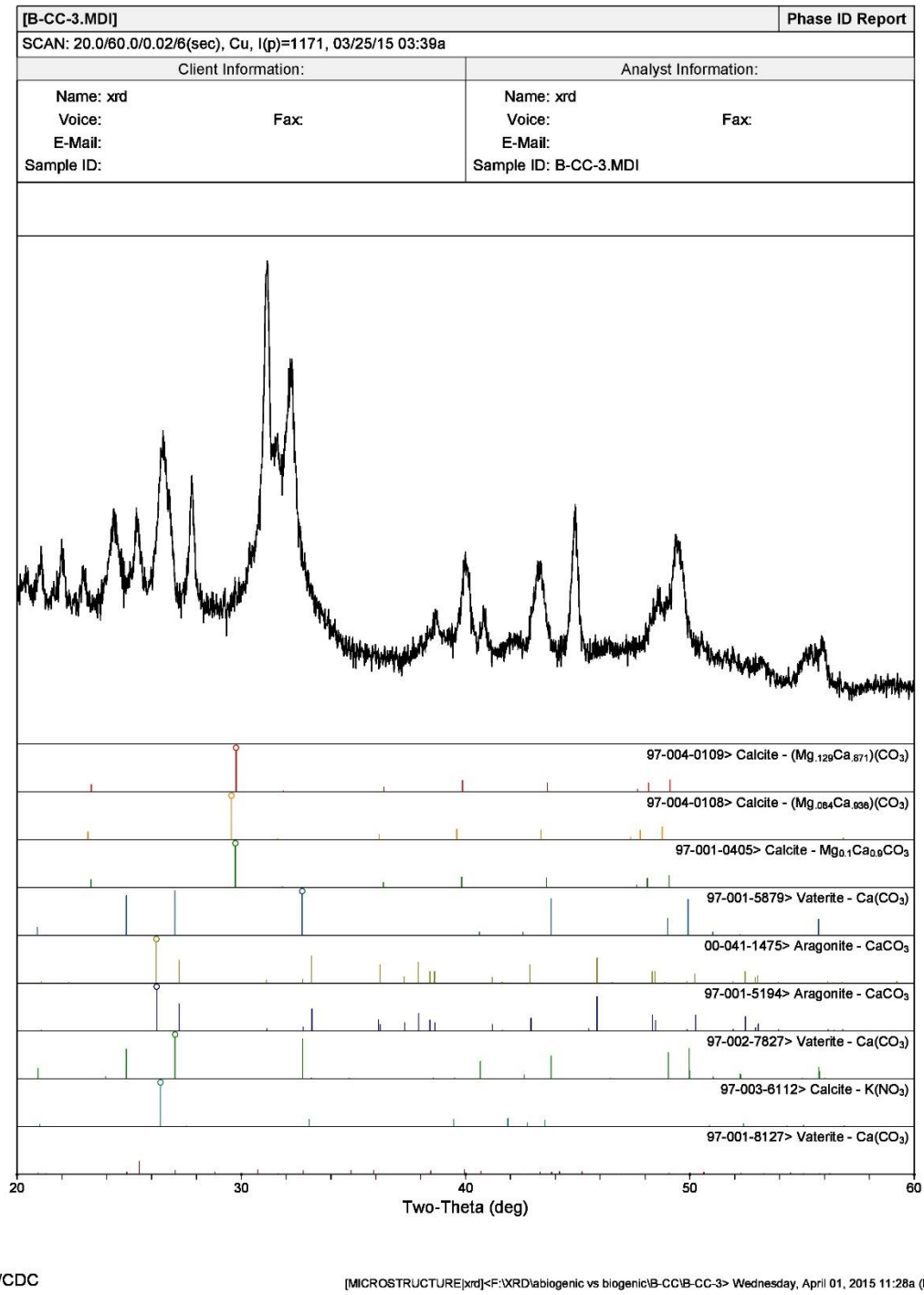

Figure A.5: B-CC-3 phase ID report showing peaks.

[B-CC-3.MDI]			Phase ID Report
SCAN: 20.0/60.0/0.02/6(sec), Cu, I(p)=1171, 03/25/15 03:39a			
Client Information:		Analyst Information:	
Name: xrd Voice: Fax: E-Mail: Sample ID:		Name: xrd Voice: Fax: E-Mail: Sample ID: B-CC-3.MDI	

#	Phase ID	PDF#	Wt%
1	Calcite - $(Mg_{.129}Ca_{.871})(CO_3)$	97-004-0109	5.5%
2	Calcite - $(Mg_{.064}Ca_{.936})(CO_3)$	97-004-0108	0.1%
3	Calcite - $Mg_{0.1}Ca_{0.9}CO_3$	97-001-0405	31.2%
4	Vaterite - $Ca(CO_3)$	97-001-5879	18.1%
5	Aragonite - $CaCO_3$	00-041-1475	11.5%
6	Aragonite - $CaCO_3$	97-001-5194	17.9%
7	Vaterite - $Ca(CO_3)$	97-002-7827	9.5%
8	Calcite - $K(NO_3)$	97-003-6112	4.2%
9	Vaterite - $Ca(CO_3)$	97-001-8127	2.1%

CMRG/CDC [MICROSTRUCTURE|xrd]<F:\XRD\abiogenic vs biogenic\B-CC\B-CC-3> Wednesday, April 01, 2015 11:28a (MDI/JADE9)

Figure A.6: B-CC-3 phase ID report showing mineralogical composition by weight.

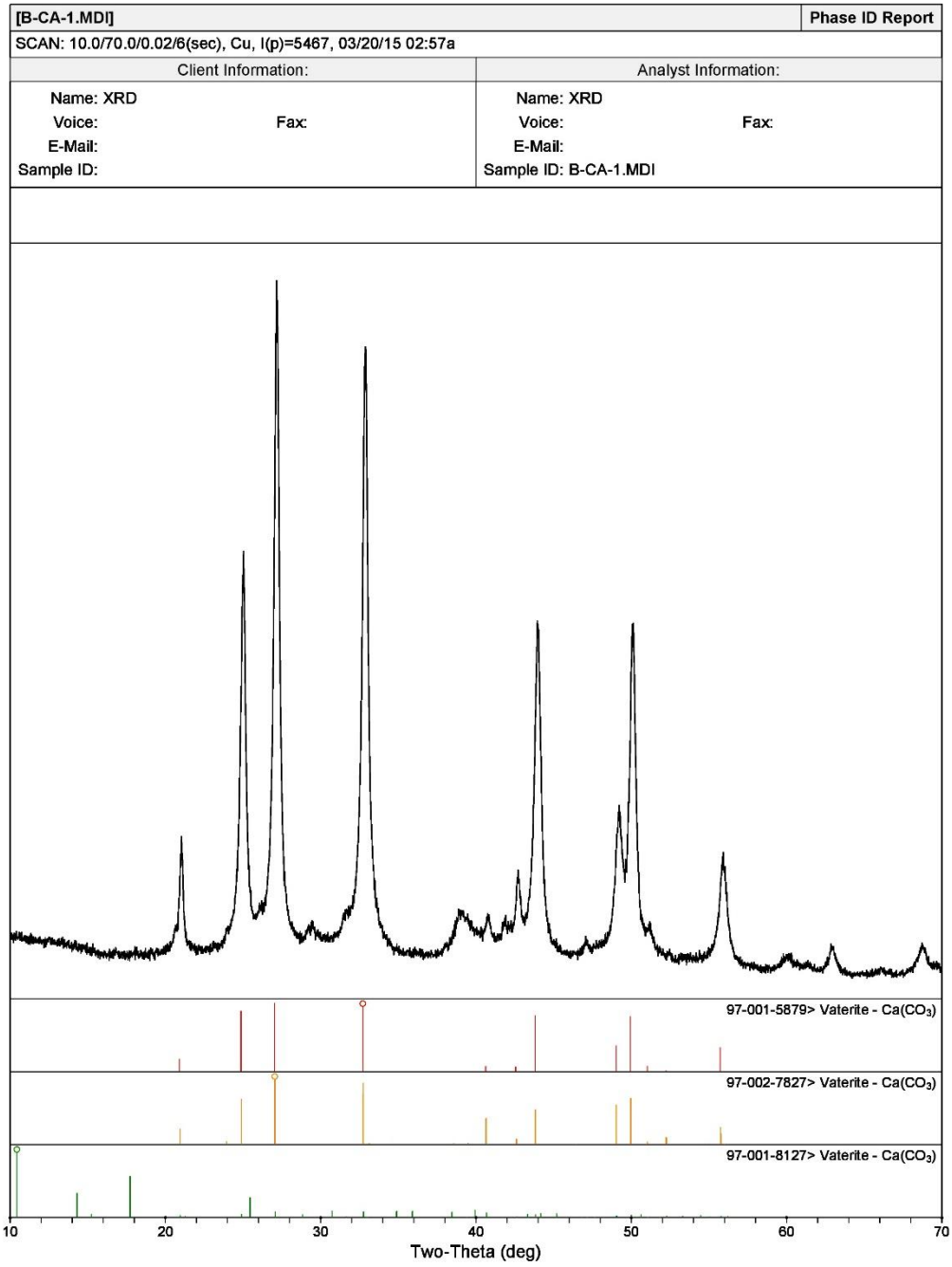

Figure A.7: B-CA-1 phase ID report showing peaks.

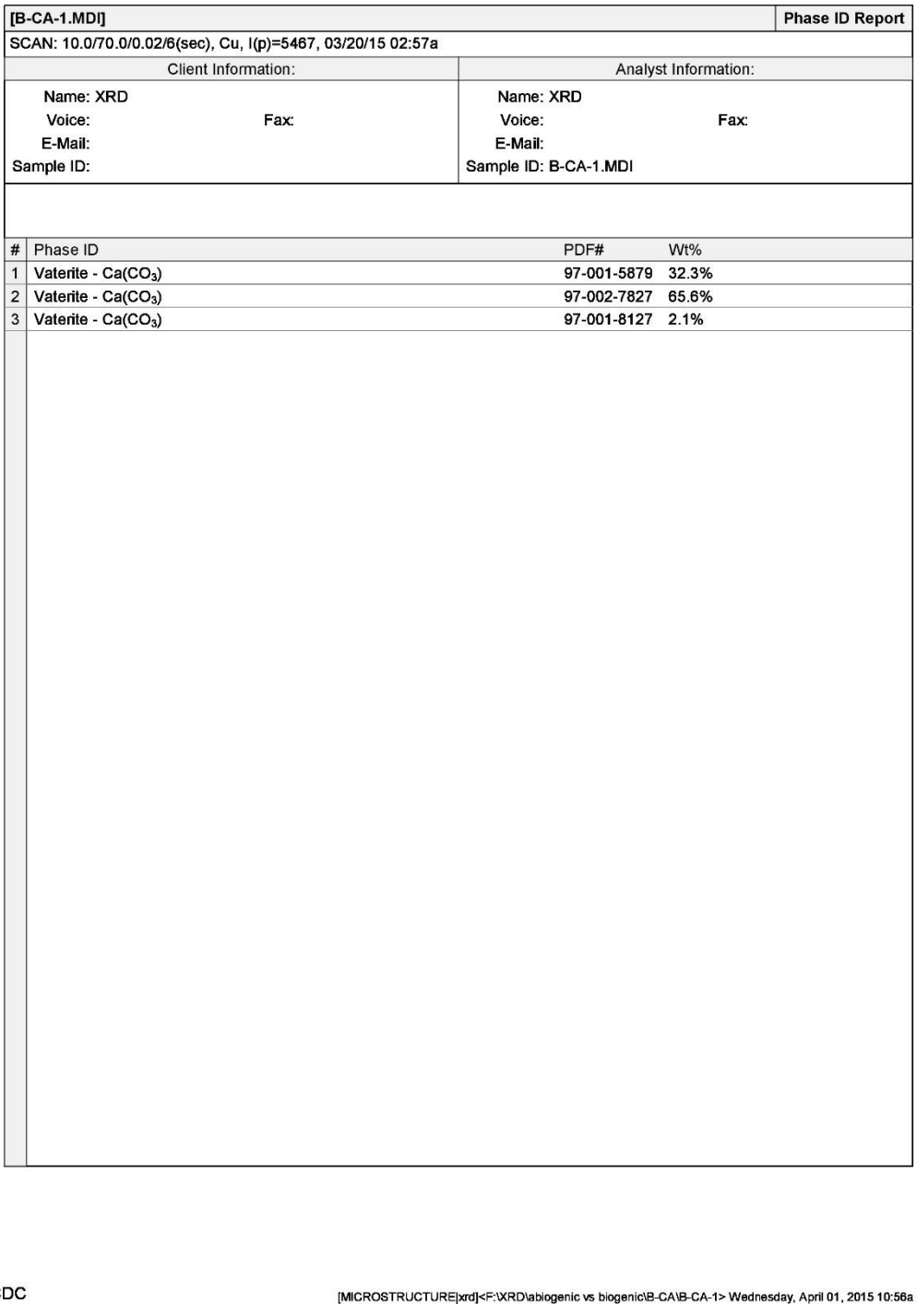

[B-CA-1.MDI] Phase ID Report

SCAN: 10.0/70.0/0.02/6(sec), Cu, I(p)=5467, 03/20/15 02:57a

Client Information:	Analyst Information:
Name: XRD	Name: XRD
Voice: Fax:	Voice: Fax:
E-Mail:	E-Mail:
Sample ID:	Sample ID: B-CA-1.MDI

#	Phase ID	PDF#	Wt%
1	Vaterite - $Ca(CO_3)$	97-001-5879	32.3%
2	Vaterite - $Ca(CO_3)$	97-002-7827	65.6%
3	Vaterite - $Ca(CO_3)$	97-001-8127	2.1%

Figure A.8: B-CA-1 phase ID report showing mineralogical composition by weight.

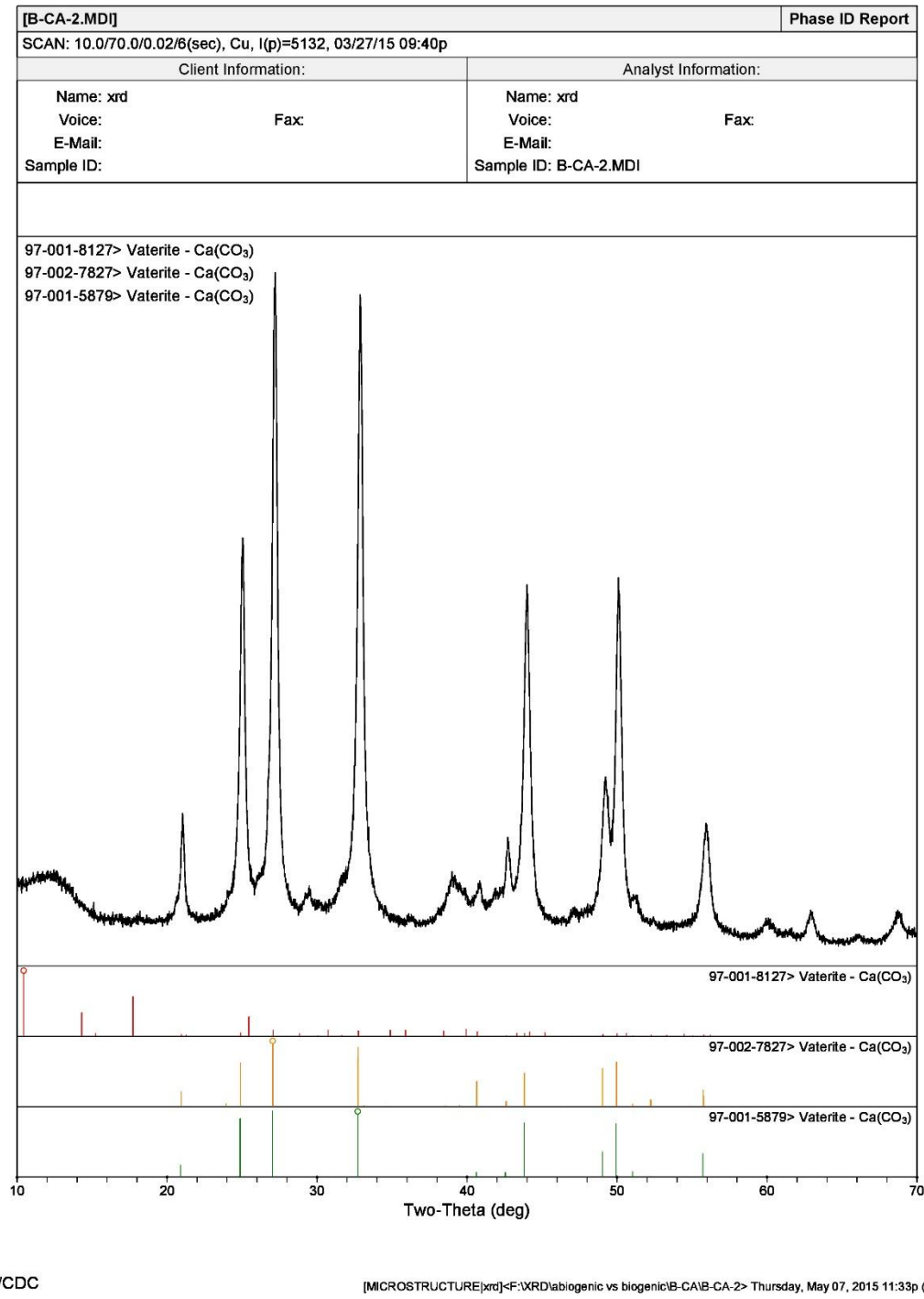

Figure A.9: B-CA-2 phase ID report showing peaks.

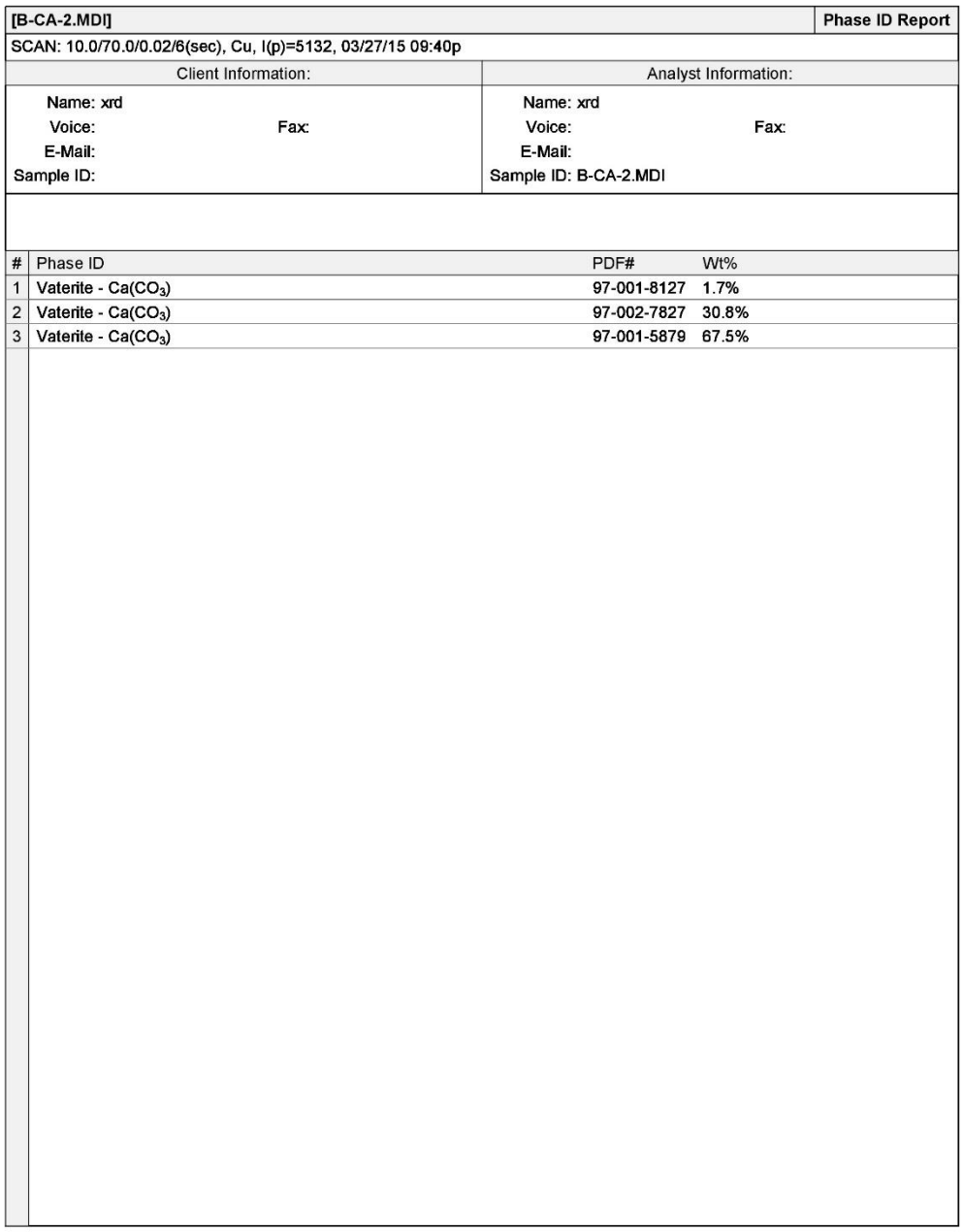

[B-CA-2.MDI] Phase ID Report

SCAN: 10.0/70.0/0.02/6(sec), Cu, I(p)=5132, 03/27/15 09:40p

Client Information:	Analyst Information:
Name: xrd	Name: xrd
Voice: Fax:	Voice: Fax:
E-Mail:	E-Mail:
Sample ID:	Sample ID: B-CA-2.MDI

#	Phase ID	PDF#	Wt%
1	Vaterite - $Ca(CO_3)$	97-001-8127	1.7%
2	Vaterite - $Ca(CO_3)$	97-002-7827	30.8%
3	Vaterite - $Ca(CO_3)$	97-001-5879	67.5%

Figure A.10: B-CA-2 phase ID report showing mineralogical composition by weight.

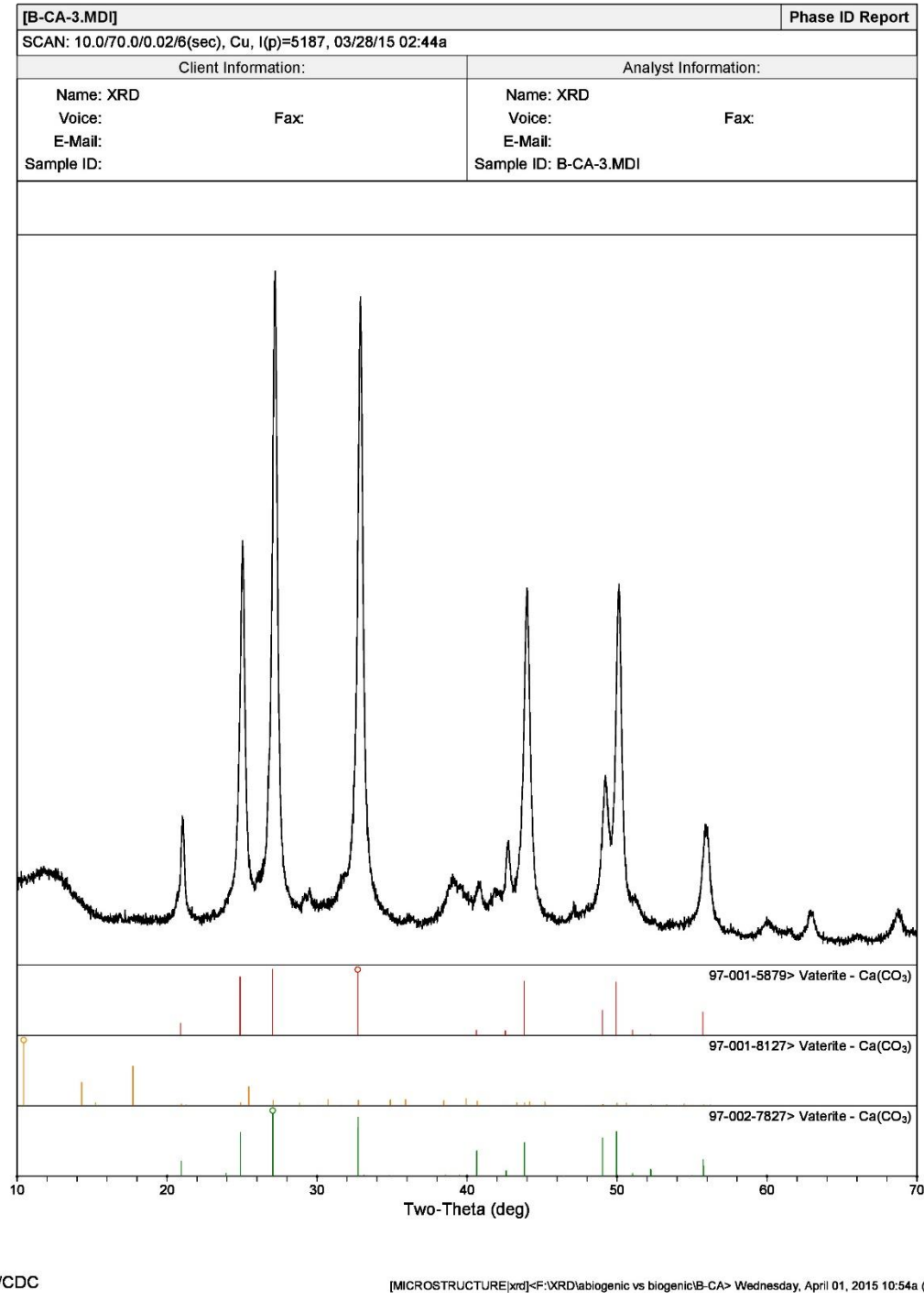

Figure A.11: B-CA-3 phase ID report showing peaks.

[B-CA-3.MDI]			Phase ID Report
SCAN: 10.0/70.0/0.02/6(sec), Cu, I(p)=5187, 03/28/15 02:44a			
Client Information:		Analyst Information:	
Name: XRD Voice: Fax: E-Mail: Sample ID:		Name: XRD Voice: Fax: E-Mail: Sample ID: B-CA-3.MDI	

#	Phase ID	PDF#	Wt%
1	Vaterite - $Ca(CO_3)$	97-001-5879	80.5%
2	Vaterite - $Ca(CO_3)$	97-001-8127	1.2%
3	Vaterite - $Ca(CO_3)$	97-002-7827	18.3%

Figure A.12: B-CA-3 phase ID report showing mineralogical composition by weight.

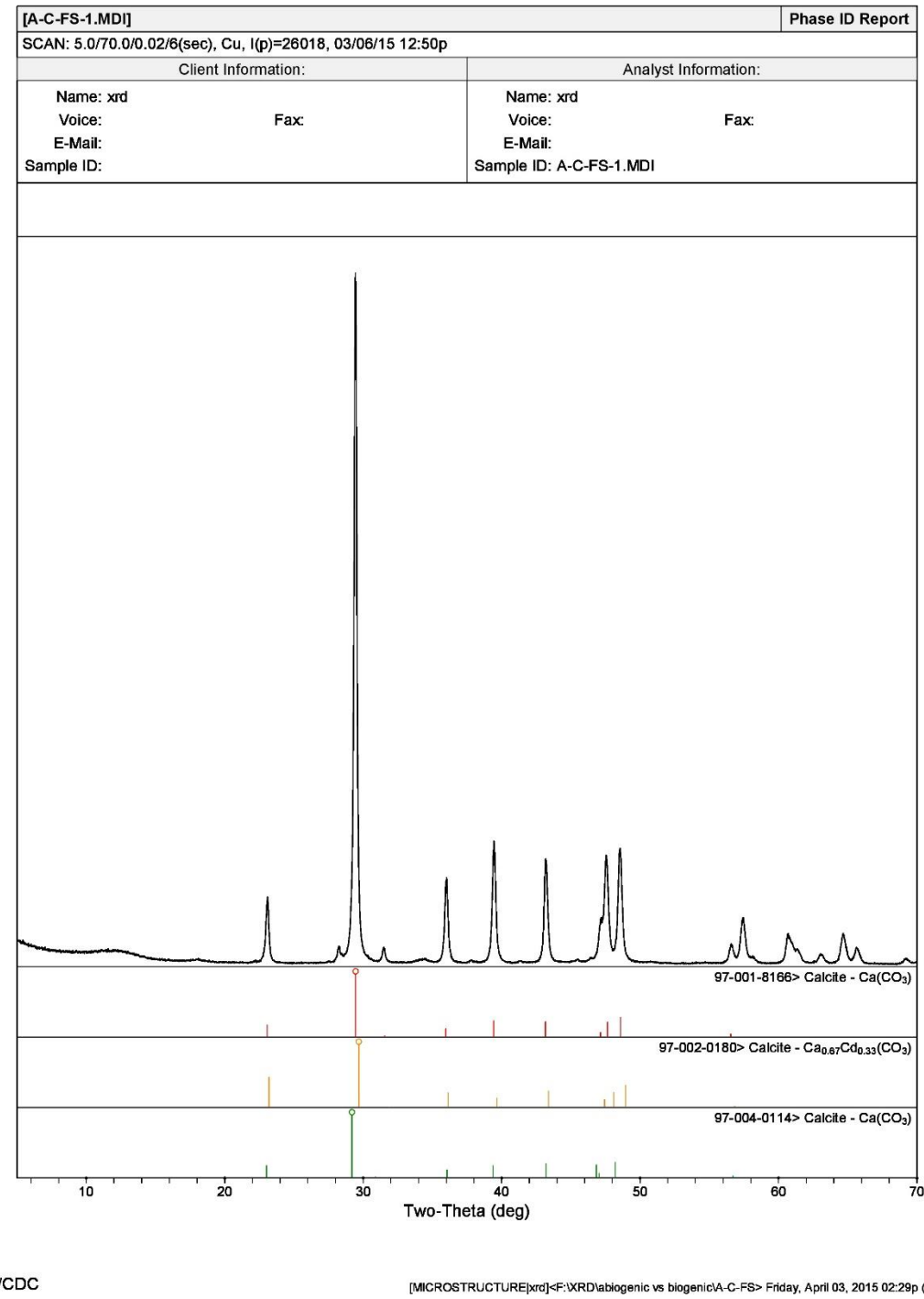

Figure A.13: A-C-FS-1 phase ID report showing peaks.

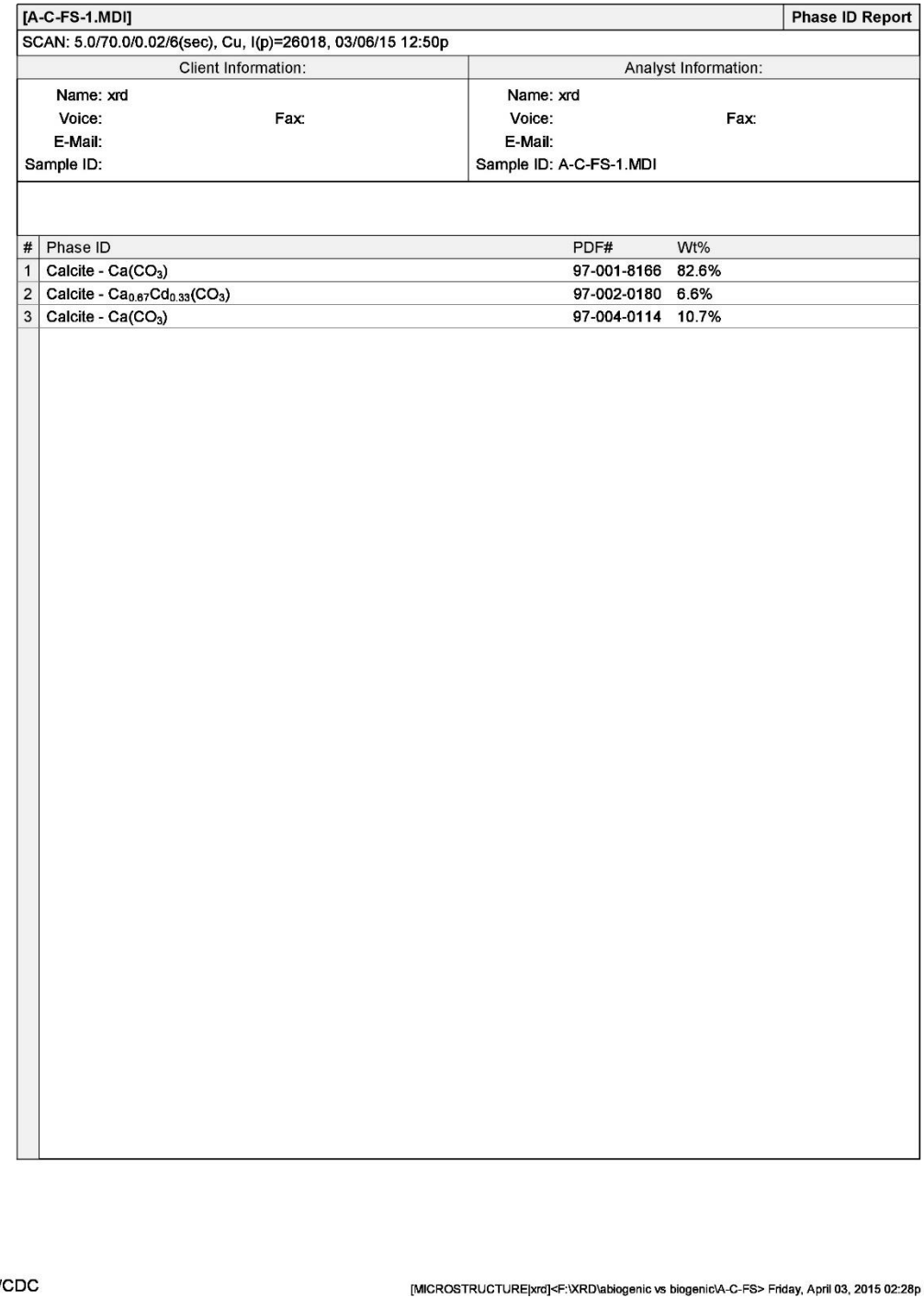

[A-C-FS-1.MDI] Phase ID Report

SCAN: 5.0/70.0/0.02/6(sec), Cu, I(p)=26018, 03/06/15 12:50p

Client Information:	Analyst Information:
Name: xrd	Name: xrd
Voice: Fax:	Voice: Fax:
E-Mail:	E-Mail:
Sample ID:	Sample ID: A-C-FS-1.MDI

#	Phase ID	PDF#	Wt%
1	Calcite - $Ca(CO_3)$	97-001-8166	82.6%
2	Calcite - $Ca_{0.67}Cd_{0.33}(CO_3)$	97-002-0180	6.6%
3	Calcite - $Ca(CO_3)$	97-004-0114	10.7%

Figure A.14: A-C-FS-1 phase ID report showing mineralogical composition by weight.

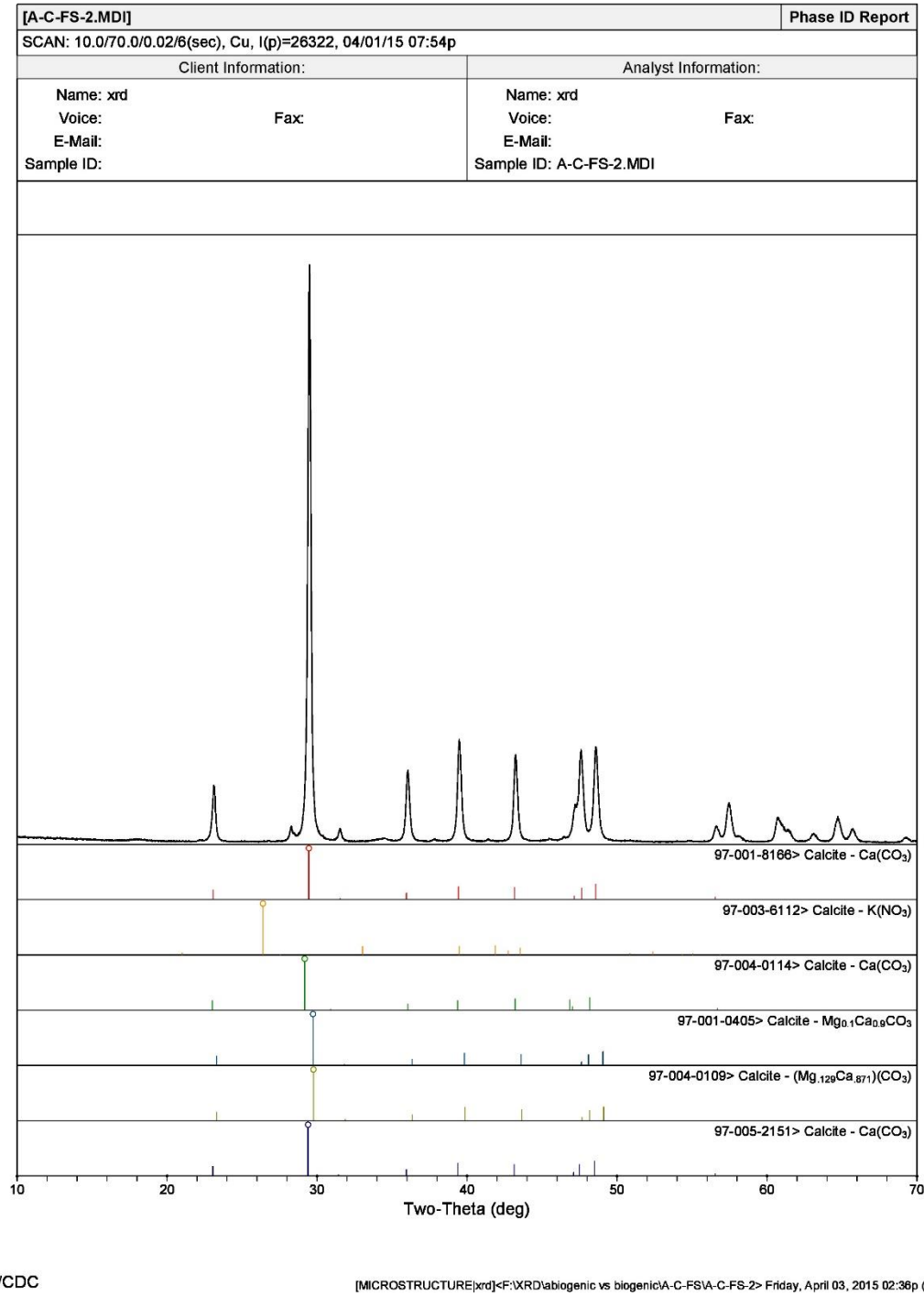

Figure A.15: A-C-FS-2 phase ID report showing peaks.

[A-C-FS-2.MDI]			Phase ID Report
SCAN: 10.0/70.0/0.02/6(sec), Cu, I(p)=26322, 04/01/15 07:54p			
Client Information:		Analyst Information:	
Name: xrd Voice: Fax: E-Mail: Sample ID:		Name: xrd Voice: Fax: E-Mail: Sample ID: A-C-FS-2.MDI	

#	Phase ID	PDF#	Wt%
1	Calcite - $Ca(CO_3)$	97-001-8166	88.0%
2	Calcite - $K(NO_3)$	97-003-6112	0.0%
3	Calcite - $Ca(CO_3)$	97-004-0114	12.0%
4	Calcite - $Mg_{0.1}Ca_{0.9}CO_3$	97-001-0405	0.0%
5	Calcite - $(Mg_{.129}Ca_{.871})(CO_3)$	97-004-0109	0.0%
6	Calcite - $Ca(CO_3)$	97-005-2151	0.0%

CMRG/CDC [MICROSTRUCTURE|xrd]<F:\XRD\abiogenic vs biogenic\A-C-FS\A-C-FS-2> Friday, April 03, 2015 02:37p (MDI/JADE9)

Figure A.16: A-C-FS-2 phase ID report showing mineralogical composition by weight.

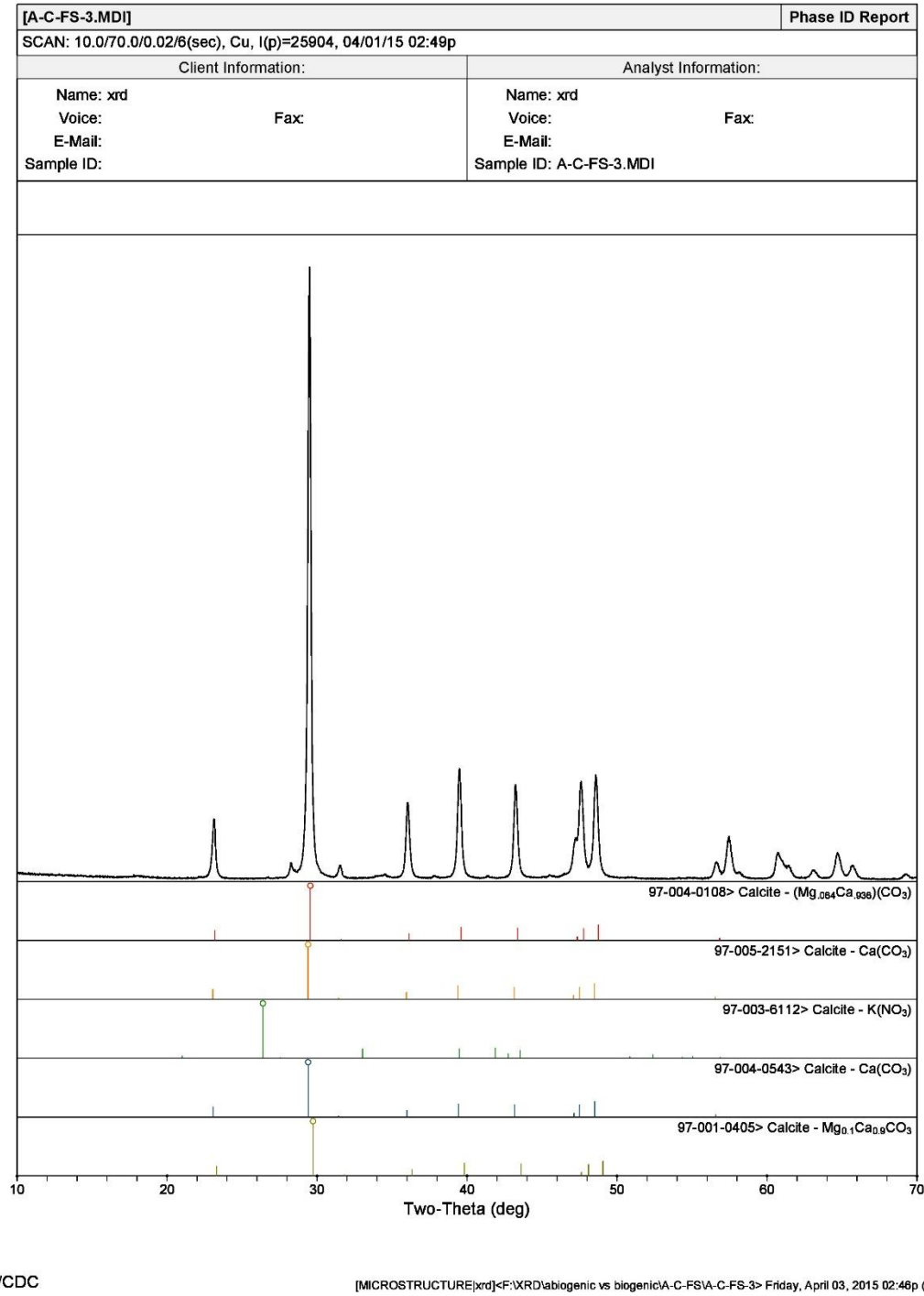

Figure A.17: A-C-FS-3 phase ID report showing peaks.

[A-C-FS-3.MDI]		Phase ID Report
SCAN: 10.0/70.0/0.02/6(sec), Cu, I(p)=25904, 04/01/15 02:49p		
Client Information:	Analyst Information:	
Name: xrd Voice: Fax: E-Mail: Sample ID:	Name: xrd Voice: Fax: E-Mail: Sample ID: A-C-FS-3.MDI	

#	Phase ID	PDF#	Wt%
1	Calcite - $(Mg_{.064}Ca_{.936})(CO_3)$	97-004-0108	27.5%
2	Calcite - $Ca(CO_3)$	97-005-2151	9.1%
3	Calcite - $K(NO_3)$	97-003-6112	0.0%
4	Calcite - $Ca(CO_3)$	97-004-0543	9.8%
5	Calcite - $Mg_{0.1}Ca_{0.9}CO_3$	97-001-0405	53.6%

CMRG/CDC

[MICROSTRUCTURE|xrd]<F:\XRD\abiogenic vs biogenic\A-C-FS\A-C-FS-3> Friday, April 03, 2015 02:46p (MDI/JADE9)

Figure A.18: A-C-FS-3 phase ID report showing mineralogical composition by weight.

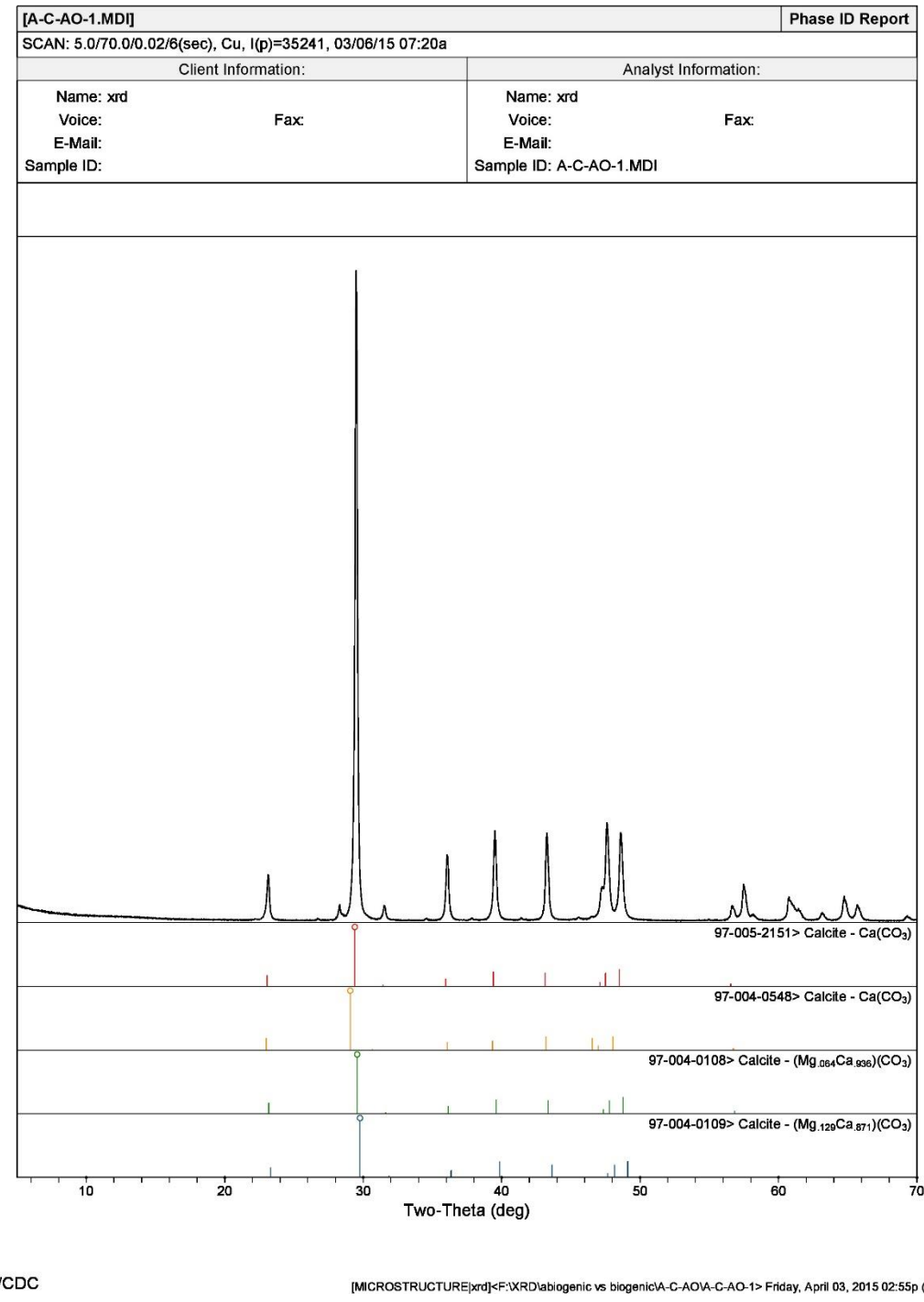

Figure A.19: A-C-AO-1 phase ID report showing peaks.

[A-C-AO-1.MDI]		Phase ID Report
SCAN: 5.0/70.0/0.02/6(sec), Cu, I(p)=35241, 03/06/15 07:20a		
Client Information:		Analyst Information:
Name: xrd Voice: Fax: E-Mail: Sample ID:		Name: xrd Voice: Fax: E-Mail: Sample ID: A-C-AO-1.MDI

#	Phase ID	PDF#	Wt%
1	Calcite - $Ca(CO_3)$	97-005-2151	29.7%
2	Calcite - $Ca(CO_3)$	97-004-0548	10.0%
3	Calcite - $(Mg_{.064}Ca_{.936})(CO_3)$	97-004-0108	60.4%
4	Calcite - $(Mg_{.129}Ca_{.871})(CO_3)$	97-004-0109	0.0%

CMRG/CDC [MICROSTRUCTURE|xrd]<F:\XRD\abiogenic vs biogenic\A-C-AO> Friday, April 03, 2015 02:53p (MDI/JADE9)

Figure A.20: A-C-AO-1 phase ID report showing mineralogical composition by weight.

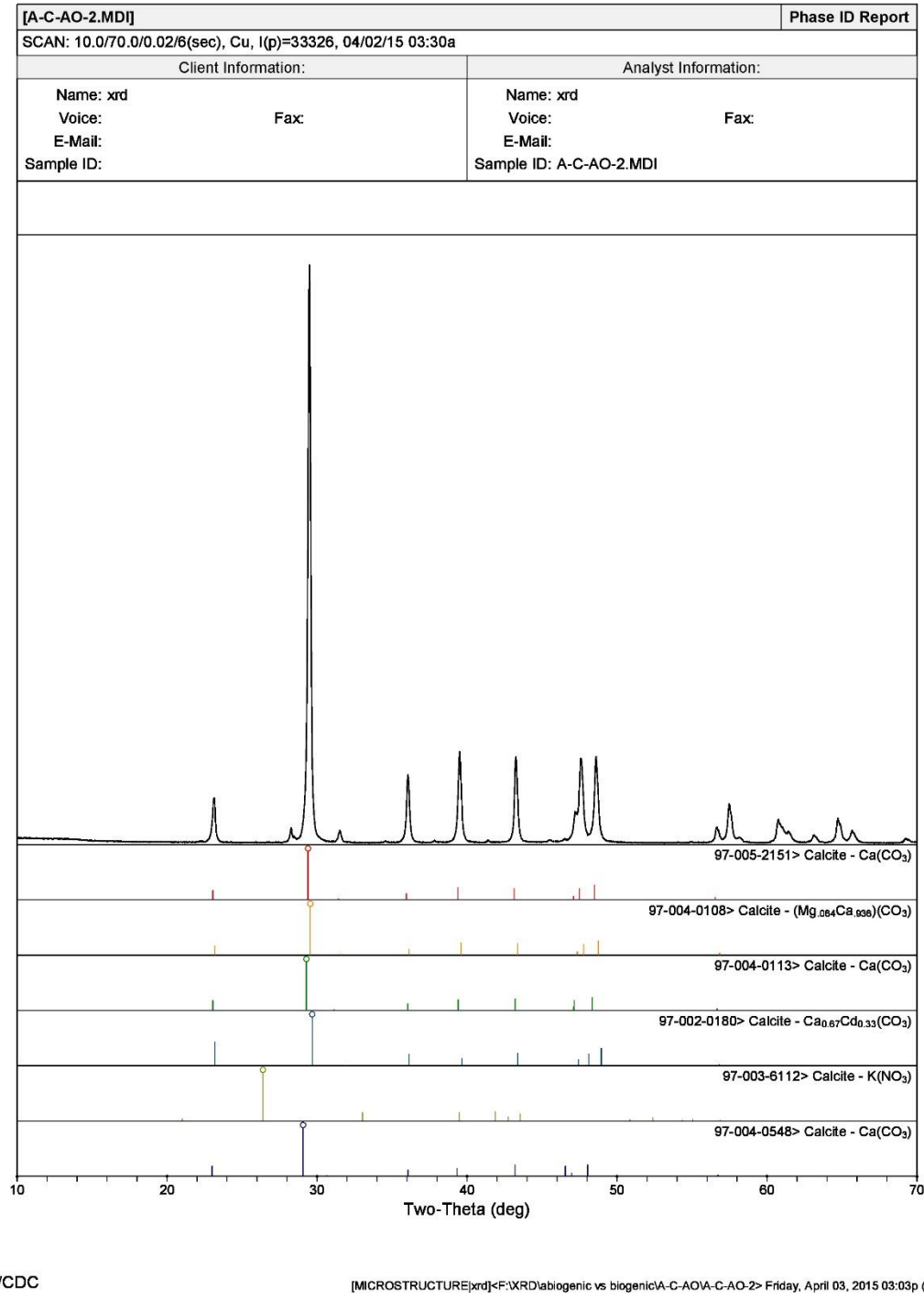

Figure A.21: A-C-AO-2 phase ID report showing peaks.

[A-C-AO-2.MDI]			Phase ID Report
SCAN: 10.0/70.0/0.02/6(sec), Cu, I(p)=33326, 04/02/15 03:30a			
Client Information:		Analyst Information:	
Name: xrd Voice: Fax: E-Mail: Sample ID:		Name: xrd Voice: Fax: E-Mail: Sample ID: A-C-AO-2.MDI	

#	Phase ID	PDF#	Wt%
1	Calcite - $Ca(CO_3)$	97-005-2151	10.9%
2	Calcite - $(Mg_{.064}Ca_{.936})(CO_3)$	97-004-0108	71.6%
3	Calcite - $Ca(CO_3)$	97-004-0113	5.0%
4	Calcite - $Ca_{0.67}Cd_{0.33}(CO_3)$	97-002-0180	1.6%
5	Calcite - $K(NO_3)$	97-003-6112	0.0%
6	Calcite - $Ca(CO_3)$	97-004-0548	11.0%

Figure A.22: A-C-AO-2 phase ID report showing mineralogical composition by weight.

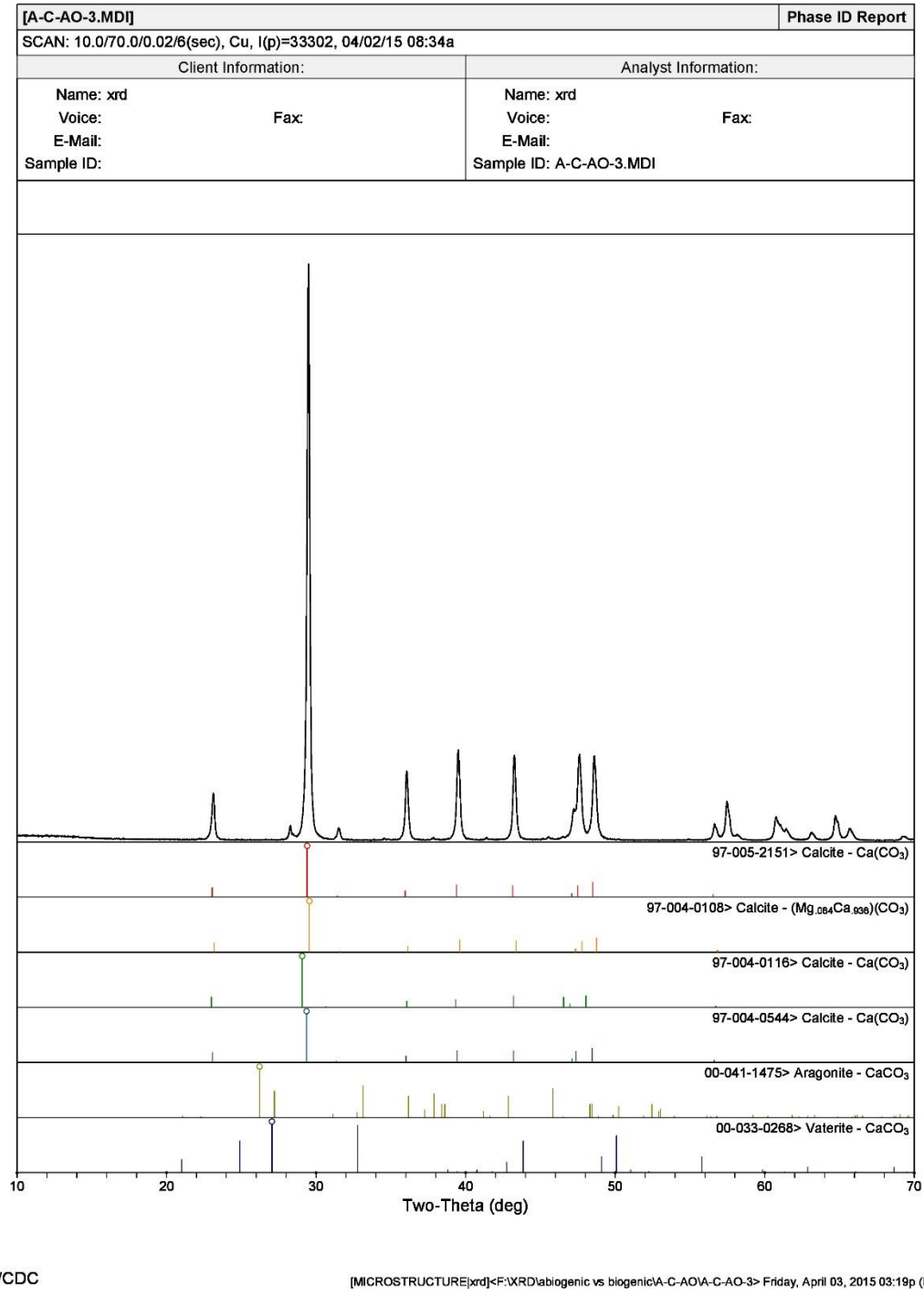

Figure A.23: A-C-AO-3 phase ID report showing peaks.

[A-C-AO-3.MDI]			Phase ID Report
SCAN: 10.0/70.0/0.02/6(sec), Cu, I(p)=33302, 04/02/15 08:34a			
Client Information:		Analyst Information:	
Name: xrd Voice: Fax: E-Mail: Sample ID:		Name: xrd Voice: Fax: E-Mail: Sample ID: A-C-AO-3.MDI	

#	Phase ID	PDF#	Wt%
1	Calcite - $Ca(CO_3)$	97-005-2151	0.0%
2	Calcite - $(Mg_{.064}Ca_{.936})(CO_3)$	97-004-0108	89.0%
3	Calcite - $Ca(CO_3)$	97-004-0116	11.0%
4	Calcite - $Ca(CO_3)$	97-004-0544	0.0%
5	Aragonite - $CaCO_3$	00-041-1475	0.0%
6	Vaterite - $CaCO_3$	00-033-0268	0.0%

CMRG/CDC

[MICROSTRUCTURE|xrd]<F:\XRD\abiogenic vs biogenic\A-C-AO\A-C-AO-3> Friday, April 03, 2015 03:18p (MDI/JADE9)

Figure A.24: A-C-AO-3 phase ID report showing mineralogical composition by weight.

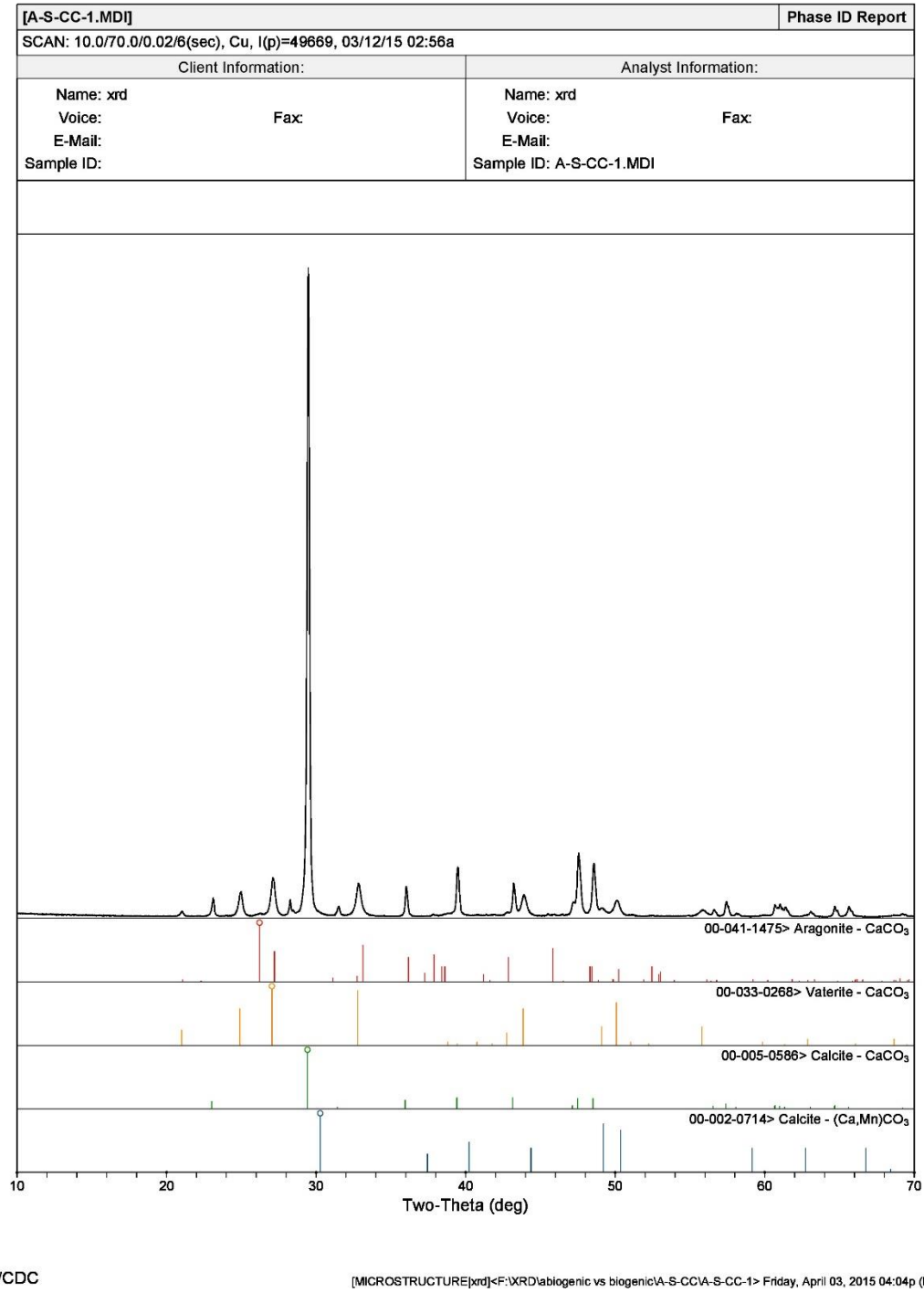

Figure A.25: A-S-CC-1 phase ID report showing peaks.

[A-S-CC-1.MDI]		Phase ID Report
SCAN: 10.0/70.0/0.02/6(sec), Cu, I(p)=49669, 03/12/15 02:56a		
Client Information:		Analyst Information:
Name: xrd Voice: Fax: E-Mail: Sample ID:		Name: xrd Voice: Fax: E-Mail: Sample ID: A-S-CC-1.MDI

#	Phase ID	PDF#	Wt%
1	Aragonite - $CaCO_3$	00-041-1475	6.0%
2	Vaterite - $CaCO_3$	00-033-0268	9.1%
3	Calcite - $CaCO_3$	00-005-0586	84.9%
4	Calcite - $(Ca,Mn)CO_3$	00-002-0714	1.0%

CMRG/CDC

[MICROSTRUCTURE]xrd]<F:\XRD\abiogenic vs biogenic\A-S-CC\A-S-CC-1> Friday, April 03, 2015 04:04p (MDI/JADE9)

Figure A.26: A-S-CC-1 phase ID report showing mineralogical composition by weight.

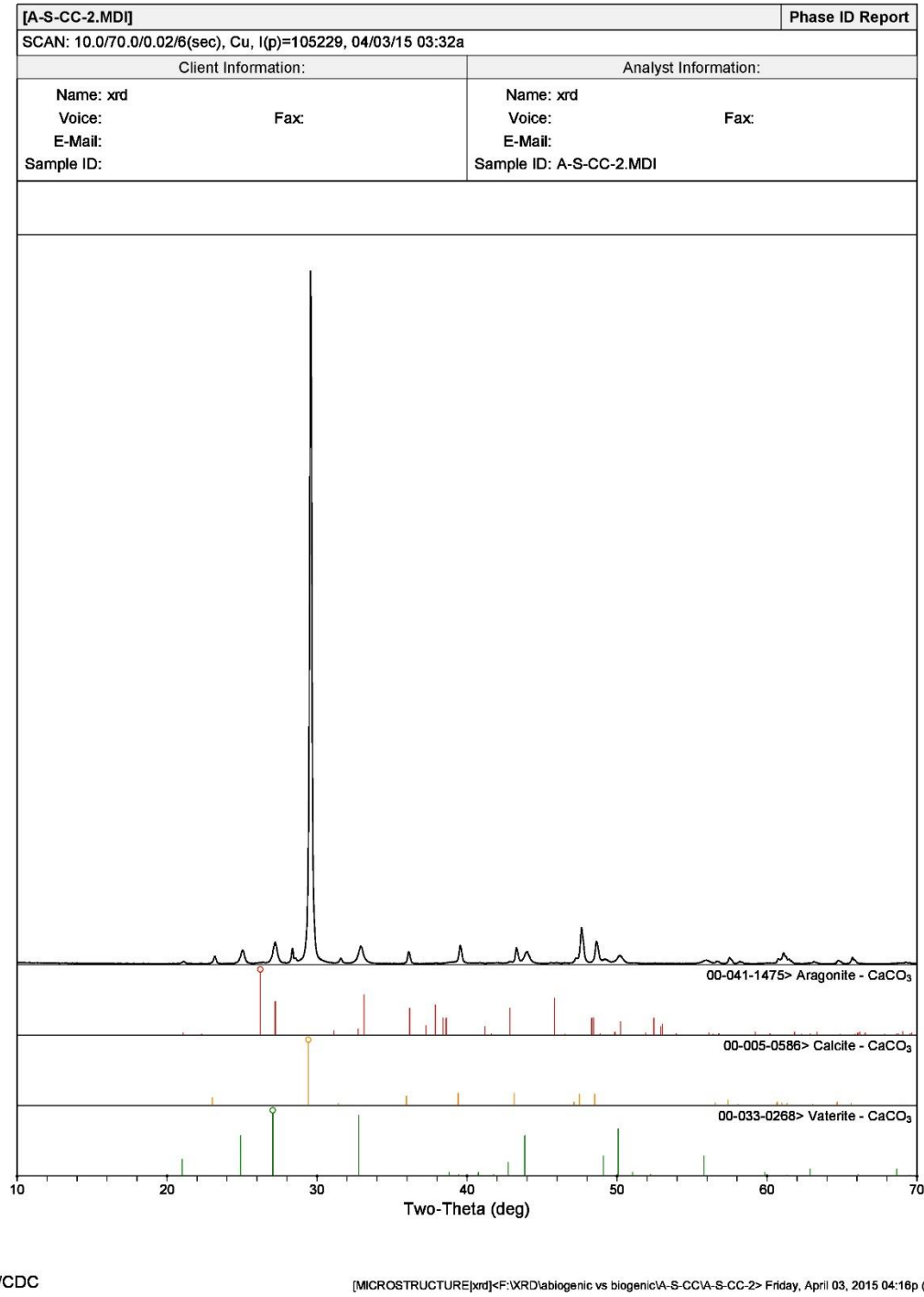

Figure A.27: A-S-CC-2 phase ID report showing peaks.

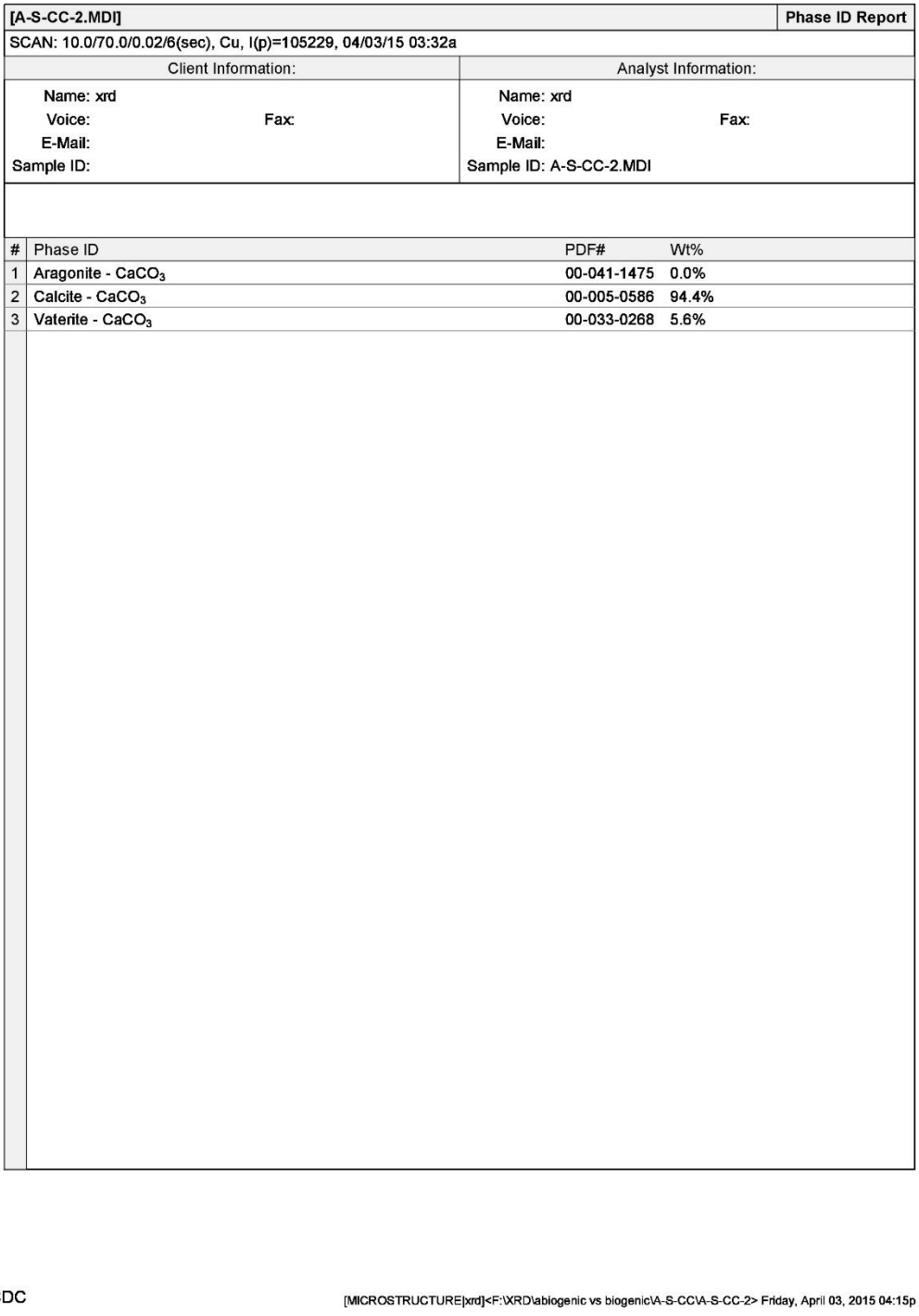

[A-S-CC-2.MDI] Phase ID Report

SCAN: 10.0/70.0/0.02/6(sec), Cu, I(p)=105229, 04/03/15 03:32a

Client Information:	Analyst Information:
Name: xrd	Name: xrd
Voice: Fax:	Voice: Fax:
E-Mail:	E-Mail:
Sample ID:	Sample ID: A-S-CC-2.MDI

#	Phase ID	PDF#	Wt%
1	Aragonite - $CaCO_3$	00-041-1475	0.0%
2	Calcite - $CaCO_3$	00-005-0586	94.4%
3	Vaterite - $CaCO_3$	00-033-0268	5.6%

Figure A.28: A-S-CC-2 phase ID report showing mineralogical composition by weight.

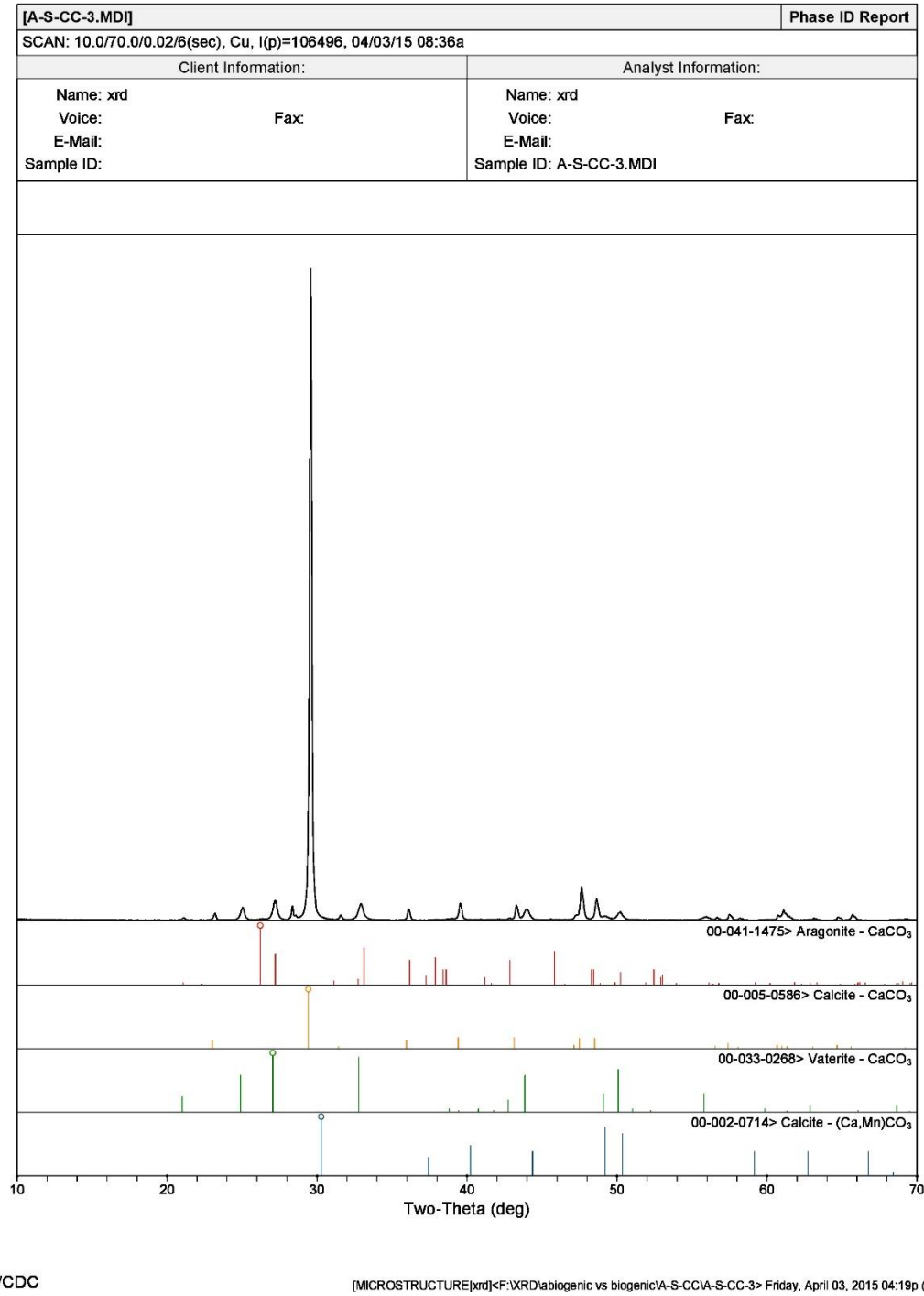

Figure A.29: A-S-CC-3 phase ID report showing peaks.

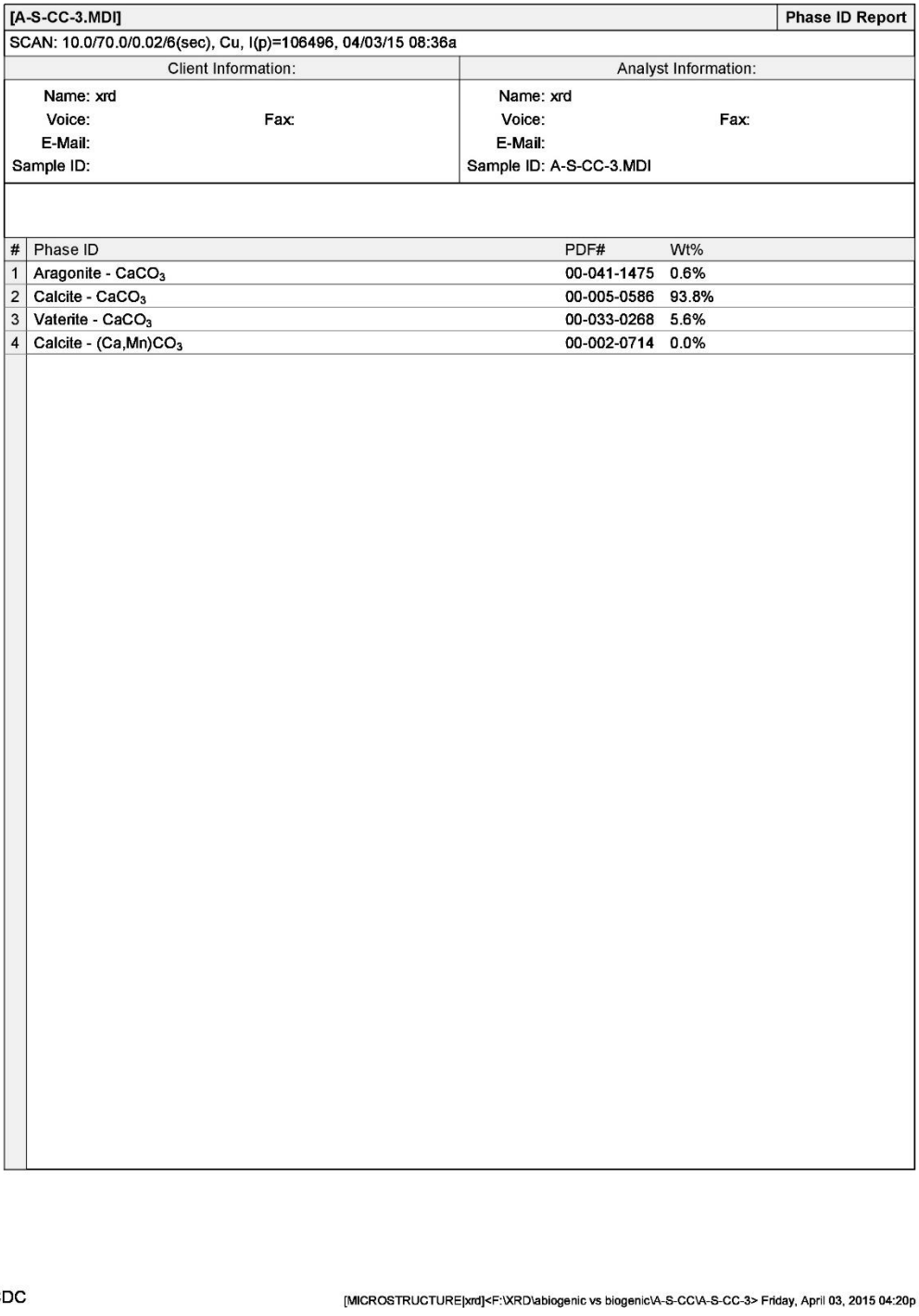

[A-S-CC-3.MDI] Phase ID Report

SCAN: 10.0/70.0/0.02/6(sec), Cu, I(p)=106496, 04/03/15 08:36a

Client Information:	Analyst Information:
Name: xrd	Name: xrd
Voice: Fax:	Voice: Fax:
E-Mail:	E-Mail:
Sample ID:	Sample ID: A-S-CC-3.MDI

#	Phase ID	PDF#	Wt%
1	Aragonite - $CaCO_3$	00-041-1475	0.6%
2	Calcite - $CaCO_3$	00-005-0586	93.8%
3	Vaterite - $CaCO_3$	00-033-0268	5.6%
4	Calcite - $(Ca,Mn)CO_3$	00-002-0714	0.0%

Figure A.30: A-S-CC-3 phase ID report showing mineralogical composition by weight.

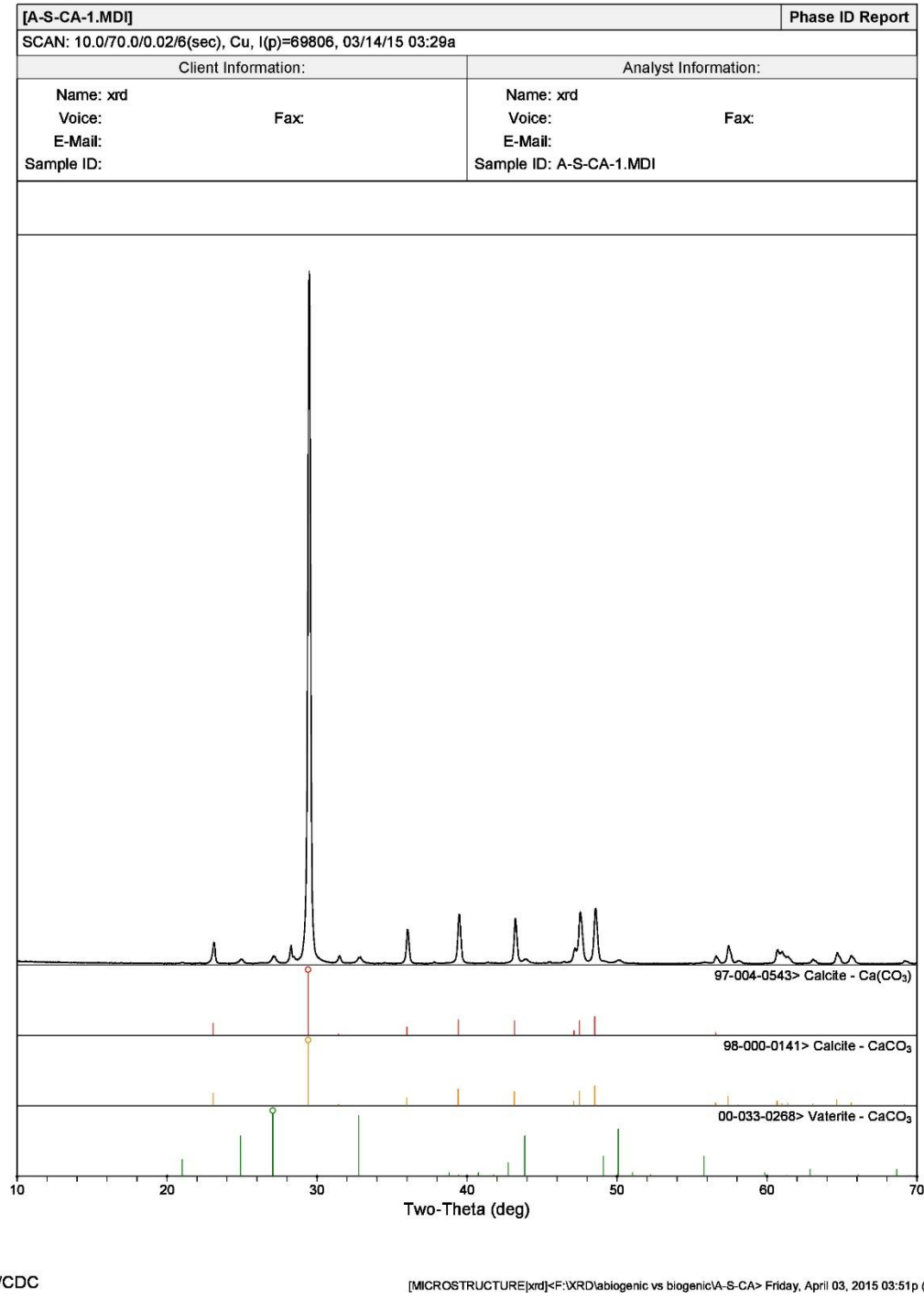

Figure A.31: A-S-CA-1 phase ID report showing peaks.

[A-S-CA-1.MDI]			Phase ID Report
SCAN: 10.0/70.0/0.02/6(sec), Cu, I(p)=69806, 03/14/15 03:29a			
Client Information:		Analyst Information:	
Name: xrd Voice: Fax: E-Mail: Sample ID:		Name: xrd Voice: Fax: E-Mail: Sample ID: A-S-CA-1.MDI	

#	Phase ID	PDF#	Wt%
1	Calcite - $Ca(CO_3)$	97-004-0543	73.8%
2	Calcite - $CaCO_3$	98-000-0141	24.1%
3	Vaterite - $CaCO_3$	00-033-0268	2.1%

Figure A.32: A-S-CA-1 phase ID report showing mineralogical composition by weight.

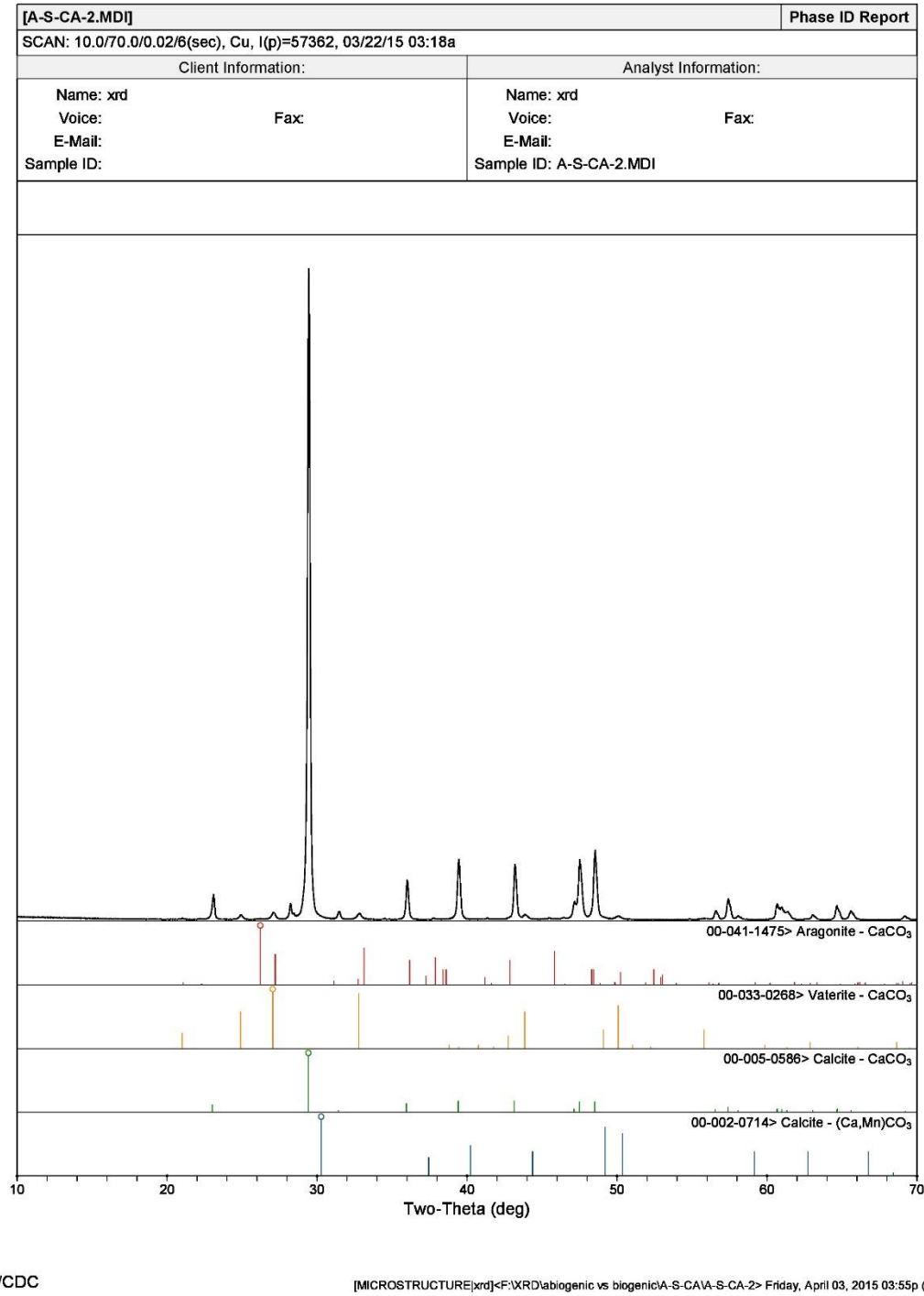

Figure A.33: A-S-CA-2 phase ID report showing peaks.

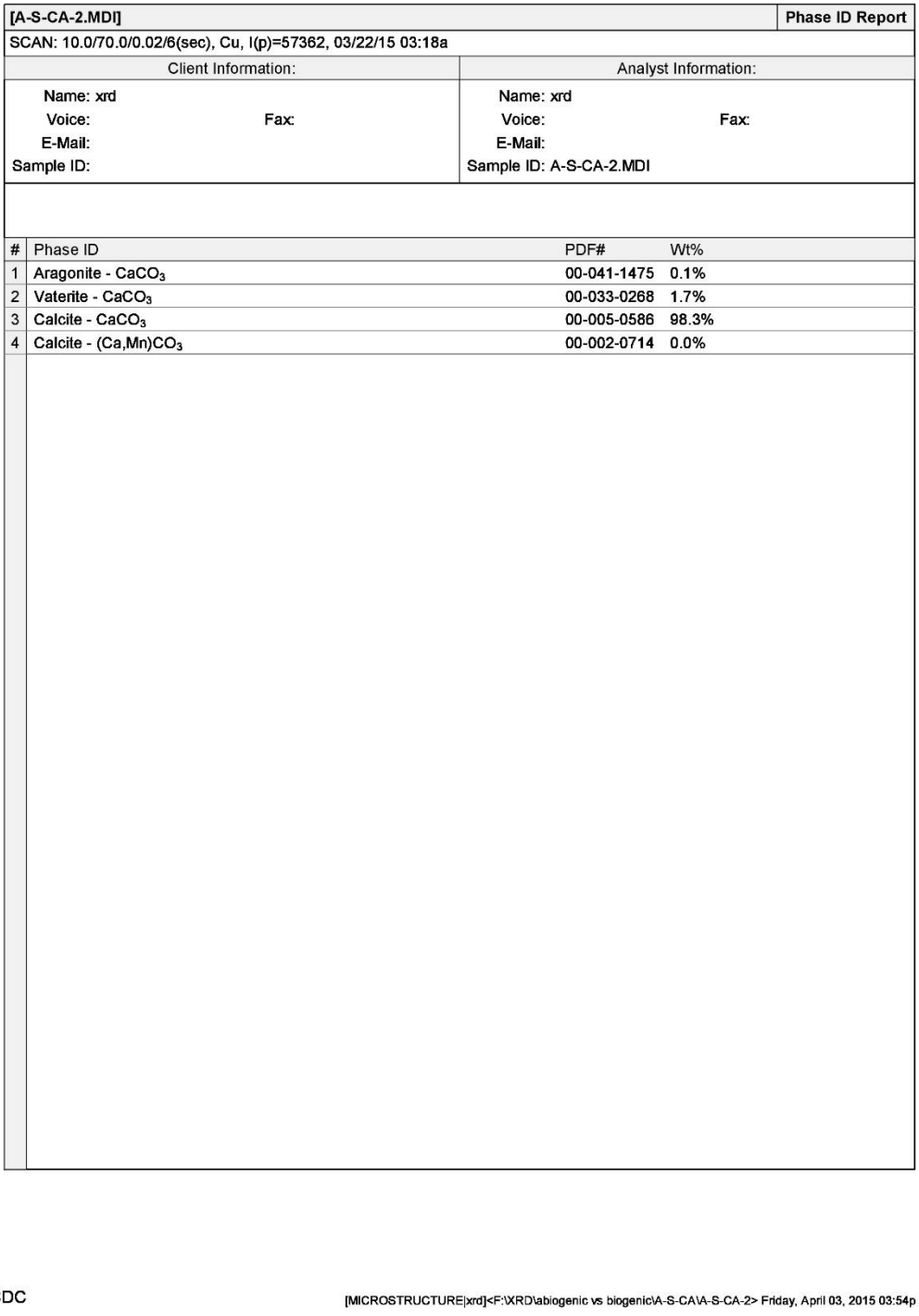

[A-S-CA-2.MDI] **Phase ID Report**

SCAN: 10.0/70.0/0.02/6(sec), Cu, I(p)=57362, 03/22/15 03:18a

Client Information:	Analyst Information:
Name: xrd	Name: xrd
Voice: Fax:	Voice: Fax:
E-Mail:	E-Mail:
Sample ID:	Sample ID: A-S-CA-2.MDI

#	Phase ID	PDF#	Wt%
1	Aragonite - $CaCO_3$	00-041-1475	0.1%
2	Vaterite - $CaCO_3$	00-033-0268	1.7%
3	Calcite - $CaCO_3$	00-005-0586	98.3%
4	Calcite - $(Ca,Mn)CO_3$	00-002-0714	0.0%

Figure A.34: A-S-CA-2 phase ID report showing mineralogical composition by weight.

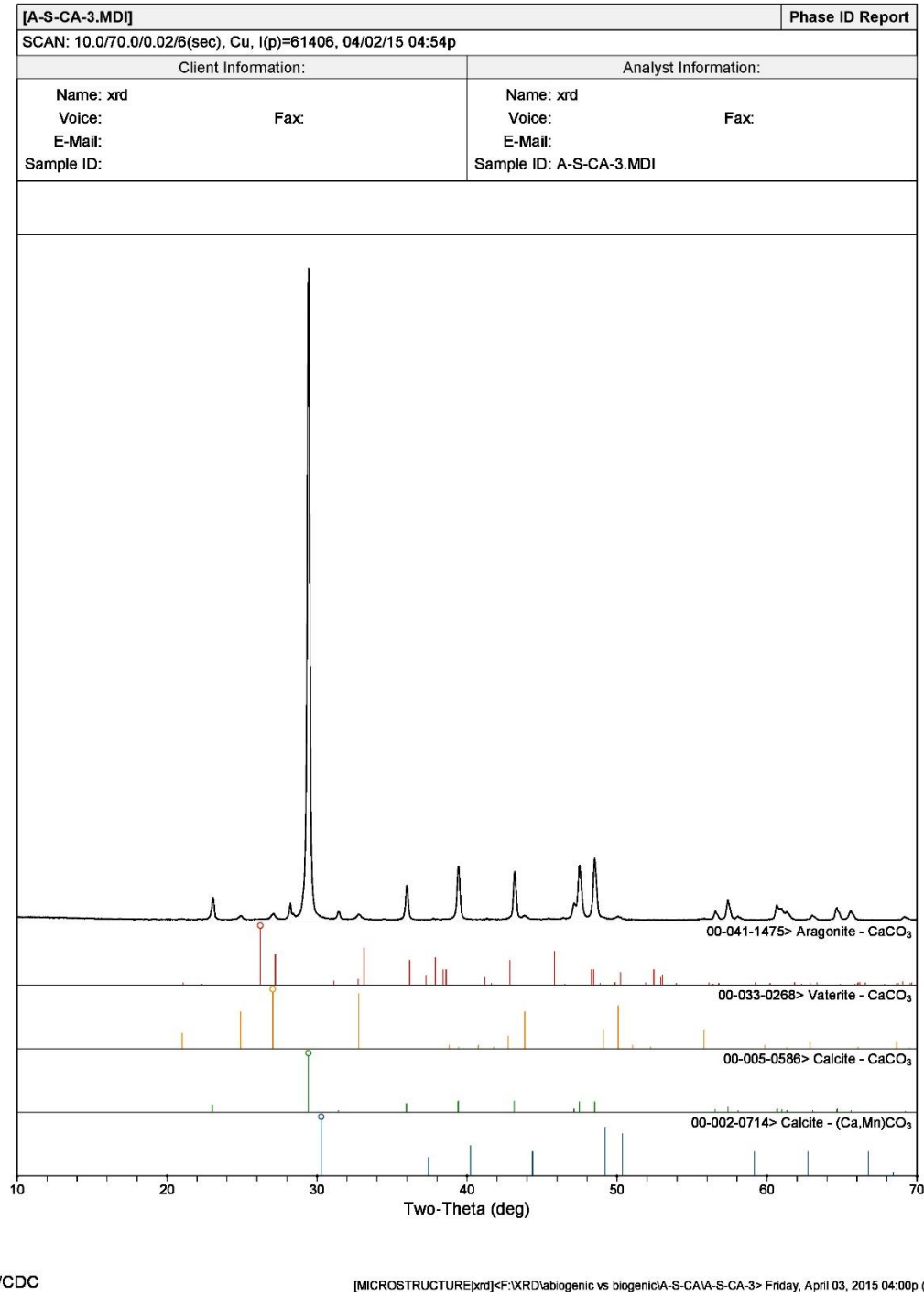

Figure A.35: A-S-CA-3 phase ID report showing peaks.

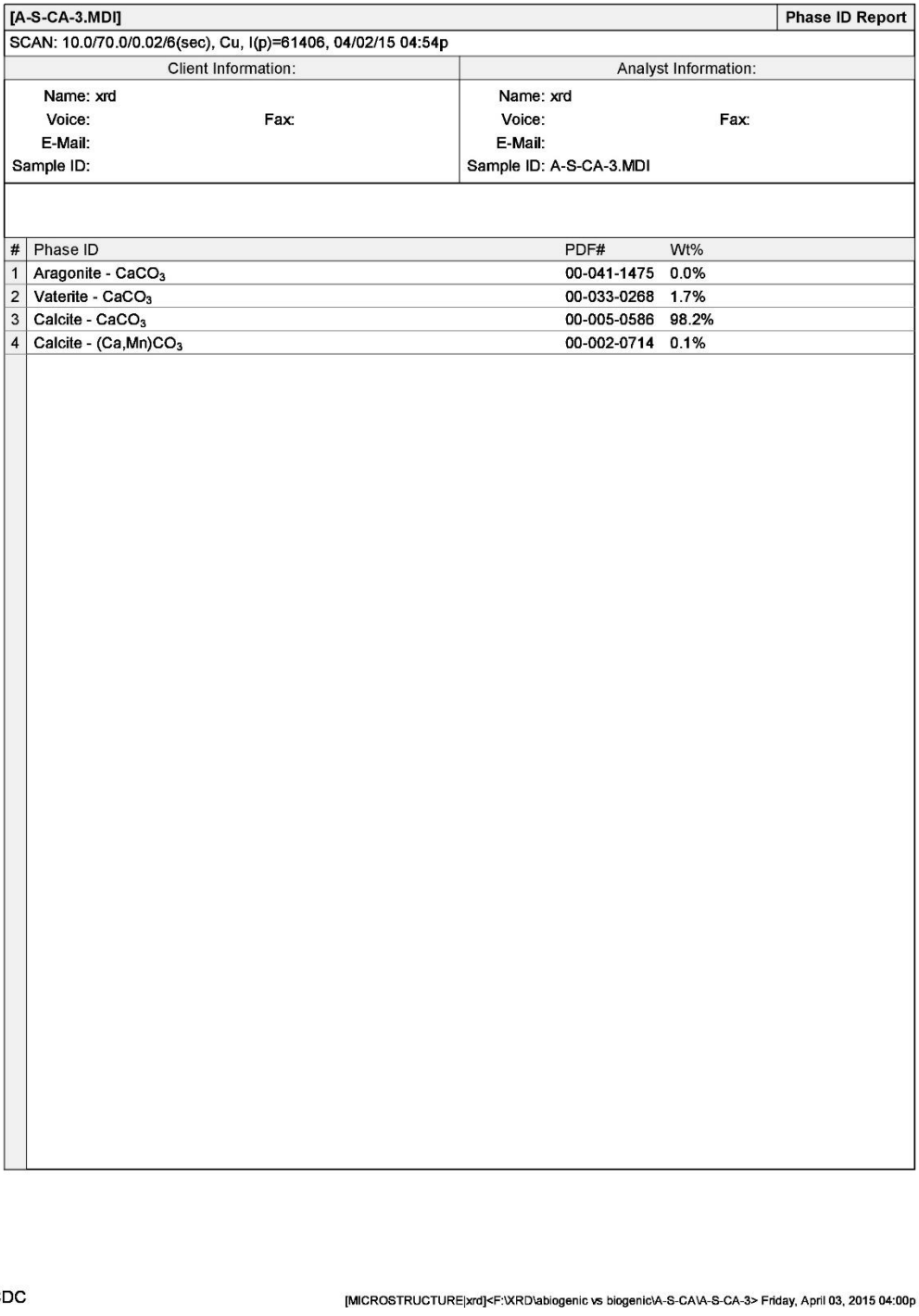

[A-S-CA-3.MDI] Phase ID Report

SCAN: 10.0/70.0/0.02/6(sec), Cu, I(p)=61406, 04/02/15 04:54p

Client Information:	Analyst Information:
Name: xrd	Name: xrd
Voice: Fax:	Voice: Fax:
E-Mail:	E-Mail:
Sample ID:	Sample ID: A-S-CA-3.MDI

#	Phase ID	PDF#	Wt%
1	Aragonite - $CaCO_3$	00-041-1475	0.0%
2	Vaterite - $CaCO_3$	00-033-0268	1.7%
3	Calcite - $CaCO_3$	00-005-0586	98.2%
4	Calcite - $(Ca,Mn)CO_3$	00-002-0714	0.1%

Figure A.36: A-S-CA-3 phase ID report showing mineralogical composition by weight.

Appendix B: Optical Images of Crack Sealing

The following optical images depict a cracked, untreated, neat beam (Figure B.1) and a treated beam from each sample group 28 days after the treatment was applied (Figures B.2 - B.11)

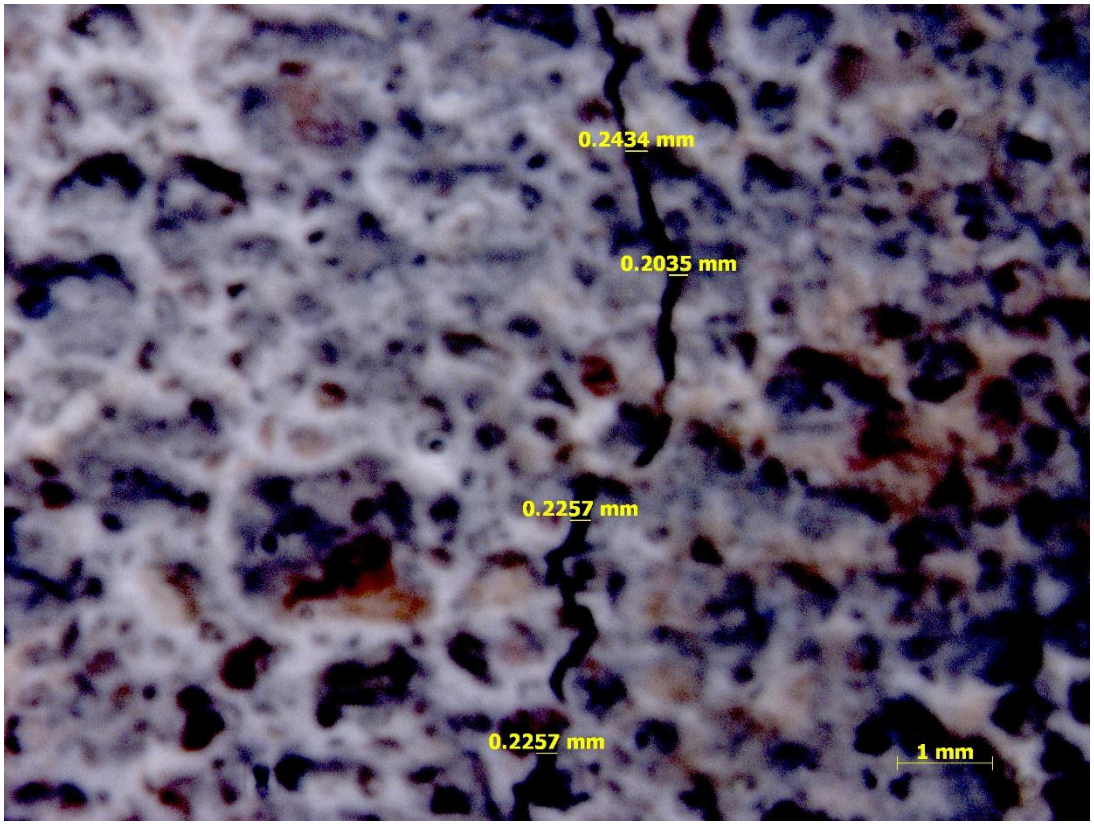

Figure B.1: An untreated, cracked, neat beam.

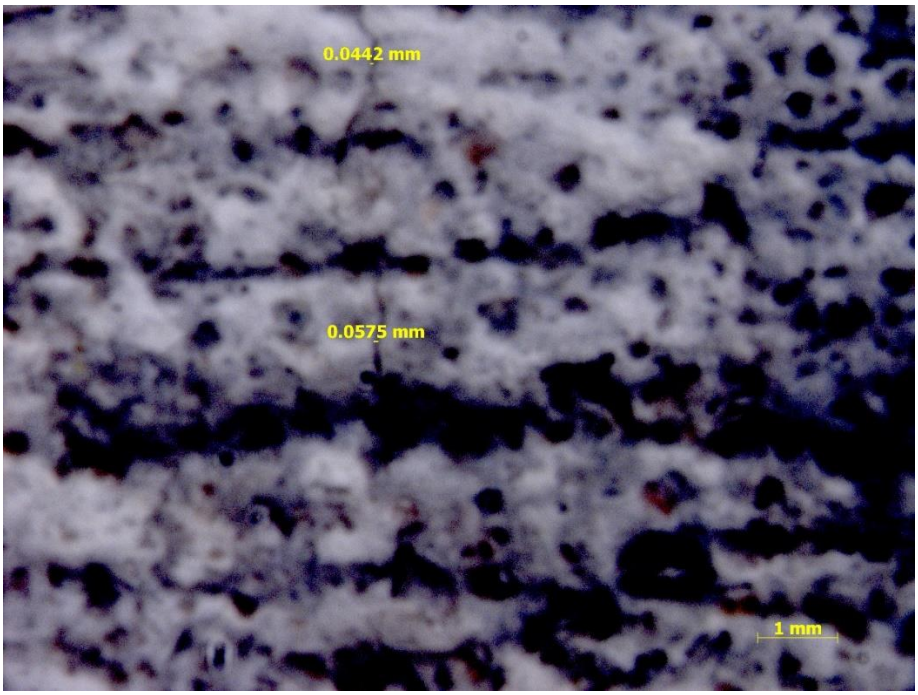

Figure B.2: A beam from group A1 28 days after treatment.

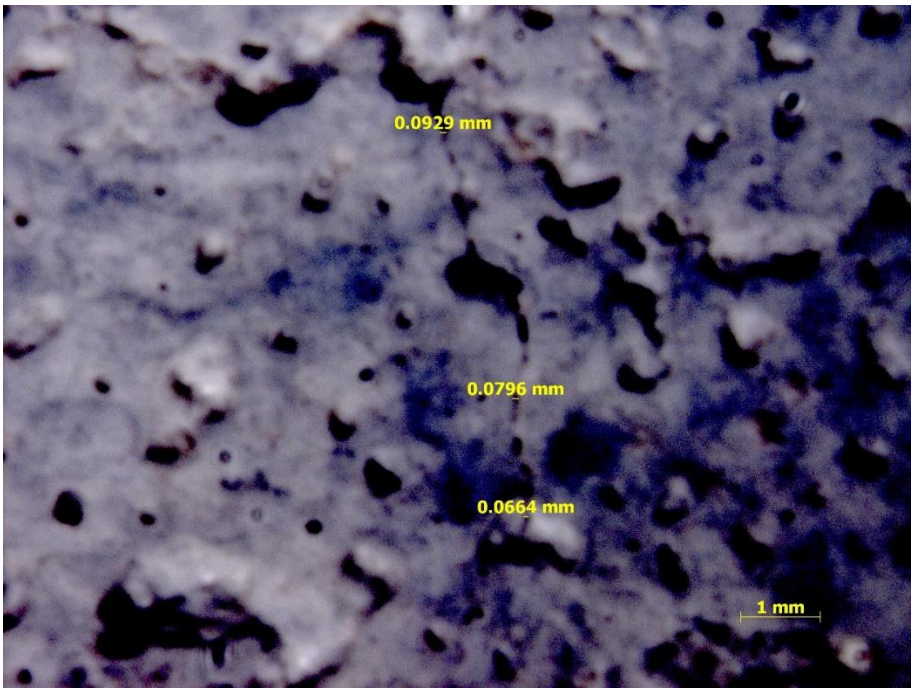

Figure B.3: A beam from group A2 28 days after treatment.

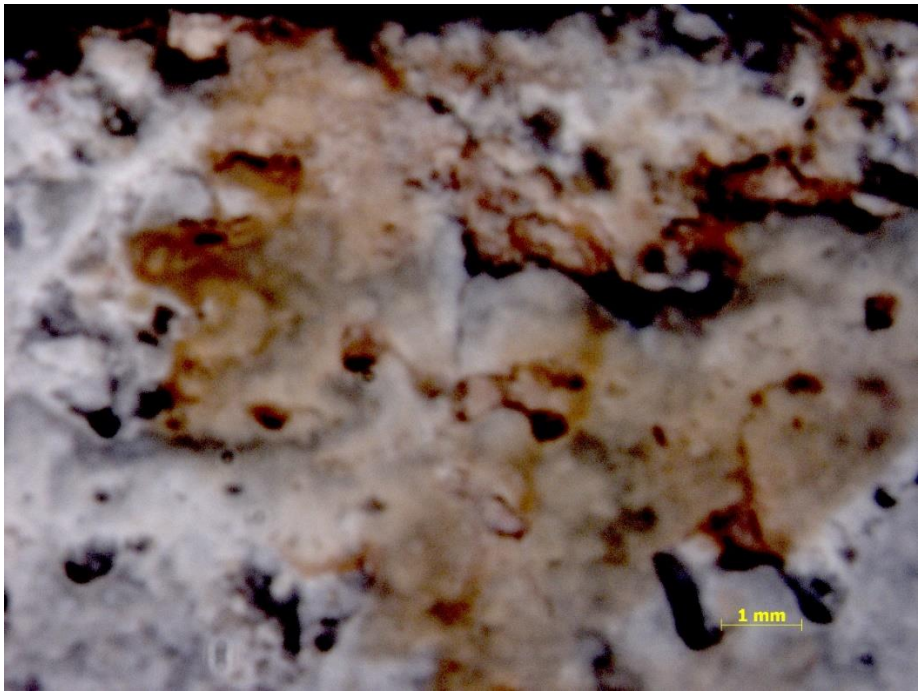

Figure B.4: A beam from group A3 28 days after treatment.

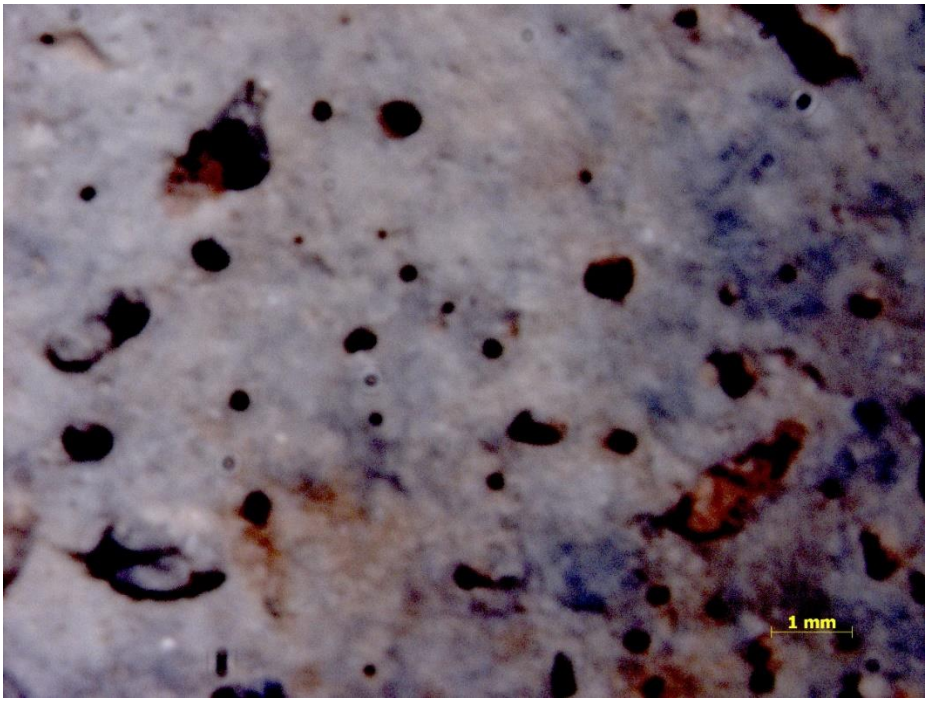

Figure B.5: A beam from group A4 28 days after treatment.

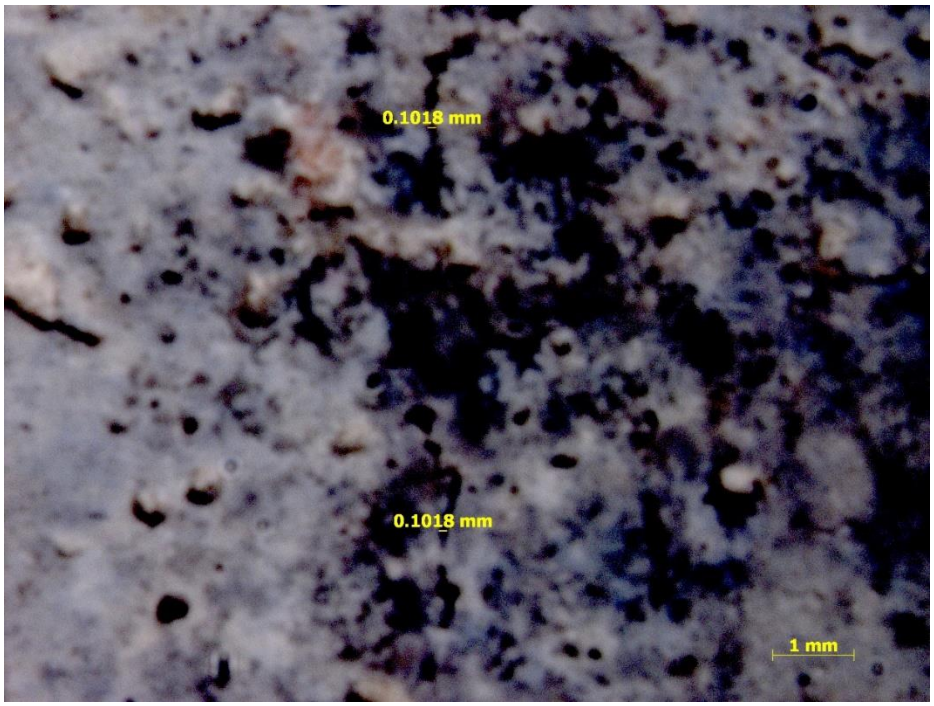

Figure B.6: A beam from group B1 28 days after treatment.

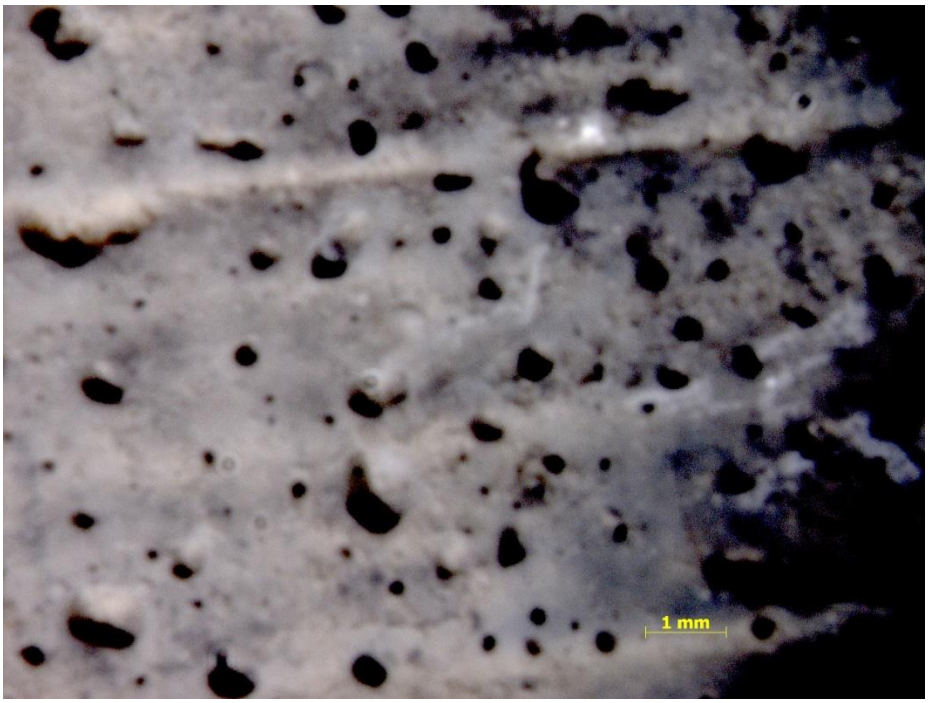

Figure B.7: A beam from group B2 28 days after treatment.

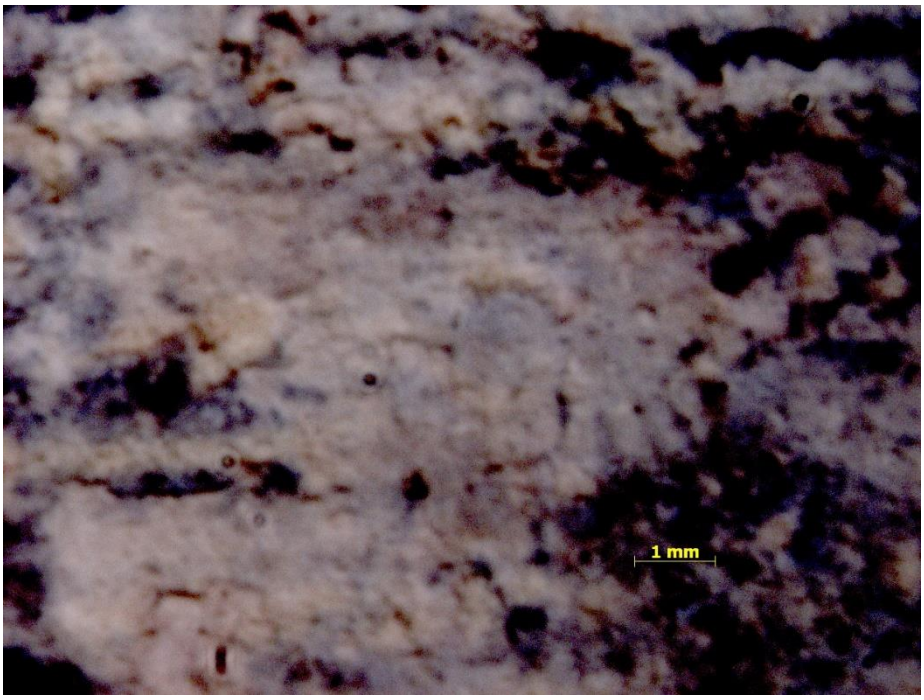

Figure B.8: A beam from group B3 28 days after treatment.

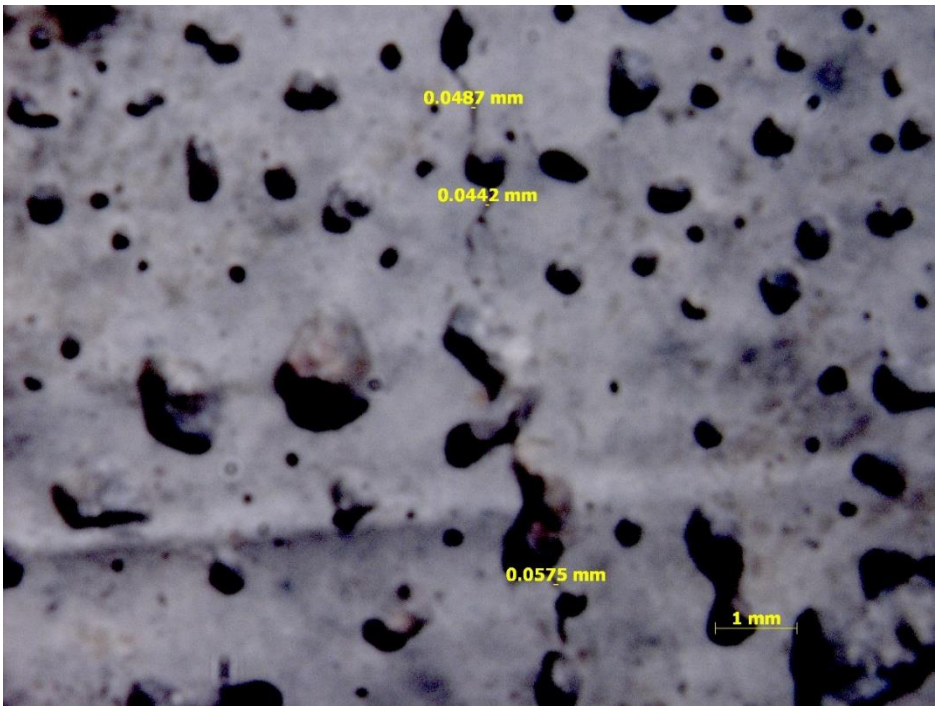

Figure B.9: A beam from group C1 28 days after treatment.

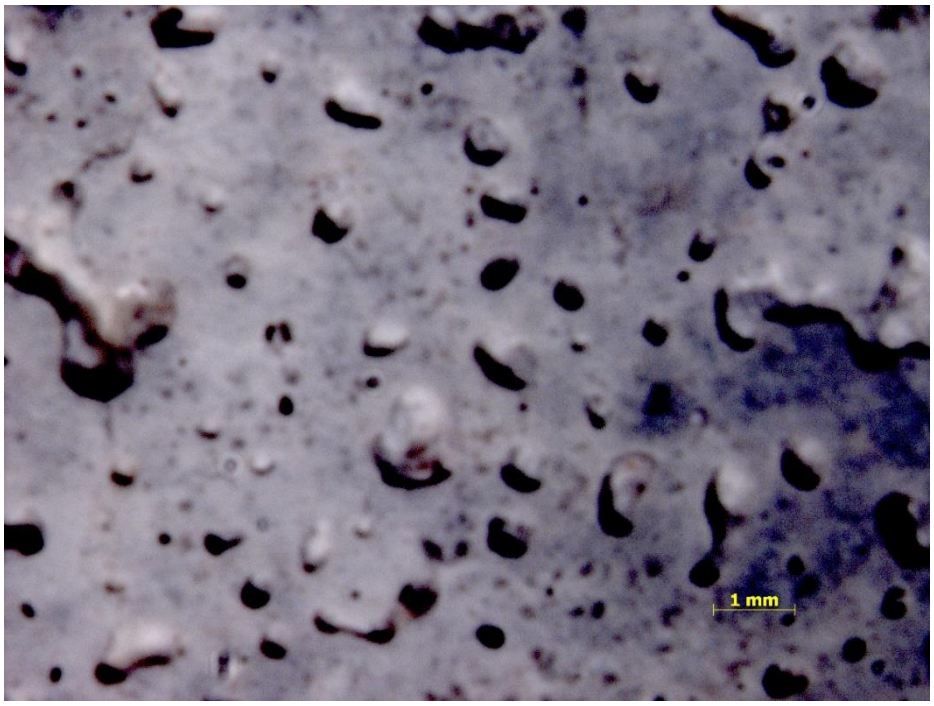

Figure B.10: A beam from group C2 28 days after treatment.

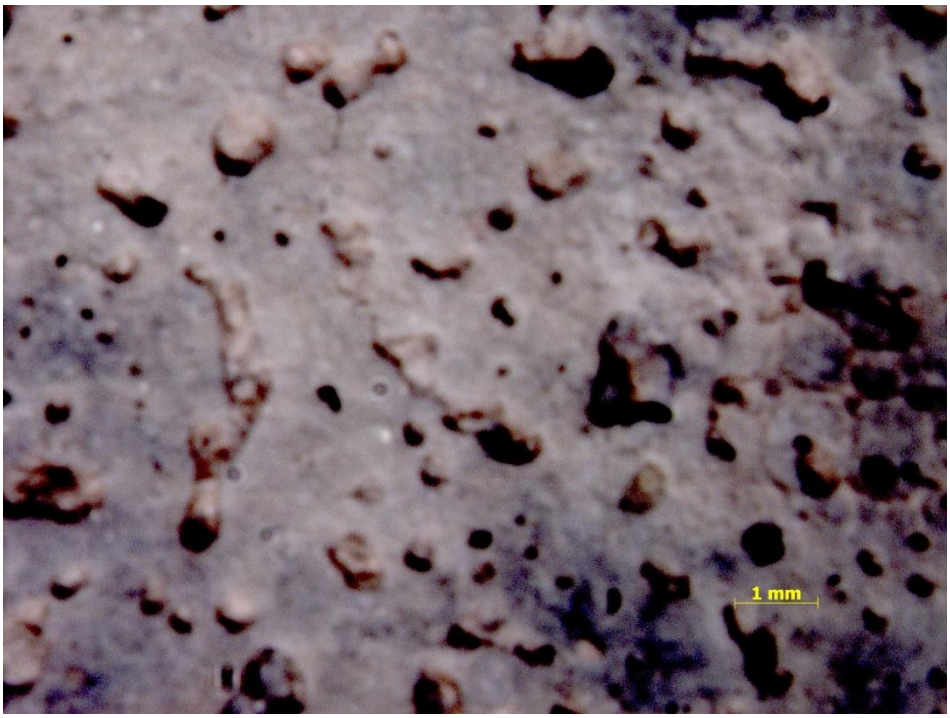

Figure B.11: A beam from group C3 28 days after treatment.

Appendix C: Flexural Loads and Stresses

Table C.1 displays the pertinent values used to calculate strength recovery in Section 8.3.3 for each beam examined in this study.

Table C.1: Initial peak load, peak load 28 days after treatment, initial peak stress, peak stress 28 days after treatment, and strength recovery for neat (A), UYE bacterial (B), and UME-SA bacterial beams subjected to various bacteria-based treatments.

Group	Initial peak load (N)	Peak load 28 days after treatment (N)	Initial peak stress (MPa)	Peak stress 28 days after treatment (MPa)	Strength recovery (%)
A1	511.36	61.37	9.51	1.14	12.00
	610.07	39.86	11.35	0.74	6.53
	539.71	32.46	10.04	0.60	6.01
A2	459.20	62.88	8.54	1.17	13.69
	497.42	40.13	9.25	0.75	8.07
	480.45	77.98	8.94	1.45	16.23
A3	510.75	71.41	9.50	1.33	13.98
	437.09	44.10	8.13	0.82	10.09
	508.73	29.52	9.46	0.55	5.80
A4	547.72	24.85	10.19	0.46	4.54
	478.13	43.04	8.89	0.80	9.00
	454.10	39.96	8.45	0.74	8.80
B1	420.24	68.56	7.82	1.28	16.31
	419.95	54.47	7.81	1.01	12.97
	416.54	59.63	7.75	1.11	14.32
B2	441.79	56.31	8.22	1.05	12.75
	425.97	80.84	7.92	1.50	18.98
	446.51	61.24	8.31	1.14	13.72
B3	427.18	49.36	7.95	0.92	11.55
	367.14	62.09	6.83	1.15	16.91
	385.99	60.31	7.18	1.12	15.62
C1	378.68	59.82	7.04	1.11	15.80
	338.41	57.97	6.29	1.08	17.13
	422.77	55.93	7.86	1.04	13.23
C2	449.09	89.08	8.35	1.66	19.84
	360.80	50.39	6.71	0.94	13.97
	397.66	48.44	7.40	0.90	12.18
C3	365.30	141.25	6.79	2.63	38.67
	328.03	97.52	6.10	1.81	29.73
	385.79	78.17	7.18	1.45	20.26

References

[1] V. Li and E. Herbert, "Robust self-healing concrete for sustainable infrastructure," *Journal of Advanced Concrete Technology,* vol. 10, pp. 207-218, 2012.

[2] L. Westra, C. Soskolne and D. Spady, Human Health and Ecological Integrity: Ethics, Law and Human Rights, London: Routledge, 2012.

[3] A. Gurtoo and S. Antony, "Environmental regulations," *Management of Environmental Quality: An International Journal,* vol. 18, no. 6, pp. 626-642, 2007.

[4] R. Jelinek, Biomimetics: A Molecular Perspective, Berlin/ Boston: Walter de Gruyter GmbH, 2013.

[5] Strategic Development Council, "Roadmap 2030: The U.S. Concrete Industry Technology Roadmap," 2020.

[6] J. Allwood, J. Cullen and R. Milford, "Options for achieving a 50% cut in industrial carbon emissions by 2050," *Environmental Science & Technology,* vol. 44, no. 6, p. 1888, 2010.

[7] Y. Liu, Y. Kuang, N. Huang, Z. Wu and C. Wang, "CO_2 emission from cement manufacturing and its driving forces in China," *International Journal of Environment and Pollution,* vol. 37, no. 4, pp. 369-382, 2009.

[8] V. M. Malhotra, "Role of fly ash in reducing greenhouse gas emissions during the manufacturing of portland cement clinker," *Advances in Concrete Technologies in the Middle East,* pp. 19-20, 2008.

[9] L. Haselbach, "Potential for Carbon Dioxide Absorption in Concrete," *Journal of Environmental Engineering,* vol. 135, no. SPECIAL ISSUE: Recent Developments in CO_2 Emission Control Technology, p. 465–472, 2009.

[10] C. Pade and M. Guimaraes, "The CO_2 uptake of concrete in a 100 year perspective," *Cement and Concrete Research,* vol. 37, no. 9, p. 1348–1356, 2007.

[11] E. Worrell, L. Price, N. Martin, C. Hendriks and L. Ozawa Meida, "Carbon dioxide emissions from the global cement industry," *Annual Review of Energy and the Environment,* vol. 26, p. 303–329, 2001.

[12] J. Benyus, Biomimicry: innovation inspired by nature, New York: Williams Morrow and Company, 1997.

[13] A. Meier, E. Bonaldi, G. M. Cella, W. Lipinski and D. Wuillemin, "Solar chemical reactor technology for industrial production of lime," *Solar Energy,* vol. 80, no. 10, pp. 1355-1362, 2006.

[14] S. Licht, H. Wu, C. Hettige, B. Wang, J. Asercion, J. Lau and J. Stewart, "STEP cement: solar thermal electrochemical production of CaO without CO_2 emission," *Chemical Communications,* vol. 48, no. 48, pp. 6019-6021, 2012.

[15] B. Klotz, "New developments in precalciners and preheaters," in *IEEE/PCA Cement Industry Technical Conference*, Hershey, 1997.

[16] V. Houšt, J. Eliáš and L. Mič̆a, "Shape optimization of concrete buried arches," *Engineering Structures,* vol. 48, pp. 716-726, 2013.

[17] J. Akbari, M. Ahmadi and H. Moharrami, "Advances in concrete arch dams shape optimization," *Applied Mathematical Modelling,* vol. 35, no. 7, p. 3316–3333, 2011.

[18] N. Oikonomou, "Recycled concrete aggregates," *Cement and Concrete Composites,* vol. 27, no. 2, pp. 315-318, 2005.

[19] V. Radonjanin, M. Malesev, S. Marinkovic and A. Malty, "Green recycled aggregate concrete," *Construction and Building Materials,* vol. 47, pp. 1503-1511, 2013.

[20] J. Sharma and S. Singla, "Study of recycled concrete aggregates," *International Journal of Engineering Trends and Technology,* vol. 13, no. 3, pp. 123-125, 2014.

[21] C. Thomas, J. Setien, J. Polanco, P. Alaejos and M. S. de Juan, "Durability of recycled aggregate concrete," *Construction and Building Materials,* vol. 40, pp. 1054-1065, 2013.

[22] K. McNeil and T. Kang, "Recycled concrete aggregates: a review," *International Journal of Concrete Structures and Materials,* vol. 7, no. 1, pp. 61-69, 2013.

[23] J. Xiao, D. Lu and J. Ying, "Durability of recycled aggregate concrete," *Journal of Advanced Concrete Technology,* vol. 11, no. 12, p. 347, 2013.

[24] J. Sanchez, "The effect of curing time and mix parameters on the sequestration of carbon dioxide in concrete," The University of Texas at San Antonio, San Antonio, 2012.

[25] P. Pipilikaki, M. Katsioti, D. Papageorgiou, D. Fragoulis and E. Chaniotakis, "Use of tire derived fuel in clinker burning," *Cement and Concrete Composites,* vol. 27, no. 7-8, p. 843–847, 2005.

[26] M. Trezza and A. Scian, "Burning wastes as an industrial resource: Their effect on Portland cement clinker," *Cement and Concrete Research,* vol. 30, no. 1, p. 137–144, 2000.

[27] M. Trezza and A. Scian, "Waste fuels: their effect on Portland cement clinker," *Cement and Concrete Research,* vol. 35, no. 3, pp. 438-444, 2005.

[28] V. Papadakis and S. Tsimas, "Supplementary cementing materials in concrete: Part I: efficiency and design," *Cement and Concrete Research,* vol. 32, no. 10, p. 1525–1532, 2002.

[29] V. Papadakis, S. Antiohos and S. Tsimas, "Supplementary cementing materials in concrete: Part II: A fundamental estimation of the efficiency factor," *Cement and Concrete Research,* vol. 32, no. 10, p. 1533–1538, 2002.

[30] A. Kiliç, C. Atis, A. Teymen, O. Karahan, F. Ozcan, C. Bilim and M. Ozdemir, "The influence of aggregate type on the strength and abrasion resistance of high strength concrete," *Cement and Concrete Composites,* vol. 30, no. 4, pp. 290-296, 2008.

[31] C. Gonilho Pereira, J. Castro-Gomes and L. Pereira de Oliveira, "Influence of natural coarse aggregate size, mineralogy and water content on the permeability of structural concrete," *Construction and Building Materials,* vol. 23, no. 2, p. 602–608, 2009.

[32] H. Beushausen and T. Dittmer, "The influence of aggregate type on the strength and elastic modulus of high strength concrete," *Construction and Building Materials,* vol. 74, pp. 132-139, 2015.

[33] H. Taylor, Cement chemistry, London: T. Telford, 1997.

[34] C. Georgopoulos and A. Minson, Sustainable Concrete Solutions, Hoboken: Wiley-Blackwell, 2014.

[35] The Sustainable Concrete Forum, "Concrete Industry Sustainability Performance Report: Based on 2009 production," MPA - The Concrete Centre, Camberley, 2010.

[36] J. Borger, R. Carrasquillo and D. Fowler, "Use of recycled wash water and returned plastic concrete in the production of fresh concrete," *Advanced Cement Based Materials,* vol. 1, no. 6, p. 267–274, 1994.

[37] F. Sandrolini and E. Franzoni, "Waste wash water recycling in ready-mixed concrete plants," *Cement and Concrete Research,* vol. 31, no. 3, p. 485–489, 2001.

[38] J. Daczko, Self-Consolidating Concrete: Applying what we know, London: CRC Press, 2012.

[39] Z. Ellis, "Ultra-high performance concrete," *Public Roads,* vol. 75, no. 2, p. 49, 2011.

[40] M. Aleem and P. Arumairaj, "Geopolymer concrete - a review," *International Journal of Engineering Sciences & Emerging Technologies,* vol. 1, no. 2, pp. 118-122, 2012.

[41] B. Zhang, Z. Bundur, P. Mondal and R. Ferron, "Use of biomineralization in developing smart concrete inspired by nature," *International Journal of Materials and Structural Integrity,* in press.

[42] S. Stocks-fischer, J. K. Galinat and S. S. Bang, "Microbiological precipitation of $CaCO_3$," *Soil Biology and Biochemistry,* no. 31, 1999.

[43] V. Whiffin, "Microbial $CaCO_3$ precipitation for the production of biocement," Murdoch University, Perth, 2004.

[44] V. Achal, A. Mukerjee and M. Reddy, "Biogenic treatment improves the durability and remediates the cracks of concrete structures," *Construction and Building Materials,* vol. 48, pp. 1-5, 2013.

[45] V. Achal, A. Mukherjee and M. Reddy, "Effect of calcifying bacteria on permeation properties of concrete," *Journal of Industrial Microbiology and Biotechnology,* vol. 38, no. 9, pp. 1229-1234, 2010.

[46] K. Van Tittelboom, N. De Belie, W. De Muynck and W. Verstraete, "Use of bacteria to repair cracks in concrete," *Cement and Concrete Research,* vol. 40, no. 1, pp. 157-166, 2010.

[47] J. Wang, H. Soens, W. Verstraete and N. De Belie, "Self-healing concrete by use of microencapsulated bacterial spores," *Cement and Concrete Research,* vol. 56, pp. 139-152, 2014.

[48] H. Patil, H. Prashant, D. Raijiwala and B. Vijay, "Bacterial concrete--a self healing concrete," *International Journal of Applied Engineering Research,* vol. 3, no. 12, pp. 1719-1725, 2008.

[49] H. Jonkers and E. Schlangen, "Self-healing of cracked concrete : A bacterial approach," in *Proceedings of FRACOS6: fracture mechanics of concrete and concrete structures*, Catania, Italy, 2007.

[50] H. Jonkers, A. Thijssen, G. Muyzer, O. Copuroglu and E. Schlangen, "Application of bacteria as self-healing agent for the development of sustainable concrete," *Ecological Engineering,* vol. 36, no. 2, pp. 230-235, 2010.

[51] V. Wiktor and H. Jonkers, "Quantification of crack-healing in novel bacteria-based self-healing concrete," *Cement and Concrete Composites,* vol. 33, no. 7, pp. 763-770, 2011.

[52] Z. Basaran, "Biomineralization of cement based materials: inoculation of vegetative cells," The University of Texas at Austin, Austin, 2013.

[53] W. De Muynck, D. Debrouwer, N. De Belie and W. Verstraete, "Bacterial carbonate precipitation improves the durability of cementitious materials," *Cement and Concrete Research,* vol. 38, pp. 1005-1014, 2008.

[54] Z. Bundur, M. Kirisits and R. Ferron, "Biomineralized cement-based materials: Impact of inoculating vegetative bacterial cells on hydration and strength," *Cement and Concrete Research,* vol. 67, pp. 237 - 245, 2015.

[55] P. Ghosh, S. Mandal, B. Chattopadhyay and S. Pal, "Use of microorganism to improve the strength of cement mortar," *Cement and Concrete Research,* vol. 35, no. 10, p. 1980–1983, 2005.

[56] S. Vempada, S. Reddy, M. Rao and C. Sasikala, "Strength enhancement of cement mortar using microorganisms - an experimental study," *International Journal of Earth Sciences and Engineering,* vol. 4, no. 6, pp. 933-936, 2011.

[57] F. Silva, N. Boon, N. De Belie and W. Verstraete, "Industrial application of biological self-healing concrete: Challenges and economic feasibility," *Journal of Commercial Biotechnology,* vol. 21, no. 1, pp. 31-38, 2015.

[58] L. Plummer and E. Busenberg, "The solubilities of calcite, aragonite and vaterite in CO_2-H_2O solutions between 0 and 90 C, and an evaluation of the aqueous model for the system $CaCO_3$-CO_2-H_2O," *Geochimica et Cosmochimica Acta,* vol. 46, no. 6, pp. 1011-1040, 1982.

[59] C. Weiss, K. Torres-Cancel, R. Moser, P. Allison, E. Gore, M. Chandler and P. Malone, "Influence of temperature on calcium carbonate polymorph formed from ammonium carbonate and calcium acetate," *Journal of Nanotechnology and Smart Materials,* vol. 1, pp. 1-6, 2014.

[60] K. Sarayu, N. Iyer and A. Murthy, "Exploration on the biotechnological aspect of the ureolytic bacteria for the production of the cementitious materials—a review," *Applied Biochemistry and Biotechnology,* vol. 172, no. 5, p. 2308–2323, 2014.

[61] A. Schenk, I. Zlotnikov, B. Pokroy, N. Gierlinger, A. Masic, P. Zaslansky, A. P. O. Fitch, T. Metzger, H. Cölfen, P. Fratz and B. Aichmayer, "Hierarchical Calcite Crystals with Occlusions of a Simple Polyelectrolyte Mimic Complex Biomineral Structures," *Advanced Functional Materials,* vol. 22, no. 22, pp. 4668-4676, 2012.

[62] S. Mann, Biomineralization: Principles and Concepts in Bioinorganic Materials Chemistry, New York: Oxford University Press, Inc., 2001.

[63] J. Vincent, O. Bogatyreva, N. Bogatyrev, A. Bowyer and A. Pahl, "Biomimetics: its practice and theory," *J Roy Soc Interf,* vol. 3, no. 9, pp. 471-482, 2006.

[64] A. Srinivasan, G. Haritos and F. Hedberg, "Biomimetics: Advancing Man-Made Materials Through Guidance From Nature," *Applied Mechanics Reviews,* vol. 44, no. 11, pp. 463-482 , 1991.

[65] B. Suprenant and W. Malisch, "The cost of waiting: Concrete contractors can lose big money when delayed concrete setting sidelines finishers," *Concrete Construction,* 2000.

[66] S. Ramachandran, V. Ramakrishnan and S. Bang, "Remediation of concrete using micro-organisms," *ACI Materials Journal,* vol. 98, pp. 3-9, 2001.

[67] J. Gordon, The New Science of Strong Materials or Why You Don't Fall through the Floor, Princeton: Princeton University Press, 2006.

[68] G. Swiegers, Bioinspiration and Biomimicry in Chemistry: Reverse-Engineering Nature, Hoboken: John Wiley & Sons, Inc., 2012.

[69] R. Bonser, "Patented Biologically-inspired Technological," *Journal of Bionic Engineering,* vol. 3, no. 1, pp. 39-41, 2006.

[70] K. Geiser, "Making Safer Chemicals," Lowell Center for Sustainable Production, University of Massachusetts, Lowell, 2005.

[71] P. Ball, "Natural strategies for the molecular engineer," *Nanotechnology,* vol. 13, no. 5, pp. R15-R28, 2002.

[72] Y. Bar-Cohen, Biomimetics: nature-based innovation, Boca Raton: CRC Press, 2012.

[73] DTI Global Watch Mission, "Biomimetics: strategies for product design inspired by nature," Department of Trade and Industry, London, 2007.

[74] M. Meyers, P. Chen, A. Lin and Y. Seki, "Biological materials: Structure and mechanical properties," *Progress in Materials Science,* vol. 53, no. 1, pp. 1-206, 2008.

[75] S. Vierra, "Biomimicry: Designing to Model Nature," National Institute of Building Sciences, Washington, D.C., 2014.

[76] H. Wolpert, "The World's Top Olympians," *Engineered Biomimicry,* p. xix–xxv, 2013.

[77] C. Nicholas and J. Peterson, "Biomimicry: the "Natural" intersection of biology and engineering," *Science Scope,* vol. 38, no. 7, p. 18, 2015.

[78] D. Schroeter, "Introducing Biomimicry," *Green Teacher,* no. 88, p. 13, 2010.

[79] K. Passino, Biomimicry for Optimization, Control, and Automation, London Berlin Heidelberg: Springer-Verlag, 2004.

[80] M. McKosky, "Graphic Design + Biomimicry: Integrating Nature into Modern Design Practices," Rochester Institute of Technology, Rochester, 2012.

[81] C. Drake, "Biomimicry: Emulating the Closed-Loops Systems of the Oak Tree for Sustainable Architecture," University of Massachusetts, Amherst, 2011.

[82] L. Lee, "Biomimicry Design for Pre-fabricated Steel Module Inspired by Beehive," Albert Nerken School of Engineering, The Cooper Union, New York, 2012.

[83] D. Chen, B. Ross and L. Klotz, "Lessons from a Coral Reef: Biomimicry for structural engineers," *Journal of Structural Engineering,* vol. 141, no. 4, 2015.

[84] Y. Fujita, F. Ferris, R. Lawson, F. Colwell and R. Smith, "Calcium carbonate precipitation by ureolytic subsurface bacteria," *Geomicrobiology Journal,* vol. 17, no. 4, pp. 305-318, 2000.

[85] D. Sarda, H. S. Choonia, D. D. Sarode and S. Lele, "Biocalcification by *Bacillus pasteurii* urease : a novel application," *Journal Of Industrial Microbiology,* vol. 36, no. 8, pp. 1111-1115, 2009.

[86] A. C. Mitchell and F. G. Ferris, "The influence of *Bacillus pasteurii* on the nucleation and growth of calcium carbonate," *Geomicrobiology Journal,* vol. 23, no. 3, pp. 213-226, 2006.

[87] J. DeJong, B. Mortensen, B. Martinez and D. Nelson, "Bio-mediated soil improvement," *Ecological Engineering,* no. 36, pp. 197-210, 2010.

[88] V. S. Whiffin, L. A. van Paassen and M. P. Harkes, "Microbial Carbonate Precipitation as a Soil Improvement Technique," *Geomicrobiology Journal,* vol. 24, no. 5, pp. 417 - 423, 2007.

[89] V. Ivanov and J. Chu, "Applications of microorganisms to geotechnical engineering for bioclogging and biocementation of soil in situ," *Reviews in Environmental Science and Bio/Technology,* vol. 7, no. 2, pp. 139-153, 2008.

[90] J. Chu, V. Ivanov, M. Naeimi, V. Stabnikov and H. Liu, "Optimization of calcium-based bioclogging and biocementation of sand," *Acta Geotechnica,* vol. 9, no. 2, pp. 277-285, 2014.

[91] R. Hui, Q. ChunXiang and W. RuiXing, "A cementation method of loose particles based on microbe-based cement," *Science China Technological Sciences,* vol. 54, no. 7, pp. 1722-1729, 2011.

[92] J. DeJong, M. Fritzges and K. Nüsslein, "Microbially Induced Cementation to Control Sand Response to Undrained Shear," *Journal of Geotechnical and Geoenvironmental Engineering,* vol. 132, no. 11, pp. 1381-1392, 2006.

[93] D. Kim, K. Park and D. Kim, "Effects of ground conditions on microbial cementation in soils," *Materials,* vol. 7, no. 1, pp. 143-156, 2013.

[94] M. Gomez, "Field Scale Bio-cementation for the Improvement of Loose Sands," University of California at Davis, Davis, 2013.

[95] R. Hui and Q. Chunxiang, "Cementation of loose sand particles based on bio-cement," *Journal of Wuhan University of Technology: Matererials Science,* vol. 29, no. 6, pp. 1208-1212, 2014.

[96] N. Soon, L. Lee, T. Khun and H. Ling, "Improvements in engineering properties of soils through microbial-induced calcite precipitation," *KSCE Journal of Civil Engineering,* vol. 17, no. 4, pp. 718-728, 2013.

[97] P. Li and W. Qu, "Bioremediation of historic architectural heritages by *Sporosarcina pasteurii*," in *International Conference on Electric Technology and Civil Engineering (ICETCE)*, Lushan, 2011.

[98] G. Métayer-Levrel, S. Castanier, G. Orial, J. Loubière and J. Perthuisot, "Applications of bacterial carbonatogenesis to the protection and regeneration of limestones in buildings and historic patrimony," *Sedimentary Geology,* vol. 126, no. 1-4, p. 25–34, 1999.

[99] M. Camaiti, G. Borselli and U. Matteoli, "Prodotti consalidanti impiegati nelle operazioni di restauro," *Edilizia,* vol. 10, pp. 125-134, 1988.

[100] A. Webster and E. May, "Bioremediation of weathered-building stone surfaces," *Trends in Biotechnology,* vol. 24, no. 6, p. 255–260, 2006.

[101] J. Dick, W. De Windt, B. De Graef, H. Saveyn, P. Van der Meeren, N. De Belie and W. Verstraete, "Bio-deposition of a calcium carbonate layer on degraded limestone by *Bacillus species*," *Biodegradation,* vol. 17, p. 357–367, 2006.

[102] C. Rodriguez-Navarro, M. Rodriguez-Gallego, K. Chekroun and M. Gonzalez-Muñoz, "Conservation of ornamental stone by *Myxococcus xanthus*-induced carbonate biomineralization," *Applied and Environmental Microbiology,* vol. 69, no. 4, p. 2182–2193, 2003.

[103] P. Tiano, L. Biagiotti and G. Mastromei, "Bacterial bio-mediated calcite precipitation for monumental stones conservation: methods of evaluation," *Journal of Microbiological Methods,* vol. 36, no. 1-2, p. 139–145, 1999.

[104] P. Tiano, E. Cantisani, I. Sutherland and J. Paget, "Biomediated reinforcement of weathered calcareous stones," *Journal of Cultural Heritage,* vol. 7, no. 1, pp. 49-55, 2006.

[105] W. De Muynck, K. Cox, N. De Belie and W. Verstraete, "Bacterial carbonate precipitation as an alternative surface treatment for concrete," *Construction and Building Materials,* vol. 22, no. 5, p. 875–885, 2008.

[106] V. Achal, A. Mukherjee, S. Goyal and M. Reddy, "Corrosion Prevention of Reinforced Concrete with Microbial Calcite Precipitation," *ACI Materials Journal,* vol. 109, no. 2, pp. 157-163, 2012.

[107] N. K. Dhami, M. S. Reddy and A. Mukherjee, "*Bacillus megaterium* mediated mineralization of calcium carbonate as biogenic surface treatment of green building materials," *World Journal of Microbiology and Biotechnology,* vol. 29, no. 12, pp. 2397-2406, 2013.

[108] V. Achal, A. Mukherjee and M. Reddy, "Biocalcification by *Sporosarcina pasteurii* using corn steep liquor as the nutrient source," *Industrial Biotechnology,* vol. 6, no. 3, pp. 170-174, 2010.

[109] V. Achal, A. Mukherjee, P. Basu and M. Reddy, "Lactose mother liquor as an alternative nutrient source for microbial concrete production by *Sporosarcina Pasteurii*," *Journal of Industrial Microbiology and Biotechnology 36,* vol. 36, no. 3, pp. 433-438, 2009.

[110] D. Paulson, Topical Antimicrobial Testing and Evaluation, New York City: Marcel Dekker, Inc., 1999.

[111] R. E. Buchanan, N. E. Gibbons, S. T. Cowan, J. G. Holt, J. Liston, R. Murray, C. F. Niven, A. W. Ravin and R. W. Stanier, Bergey's Manual of Determinative Bacteriology 8th Edition, Baltimore: The Williams & Wilkin Company, 1974.

[112] E. Ricca and S. Cutting, "Emerging applications of bacterial spores in nanobiotechnology," *Journal of Nanobiotechnology,* vol. 1, no. 1, p. 6, 2003.

[113] J. Wang, N. De Belie and W. Verstraete, "Diatomaceous earth as a protective vehicle for bacteria applied for self-healing concrete," *Journal of Industrial Microbiology & Biotechnology,* vol. 39, no. 4, pp. 567-577, 2012.

[114] S. Bang, J. Galinat and V. Ramakrishnan, "Calcite precipitation induced by polyurethane-immobilized *Bacillus pasteurii*," *Enzyme and Microbial Technology,* vol. 28, no. 4-5, p. 404–409, 2001.

[115] C. Rodriguez-Navarro, F. Jroundi, M. Schiro, E. Ruiz-Agudo and M. T. González-Muñoz, "Influence of substrate mineralogy on bacterial mineralization of calcium carbonate: implications for stone conservation," *Applied and environmental microbiology,* no. 78, p. 4017–4029, 2012.

[116] N. Dhami, M. Reddy and A. Mukherjee, "Biomineralization of calcium carbonate polymorphs by the bacterial strains isolated from calcareous sites," *Journal of Microbiology and Biotechnology,* vol. 23, no. 5, pp. 707-714, 2013.

[117] F. Hammes, N. Boon, J. de Villiers, W. Verstraete and S. Siciliano, "Strain-specific ureolytic microbial calcium carbonate precipitation," *Applied and Environmental Microbiology,* vol. 69, no. 8, pp. 4901-4909, 2003.

[118] M. Ferrer, J. Quevedo-Sarmiento, M. Rivadeneyra, V. Bejar, R. Delgado and A. Ramos-Cormenzana, "Calcium carbonate precipitation by two groups of moderately halophilic microorganisms at different temperatures and salt concentrations," *Current Microbiology,* vol. 17, no. 4, pp. 221-227, 1988.

[119] I. Sondi and E. Matijević, "Homogeneous precipitation of calcium carbonates by enzyme catalyzed reaction," *Journal of Colloid And Interface Science,* vol. 238, no. 1, pp. 208-214, 2001.

[120] I. Sondi and B. Salopek-Sondi, "Influence of the primary structure of enzymes on the formation of $CaCO_3$ polymorphs: a comparison of plant (*Canavalia ensiformis*) and bacterial (*Bacillus pasteurii*) ureases," *Langmuir,* vol. 21, no. 19, p. 8876–8882, 2005.

[121] T. Kawaguchi and A. Decho, "A laboratory investigation of cyanobacterial extracellular polymeric secretions (EPS) in influencing $CaCO_3$ polymorphism," *Journal of Crystal Growth,* vol. 240, no. 1-2, pp. 230-235, 2002.

[122] B. Lian, Q. Hu, J. Chen, J. Ji and H. Teng, "Carbonate biomineralization induced by soil bacterium *Bacillus megaterium*," *Geochimica et Cosmochimica Acta,* vol. 70, no. 22, p. 5522–5535, 2006.

[123] Y. Zhang, H. Guo and X. Cheng, "Role of calcium sources in the strength and microstructure of microbial mortar," *Construction and Building Materials,* vol. 77, pp. 160-167, 2015.

[124] O. Meiron, E. Bar-David, E. Aflalo, A. Shechter, D. Stepensky, A. Berman and A. Sagi, "Solubility and bioavailability of stabilized amorphous calcium carbonate," *Journal of Bone and Mineral Research,* vol. 26, no. 2, pp. 364-372, 2011.

[125] A. Kantzas, F. Ferris, L. Stehmeier, D. Marentette, K. Jha and F. Mourits, "A novel method of sand consolidation through bacteriogenic mineral plugging," in *Proceedings of the CIM 1992 Annual Technical Conference, vol. 2*, Calgary, 1992.

[126] K. Bachmeier, A. Williams, J. Warmington and S. Bang, "Urease activity in microbiologically-induced calcite precipitation," *Journal of Biotechnology,* vol. 93, pp. 171-181, 2002.

[127] V. Achal, A. Mukherjee, P. Basu and M. Reddy, "Strain improvement of *Sporosarcina pasteurii* for enhanced urease and calcite production," *Journal of Industrial Microbiology,* vol. 36, no. 7, pp. 981-988, 2009.

[128] I. Hammad, F. Talkhan and A. Zoheir, "Urease activity and induction of calcium carbonate precipitation by *Sporosarcina pasteurii* NCIMB 8841," *Journal of Applied Sciences Research,* vol. 9, no. 3, pp. 1525-1533, 2013.

[129] C. Gorospe, S. Han, S. Kim, J. Park, C. Kang, J. Jeong and J. So, "Effects of different calcium salts on calcium carbonate crystal formation by *Sporosarcina pasteurii* KCTC 3558," *Biotechnology and Bioprocess Engineering,* vol. 18, pp. 903-908, 2013.

[130] A. Grabiec, J. Klama, D. Zawal and D. Krupa, "Modification of recycled concrete aggregate by calcium carbonate biodeposition," *Construction and Building Materials,* vol. 34, no. 1, pp. 145-150, 2012.

[131] W. Wilson, M. Wade, S. Holman and F. Champlin, "Status of methods for assessing bacterial cell surface charge properties based on zeta potential measurements," *Journal of Microbiological Methods,* vol. 43, no. 3, pp. 153-164, 2001.

[132] M. Fletcher, Bacterial Adhesion: Molecular and Ecological Diversity, Hoboken: John Wiley & Sons, Inc., 1996.

[133] P. Lee, M. Misran and W. Wan Abdullah, "Effects of Joule Heating on Electrophoretic Mobility of Titanium Dioxide (TiO_2), *Escherichia Coli* and *Staphylococcus Aureus* (Live and Dead)," in *IFMBE Proceedings 35*, Kuala Lumpur, 2011.

[134] A. Weerkamp, H. Uyen and H. Busscher, "Effect of zeta potential and surface energy on bacterial adhesion to uncoated and saliva-coated human enamel and dentin," *Journal of Dental Research,* vol. 67, pp. 1483-1487, 1988.

[135] E. Kłodzińska, M. Szumski, E. Dziubakiewicz, K. Hrynkiewicz, E. Skwarek, W. Janusz and B. Buszewski, "Effect of zeta potential value on bacterial behavior during electrophoretic separation," *Electrophoresis,* vol. 31, no. 9, pp. 1590-1596, 2010.

[136] G. Logsdon, Water Filtration Practices: Including Slow Sand Filters and Precoat Filtration, Denver: American Water Works Association, 2008.

[137] I. Bundeleva, L. Shirokova, P. Bénézeth, O. Pokrovsky, E. Kompantseva and S. Balor, "Zeta potential of anoxygenic phototrophic bacteria and Ca adsorption at the cell surface: Possible implications for cell protection from $CaCO_3$ precipitation in alkaline solutions," *Journal of Colloid and Interface Science,* vol. 360, no. 1, pp. 100-109, 2011.

[138] H. Hayashi, S. Tsuneda, A. Hirata and H. Sasaki, "Soft particle analysis of bacterial cells and its interpretation of cell adhesion behaviors in terms of DLVO theory," *Colloids and Surfaces B: Biointerfaces,* vol. 22, no. 2, pp. 149-157, 2001.

[139] K. Soni, A. Balasubramanian, A. Beskok and S. Pillai, "Zeta potential of selected bacteria in drinking water when dead, starved, or exposed to minimal and rich culture media," *Current Microbiology,* vol. 56, no. 1, pp. 93-97, 2008.

[140] F. Hammes and W. Verstraete, "Key roles of pH and calcium metabolism in microbial carbonate precipitation," *Reviews in environmental science and biotechnology,* vol. 1, no. 1, pp. 3-7, 2002.

[141] C. Rodriguez-Navarro, C. Jimenez-Lopez, A. Rodriguez-Navarro, M. Gonzalez-Muñoz and M. Rodriguez-Gallego, "Bacterially mediated mineralization of vaterite," *Geochimica et Cosmochimica Acta,* vol. 71, no. 5, p. 1197–1213, 2007.

[142] G. W. Claus, Understanding Microbes: A Laboratory Textbook for Microbiology, W. H. Freeman, 1988.

[143] V. Ramachandran, Concrete Admixtures Handbook: 2nd edition, Norwich: William Andrew, Inc., 1996.

[144] A. Neville, Properties of Concrete: 5th edition, Philadelphia: Trans-Atlantic Publications, Inc., 2012.

[145] N. Chikh, M. Cheikh-Zouaoui, S. Aggoun and R. Duval, "Effects of calcium nitrate and triisopropanolamine on the setting and strength evolution of Portland cement pastes," *Materials and Structures,* vol. 41, no. 1, pp. 31-36, 2008.

[146] S. Bang, J. Lippert, U. Yerra and S. R. V. Mulukutla, "Microbial calcite, a bio-based smart nanomaterial in concrete remediation," *International Journal of Smart and Nano Materials,* vol. 1, no. 1, pp. 28-39, 2010.

[147] S. Park, W. Chun, W. Kim and S. Ghim, "Application of alkaliphilic biofilm-forming bacteria to improve compressive strength of cement-sand mortar," *Journal of Microbiology and Biotechnology,* vol. 22, no. 3, p. 385, 2012.

[148] T. Matsuno and I. Yumoto, "Bioenergetics and the Role of Soluble Cytochromes *c* for Alkaline Adaptation in Gram-Negative Alkaliphilic *Pseudomonas*," *BioMed Research International,* 2015.

[149] S. Raut, D. Sarode and S. Lele, "Biocalcification using *B. pasteurii* for strengthening brick masonry civil engineering structures," *World Journal of Microbiology and Biotechnology,* vol. 30, no. 1, pp. 191-200, 2014.

[150] B. Mortensen, M. Haber, J. DeJong, L. Caslake and D. Nelson, "Effects of environmental factors on microbial induced calcium carbonate precipitation," *Journal of Applied Microbiology,* vol. 111, no. 2, pp. 338-349, 2011.

[151] C. Tai and F.-B. Chen, "Polymorphism of $CaCO_3$, precipitated in a constant-composition environment," *AIChE Journal,* vol. 44, no. 8, pp. 1790-1798, 1998.

[152] T. Evans, "Influence of ionic strength on calcium carbonate ($CaCO_3$) polymorphism," 2012.

[153] K. Tasneem, S. Kim, J. Kim, B. Nam and Y. Park, "Effects of aggregate mineralogy on the thermal expansion behavior of concrete," in *T&DI Congress*, Orlando, 2014.

[154] M. Sherwood, "Inhibition of *Rhizobium trifolii* by yeast extracts or glycine is prevented by calcium," *Journal of General Microbiology,* vol. 71, no. 2, pp. 351-358, 1972.

[155] L. Abelovska, M. Bujdos, J. Kubova, S. Petrezselyova, J. Nosek and L. Tomaska, "Comparison of element levels in minimal and complex yeast media," *Canadian Journal of Microbiology,* vol. 53, no. 4, pp. 533-535, 2007.

[156] R. T. Chancey, " Characterization of Crystalline and Amorphous Phases and Respective Reactivities in a Class F Fly Ash," The University of Texas at Austin, Austin, 2008.

[157] R. Ferron, "Formwork Pressure of Self-Consolidating Concrete: Influence of Flocculation Mechanisms, Structural Rebuilding, Thixotropy, and Rheology," Department of Civil and Environmental Engineering, Northwestern University, Evanston, IL, 2008.

[158] J. Zhang and G. W. Scherer, "Comparison of methods for arresting hydration of cement," *Cement and Concrete Research,* no. 41, p. 1024–1036, 2011.

[159] T. Ogino, T. Suzuki and K. Sawada, "The formation and transformation mechanism of calcium carbonate in water," *Geochimica et Cosmochimica Acta,* vol. 51, no. 10, pp. 2757-2767, 1987.

[160] F. Meldrum and H. Cölfen, "Controlling mineral morphologies and structures in biological and synthetic systems," *Chemical Reviews,* vol. 108, no. 11, pp. 4332-4432, 2008.

[161] S. Amidi and J. Wang, "Surface treatment of concrete bricks using calcium carbonate precipitation," *Construction and Building Materials,* vol. 80, p. 273–278, 2015.

[162] P. E. Stutzman, "Pattern fitting for quantitative x-ray powder diffraction analysis of portland cement and clinker," in *International Conference on Cement Microscopy, 18th*, Houston, 1996.

[163] S. Chipera and D. Bish, "Fitting full x-ray diffraction patterns for quantitative analysis: a method for readily quantifying crystalline and disordered phases," *Advances in Materials Physics and Chemistry,* vol. 3, no. 1A, pp. 47-53, 2013.

[164] C. R. Hubbard and R. L. Snydera, "RIR - Measurement and Use in Quantitative XRD," *Powder Diffraction,* vol. 3, no. 02, pp. 74-77, 1988.

[165] R. D. Moser, "High-strength stainless steels for corrosion mitigation in prestressed concrete: development and evaluation," Georgia Institute of Technology, Atlanta, 2011.

[166] Z. Siddiqi, Concrete Structures Part-II, 2nd Edition, Lahore: Help Civil Engineering Publishers, 2012.

[167] B. Diaz, L. Freire, X. Nóvoa and M. Pérez, "Electrochemical behaviour of high strength steel wires in the presence of chlorides," *Electrochimica Acta,* vol. 54, no. 22, pp. 5190-5198, 2009.

[168] C. Pereira, F. Jorge and J. Ferreira, "Adsorption of cations from a cement suspension onto lignocellulosic substrates and its influence on cement setting," *Journal of Wood Chemistry and Technology,* vol. 25, pp. 231-244, 2005.

[169] J. Gajda and M. Vangeem, "Controlling Temperatures in Mass Concrete," *Concrete International,* 59-62 January 2002.

[170] United States Department of Agriculture, "Most Probable Number Procedure and Tables," Athens, 2014.

[171] E. Olson, "Zeta potential and colloid chemistry," *Journal of GXP Compliance,* vol. 1, no. 16, p. 81, 2012.

[172] Y. Ballim and P. Graham, "The effects of supplementary cementing materials in modifying the heat of hydration of concrete," *Materials and Structures,* vol. 42, no. 6, pp. 803-811, 2009.

[173] A. Mansur, O. Do Nascimento and H. Mansur, "Controlling alkalinity of cement matrix: A key approach to improve fiber-cement durability," in *IIBCC: 11th International Inorganic-Bonded Fiber Composites Conference*, Madrid, 2008.

[174] R. Winston Liggett and H. Koffler, "Corn Steep Liquor in Microbiology," *Bacteriological reviews,* vol. 12, pp. 297-311, 1948.

[175] G. Tortora, B. Funke and C. Case, Microbiology: An Introduction 8th Edition, Benjamin-Cummings Pub Co, 2004.

[176] N. Thomas and J. Birchall, "The retarding action of sugars on cement hydration," *Cement and Concrete Research,* vol. 13, no. 6, pp. 830-842, 1983.

[177] "ASTM D1252 Standard Test Methods for Chemical Oxygen Demand (Dichromate Oxygen Demand) of Water," ASTM International, West Conshohocken, PA, 2012.

[178] L. Connelly, "T-tests," *Medsurg nursing : Official journal of the Academy of Medical-Surgical Nurses,* vol. 20, no. 6, p. 341, 2011.

[179] NIST/SEMATECH , "1.3.6.7.2. Critical Values of the Student's t Distribution," in *e-Handbook of Statistical Methods*, National Institute of Standards and Technology, 2003.

[180] R. B. Head and K. L. Sutherland, "Heterogeneous nucleation by aggregates of particles," *Australian Journal of Physics,* vol. 13, pp. 584-598, 1960.

[181] T. Lee, "Surface Characterization by Heterogeneous Nucleation from the Vapor," Harvard University, Cambridge, 1998.

[182] N. Salkind and K. Rasmussen, "Shapiro-Wilk Test for Normality," in *Encyclopedia of Measurement and Statistics*, SAGE Publications, Inc., 2007.